HYDROGEOLOGICAL MODELLING OF THE ESPERANCE DRINKING WATER AQUIFER SUBJECTED TO SEAWATER INTRUSION

ESPERANCE, WA, AUSTRALIA

BY

HUIBERT SEBASTIAAN VREEBURG

in partial fulfilment of the requirements for the degree of

Master of Science
in Water Management

at the Delft University of Technology,

to be defended publicly on Monday March 14, 2022 at 9:00 am (CET)

Thesis Committee:	Dr. Boris van Breukelen	Delft University of Technology
	Dr.Ir. Gerrit Schoups	Delft University of Technology
	Dr. Henning Prommer	CSIRO and University of Western Australia

TU Delft
Delft University of Technology

CSIRO

WATER CORPORATION

Abstract

Saltwater intrusion in groundwater is a concern in many aquifers around the world. It results in deterioration of potable and irrigation water quality and degradation of ecosystems. The problem is exacerbated by fresh groundwater abstraction, drying climates and a rising seawater level.

Esperance is a small town situated on the south coast of Western Australia. The drinking water is supplied by a borefield located on the coastal plain in between the Southern Ocean and the saline lakes: Lake Warden and the terminal Pink Lake. Saltwater intrusion has been monitored for over two decades in this aquifer.

Managing Saltwater intrusion has been a priority for the local water company and the regulator for decades yet a numerical model of the aquifer capable of quantifying flows and salinity distributions does not exist.

In this study, a numerical flow model was developed as a first step towards a model that also includes saltwater movement, i.e. density-dependent flow. A site-specific literature review is documented in this report, as well as relevant saltwater intrusion studies.

A 3-dimensional hydrogeological model was created with a kriging geostatistical algorithm with data from Airborne Electromagnetic (AEM) surveys and borehole logs. A database including climatological fluxes, abstraction rates, groundwater heads, lake stages and lithographic data was created. The salinity distribution in the catchment was analysed using borehole observations and AEM data. Groundwater salinity is more prevalent in the east and northeast of the domain. Salts from inland sources are transported to the coastal lakes by a combination of groundwater and surface water.

The flow model was calibrated with PEST++ and a linear parameter error and sensitivity reduction was carried out with GENLINPRED from the PEST++ suite. The result of the study is a groundwater flow model that is able to quantify the approximate fluxes and heads within the catchment. However, it must be noted that the calibration can be improved. The relative error reduction for some parameters is large, for example groundwater recharge in areas with sparse and dense vegetation (0.91, 0.84

respectively), the runoff/quickflow factors towards the lakes (0.87, 0.95 and 0.88 for the Pink Lake, Lake Warden and Windabout/Woody lakes respectively) and reasonable for some of the hydraulic conductivities. The identifiability for other parameters (such as specific yields and vertical hydraulic conductivity) is low.

Zone budget calculations show that groundwater annual recharge and evaporation are the largest fluxes in the catchment and are equal in magnitude. The annual average evaporation rate over the entire catchment is 0.74 mm/d. The annual average groundwater abstraction is the same order of magnitude of the flow that enters the ocean, 5,656 m^3/d vs. 8,169 m^3/d respectively.

Modelling indicates that abstraction has a large effect on groundwater levels. The decline is the largest (> 1 m) a couple of kilometres west from the town area where abstraction decreases the water table. The effect is less south of the Pink Lake (~0.40 m).

(Hyper) salinity is the result of the net transport of saline groundwater entering into the lakes in combination with net evaporation. Water budget calculations show that the groundwater inflow in the hypersaline lakes exceeds groundwater outflow by a factor 8.1 for the Pink Lake and 1.7 for Lake Warden. Freshwater entering the lakes originates from direct precipitation and a calibrated runoff/quickflow component. This results in an effective lake area for precipitation of 1.6 times for the Pink Lake and 2 times for Lake Warden. In the lakes the evaporation exceeds the freshwater inflow by a factor of 1.5 and 1.1 for the terminal Pink Lake and Lake Warden respectively.

The low flow velocities towards the ocean in the eastern part of the catchment underline the risk of saltwater intrusion in this area. Flow field modelling suggests that groundwater abstracted in areas directly south of the Pink Lake is saline.

Finally, the current model is able to support recommendations for expansion of the borefield towards the area in the west of the catchment.

Table of Contents

Abstract 2
Table of Contents iii
List of Figures vi
List of Tables ix
Acknowledgements x
Chapter 1: Introduction 11
1.1 Saltwater Intrusion 11
1.2 This Study 11
1.3 What is New? 14
1.4 Literature 15
1.4.1 Overview 15
1.4.2 Saltwater Intrusion Modelling - 2D Models 16
1.4.3 Saltwater Intrusion Modelling - 3D Models 18
1.4.4 Remarks 19
1.5 Saltwater Intrusion Computer Codes 20
1.6 Research Questions 21
1.7 Report Structure 22
Chapter 2: Site Description 23
2.1 Previous Work 23
2.1.1 Introduction 23
2.1.2 Overview 24
2.1.3 Reports by Departments and Water Corporation 25
2.1.4 PhD Studies 27
2.1.5 Other Water-Related Issues 30
2.2 The Conceptualisation of Groundwater Flow and Salinity 32
2.2.1 Sources of Salinity 32
2.2.2 Conceptual hydrological models 35
2.3 Data Used for Model Input 38
2.3.1 Subcatchment Delineation 38
2.3.2 Geology and Soils 40
2.3.3 Environmental Fluxes 40
2.3.4 Geology and Topography 44
2.3.5 Groundwater Abstraction 48
2.3.6 Population and Monthly Water Abstraction Rates 49
2.4 Data used for Model Evaluation 53
2.4.1 Public Water Aquifer 53
2.4.2 Water Levels 55
2.4.3 Salinity Data 58

Chapter 3: Methodology and Model Setup 64

3.1 Introduction 64

3.2 Gridded Rectilinear Approach 65

3.3 Geological Model 65
3.3.1 3D Kriging Introduction 65
3.3.2 3D Kriging Algorithm Selection 66
3.3.3 AEM Data Rendering 68
3.3.4 Construction and Manual Adjustments 69

3.4 Hydrogeological Model 69
3.4.1 Introduction 69
3.4.2 Lakes 69
3.4.3 Topological Features 70

3.5 MODFLOW 73
3.5.1 Software 73
3.5.2 Model Boundaries 73
3.5.3 Packages 75
3.5.4 FLOPY 81

3.6 Parameter Estimation (Pest++) 81
3.6.1 Introduction 81
3.6.2 PEST++ Algorithm Overview 82
3.6.3 Sensitivity Analysis with PEST++ 83

Chapter 4: Results and Discussion 86

4.1 Introduction 86

4.2 Salinity Distribution Analysis 86
4.2.1 Groundwater Salinity - Borehole Observations 86
4.2.2 Groundwater Salinity - AEM Data (2013) 87
4.2.3 Groundwater Salinity Discussion 88

4.3 Geological Model 89
4.3.1 Observations 89
4.3.2 Cross Sections 90

4.4 Hydrogeological model 92
4.4.1 Overview and Boundaries 92
4.4.2 Lakes 92

4.5 Calibration Results 93
4.5.1 Running PEST++ 93
4.5.2 Calibrated and Selected Parameters 93
4.5.3 Parameter Uncertainty Statistics 96
4.5.4 Head Observations vs Modelled Heads 100
4.5.5 Simulated vs Observed Water Tables 101
4.5.6 Lakes Time Series 104
4.5.7 Observation Bores Timeseries 105
4.5.8 Improving Modelling Accuracy 109

4.6 Quantification of Flows and Water Budgets 111
4.6.1 Introduction 111
4.6.2 Groundwater Inflow Estimation and Model Selection 112
4.6.3 Net Recharge and Evapotranspiration 112
4.6.4 Wetlands / Coramup Creek Inflow 113
4.6.5 Pink Lake, Lake Warden and Windabout/Woody Lakes 114
4.6.6 Interaction Ocean and Groundwater 116

4.6.7 Discussion Water Budgets....117
4.6.8 Overview of Flows....120
4.7 Groundwater Abstraction and Borefield Operation....122
4.7.1 Modelled Impact on Water Levels due to Abstraction....122
4.7.2 Vector Flow Fields....127
4.7.3 Production Borefield Design and Past Operation....135
4.7.4 Preferred Abstraction Location....138
Chapter 5: Summary and Conclusions....140
5.1 Introduction....140
5.2 Development of a numerical groundwater model....140
5.3 Extent of Saline Groundwater in the System and Sources....142
5.4 Major Hydrogeological and Hydrological Connections and Flows....142
5.5 effect of groundwater abstraction on the groundwater levels....143
5.6 role of the hypersaline lakes on saltwater intrusion....144
5.7 Borefield Design, Operation and Suggested Modifications....144
5.8 Preferred Location for future Borefield Expansions to Limit Saltwater Intrusion....145
5.9 Final Remarks....145
Chapter 6: Future Work and Recommendations....146
6.1 Introduction....146
6.2 Inclusion of variable-density flow and model calibration....146
6.3 Further develop the understanding of the interaction between the hypersaline lakes, the superficial groundwater aquifer and the ocean....148
6.4 Estimating the sustainable abstraction rates....149
6.5 Optimising existing borefield utilisation and engineering solutions with scenario testing....149
Chapter 7: References....150

List of Figures

Figure 1 – The Esperance Western Lakes Catchment, Location of the Study Area 12

Figure 2 – Esperance Western Lakes Catchment and Lake Warden Catchment (Source: Short [2], adapted) 12

Figure 3 – Esperance Geology Report Describing Water Supply, 1911 24

Figure 4 – Esperance Hydrological Field Map 26

Figure 5: Moving of the saltwater interfaces between 2000 – 2016 [source: unknown] 27

Figure 6 – The pink area identifies reliable HoistEM data (source: Abbott [28]). 28

Figure 7: Esperance Lithographic Information Field Map 29

Figure 8: Typical Stratigraphic Column with Geological Formation Notes and Schematic Cross Section (Source: Abbot [28]) 29

Figure 9 – Original basement flow accumulation interpretation is shown in red for comparison with the revised basement flow accumulation shown in black (source: Abbott [28]) 30

Figure 10 – TEMPEST CDI (Conductivity Depth Images) profiles located on their respective flight lines as a fence diagram (source: Abbott [28]) 31

Figure 11 – Typical of Australian coastal salt lakes (after Warren 1982a), (source: Mernagh [40]) 33

Figure 12 – Groundwater Salinity Distribution in the Yilgarn Craton (Source: Mernagh [40] 34

Figure 13 – Conceptual model of the interaction between the regional groundwater and groundwater discharge zone (source: Marimuthu [26]) 36

Figure 14 – Basement topography with lakes, coastline and interpreted subsurface drainage paths superimposed (source: Street [43]) 37

Figure 15 – Current salinity risk areas (source: DWER [44]) 37

Figure 16 – conceptual understanding and diagram of saltwater intrusion and saline upcoming in Esperance townsite (source: DWER [44]) 38

Figure 17 – Esperance Western Lakes 'Subcatchment' (source: Gee [45]) 39

Figure 18: Open Water Evaporation and Precipitation in Esperance 42

Figure 19: Land use Map Esperance 43

Figure 20: Typical Operation of Groundwater Bores in Esperance 2010 to 2019 44

Figure 21: AEM data showing the elevations of the dominant 4 soil formations in Esperance. The top soil (Quaternary) overlays the Pallinup formations and the elevation is shown in Figure 22 46

Figure 22: DWER - DEM LiDAR and Landsat in Esperance, 15m contour lines 47

Figure 23: Measured SCADA data, Saved Database Values and Modelled Values 48

Figure 24: Population Size and Drinking Water Abstraction Rate 50

Figure 25: Assumed Abstraction for Production Bore (15) 51

Figure 26: Assumed Normalised Annual Abstraction Pattern for Private Irrigation Bores 52

Figure 27: Population Size and Assumed Annual Water Abstraction Rate by Private Bores 52

Figure 28: Assumed Monthly Groundwater Abstraction Rates from 1993 to 2019 53

Figure 29: Location of the drinking water aquifer and of Water Corporation's boreholes. (source: unknown) 54

Figure 30: Lake Levels from 2001 to 2019, from west a, to east e 58

Figure 31: Calculated Salinity (TDS) and Measured Electrical Conductivity (EC) of the Pink Lake Between 2016 and 2020 (source: Lizamore [29]) 60

Figure 32: Calculated Salinity (TDS) and Measured Electrical Conductivity (EC) of Lake Warden Between 2016 and 2020 (source: Lizamore [29]) 61

Figure 33: Salinity measurements (TDS) of Lake Warden between 1979 and 2007 (source: DEC [23]) 62

Figure 34: Salinity (TDS) of Lake Wheatfield, Woody Lakes and Lake Windabout between 1997 and 2009 (source: DEC [23]) 62

Figure 35: Discharge and EC Observations in Coramup Creek. Calculated from EC Measurements by applying factor 0.65 to µS/cm obtain TDS in mg/L 63

Figure 36: Representation of the Inclusion of Lakes in the Hydrogeological Model 70

Figure 37: Landscape Features Used to Determine Boundary Conditions. The Resulting Model Boundaries Outlining the Subcatchment are Shown 71

Figure 38: Historical Aerial Imaginary of the Small Lakes North in the Subcatchment 72

Figure 39: Digital elevation mapping showing drainage patterns and catchment areas surrounding the lakes 78

Figure 40: Schematic plot of Evapotranspiration Flux 80

Figure 41: Groundwater Salinity in TDS (mg/L) indicated in Numbers and Colours, based on bore observations 87

Figure 42: Groundwater Salinity distribution in TDS (mg/L), based on AEM survey (2013) 88

Figure 43: 3D Geological Layers (30 layers x 275 rows x 223 columns) and Slices through Column 110 indicating the Sequence of Development of the Geological Model 91

Figure 44: 3D Overview of Hydrogeological Model, 10 x Vertically Exacerbated 92

Figure 45: Linear Uncertainty Analysis 100

Figure 46: Scatter Plots of Groundwater Model Results 101

Figure 47: Water Table Contour Map Summer Conditions (Mar 2018) 102

Figure 48: Water Table Contour Map Winter Conditions (Sept 2017) 103

Figure 49: Lake Levels Calculated and Observed (1993 – 2019) 104

Figure 50: Map of the Observation Bores Used for Calibration 105

Figure 51: Groundwater Levels Calculated and Observed (1993 – 2019) 109

Figure 52: Water Balance and Flows within the Subcatchment as Applied in the Groundwater Model 111

Figure 53: Water Balance and Flows within the Lakes as Applied in the Groundwater Model 111

Figure 54: Regional Flow Entering the Model Domain (Averaged 1993 – 2019) 112

Figure 55: Recharge and Evapotranspiration Fluxes (Averaged 1993 – 2019) 113

Figure 56: Coramup Creek Wetland Flows (Averaged 1993 – 2019) 114

Figure 57: Pink Lake Flows (Averaged 1993 – 2019) 115

Figure 58: Lake Warden Flows (Averaged 1993 – 2019) 115

Figure 59: Lake Windabout/Woody Lakes Fluxes (Averaged 1993 – 2019) 116

Figure 60: Ocean Groundwater Flows (Averaged 1993 – 2019) 117

Figure 61: Annual Net Recharge in the Subcatchment Compared to Abstraction Rates 118

Figure 62: Time Series of Groundwater Levels between 1993 and 2019 with Pumping and without Pumping 126

Figure 63: Modelled Absolute Effect on (Ground) Water Levels in Monitoring Bores as a Result of Historical Abstraction Rates 126

Figure 64: Ghyben-Herzberg's Interface Model 127

Figure 65: Locations of Flow Fields as Presented in Figure 66 129

Figure 66: Simulated Flow Vector Fields of Various Layers in November 2018 135

List of Tables

Table 1 – Stratigraphy and Soil Properties (Hydraulic Conductivities)..... 40

Table 2 – Water Availability in the Esperance Groundwater Area (source: DWER [3]) 55

Table 3 – Overview of Data Sources..... 56

Table 4 – Salinity Levels Classification..... 59

Table 5 – Selected PyKrige [64] Parameters and Algorithm 68

Table 6 – Multiplier (Recharge = Multiplier x Net Precipitation. Evapotranspiration = Multiplier x Open Water Evaporation) 79

Table 7 – Selected Root Zone Depths 80

Table 8 – Parameter Selection and Calibration Overview..... 95

Table 9 – Parameter Identifiability, Relative Error Reduction and Relative Uncertainty Reduction...... 98

Table 10 – Water Balance Pink Lake Comparison Finite Difference Method vs. Daily Water Balance Modelling..... 119

Table 11 – Overview of Average Annual Flows (1993 – 2019). Positive values indicate that flows enter and negative values indicate flows leaving the domain. 121

Table 12 – Production Bores Screen Depths and Distance to Pallinup Layer. Bores Arranged from West to East (Green Bores: East; Pink Bores: South of Pink Lake; Blue Bores: Between Pink Lake and Lake Warden; Yellow Bores: Town Area/South Lake Warden) 137

Table 13 – Groundwater Abstraction of Water Corporation Production Bores (Green: > 100 m^3/d; Yellow: 10 to 100 m^3/d; Red: < 10 m^3/d). Bores Arranged from West to East (Green Bores: East; Pink Bores: South of Pink Lake; Blue Bores: Between Pink Lake and Lake Warden; Yellow Bores: Town Area/South Lake Warden) 139

Acknowledgements

I am extremely thankful to the following people for your help, discussions and endless patience:

- My supervisors Boris van Breukelen, Henning Prommer and Gerrit Schoups
- Adam Siade (CSIRO), James Jamieson (CSIRO), Selva Marimuthu, Clive Hampton (Water Corporation), Zoe Thiele (Water Corporation) and Aine Patterson (DWER)
- The fantastic staff of the Delft University of Technology
- My family and friends, the Brockett family, Clare and Hazel

Without you the completion of my study would not have been possible.

Chapter 1: Introduction

1.1 SALTWATER INTRUSION

Saltwater intrusion is a common problem in coastal aquifers around the world. Freshwater abstraction, a drying climate and rising saltwater levels cause imbalances to the natural system resulting in the landward incursion of a salt groundwater wedge.

With 28% of the world population living within 100 km from the coastline, Kummu [1], coastal aquifers are extensively used as freshwater source. This is especially the case in arid or semi-arid regions where surface water is not readily available. As freshwater is removed from the aquifer by production bores, the natural water table is decreases and saltwater intrudes. This process of saltwater intrusion is a serious threat to the drinking water resources in many regions around the world. A thorough understanding of the hydrology in these aquifers will help to manage and protect the water resources and ecosystems.

1.2 THIS STUDY

Esperance is a town in Western Australia, on the Southern Ocean coastline 720 kilometres east-southeast of the state capital, Perth. The current urban population of Esperance is approximately 15,000. Esperance is a major regional port and service centre for the surrounding agricultural and inland mining areas. Figure 1 and Figure 2 shows the location of Esperance and the outlines of the Esperance Western Lakes Catchment which is part of the Lake Warden catchment, Short [2].

The climate is Mediterranean, characterised by winter rainfall and dry summers with evaporation rates that greatly exceed precipitation in summer. Drinking water is abstracted from a local aquifer with production bores located in the town itself and to the west of town. A pipeline located around 3 km inland with an approximate length of 12 km connects the approximate 30 active production bores.

The aquifer is not only under threat by the saltwater intrusion but also by hypersaline lakes just a couple of kilometres north of the borefield pipeline. Moreover, it is possible that the upwelling of artesian saline water underneath the aquifer also contributes to the salinisation of the aquifer.

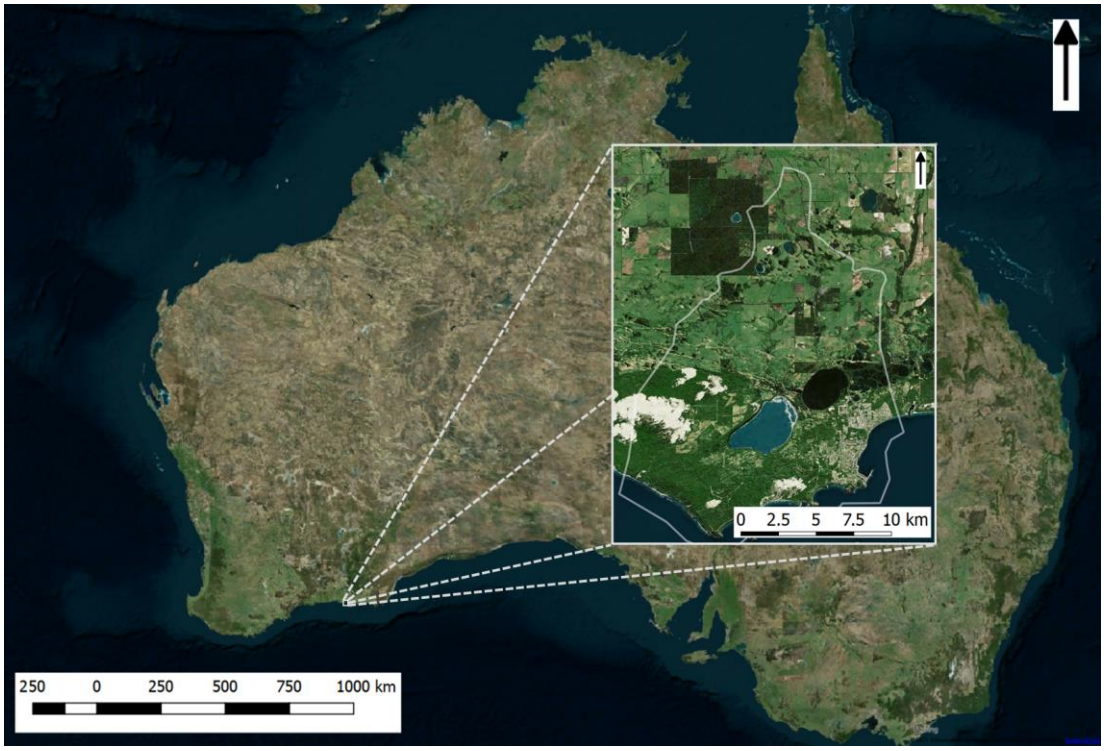

Figure 1 – The Esperance Western Lakes Catchment, Location of the Study Area

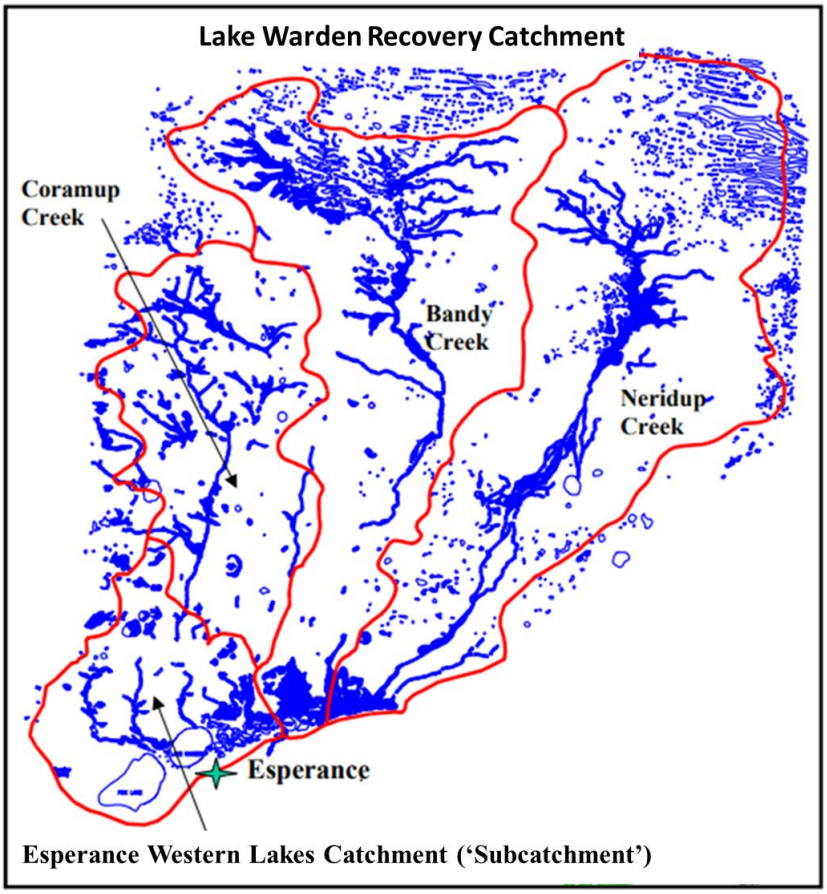

Figure 2 – Esperance Western Lakes Catchment and Lake Warden Catchment (Source: Short [2], adapted)

The Department of Water and Environmental Regulation (DWER)[1] recognise the need to manage the groundwater in the Esperance aquifer to protect the drinking water resource and limit potential environmental impacts. The Water Corporation[2], operates a superficial borefield to supply drinking water to the public and local industries.

Increasing demands for groundwater in the last decades is exerting more stress on the water resource and despite Water Corporation limiting abstraction in some bores and complying with the abstraction limits from DWER, upconing of saline water is observed in some of the bores. Currently, DWER estimates that the sustainable yield is 70 per cent of the total recharge DWER [3]. This value was estimated without the help of a numerical groundwater model.

This study aims to develop a numerical groundwater model for the Water Corporation to improve their understanding of the dynamics of the groundwater system in terms of the following:

- Salinity distribution in the catchment
- The overall hydrology and water balance of the aquifer
- Indication of areas at risk of saltwater intrusion
- Locate the most sustainable area for groundwater abstraction
- Preferred location of future borefield upgrades
- Increase understanding around the interaction of the hypersaline lakes, the superficial groundwater aquifer and borefield.

And as part of future work that includes density-dependent flow:

- Estimating the sustainable abstraction rates
- Optimising existing borefield utilisation and engineering solutions with scenario testing
- Further develop the understanding of the interaction between the hypersaline lakes, the superficial groundwater aquifer and the ocean.

1 The Department of Water and Environmental Regulation manages and regulates Western Australia's water resources.

2 Water Corporation is the principal supplier of water, wastewater & drainage services in Western Australia.

The tool required to meet the goals is a numerical model of the Esperance Western Lakes Catchment, which is from here on referred to as 'subcatchment'. The model should be used to investigate the most influential parameters on the saltwater intrusion and to help the decision and policy-makers to challenges related to population growth and climate change.

To our knowledge, no other studies have been conducted on saltwater intrusion where the aquifer is located between a salt lake and an ocean. Saltwater intrusion is a somewhat unfortunate name in the context of the aquifer in Esperance. A more appropriate term would be 'saltwater' intrusion as the saline water source is not only the sea but also the hypersaline lakes. Therefore, the term 'saltwater intrusion' is consistently used throughout this report.

A transport model has been made of the Esperance wetlands using the FEFLOW code by Marimuthu [4] however, this model did not include variable-density and also did not aim to model saltwater intrusion. The FEFLOW model was not further developed in this study as it would require a complete reworking of the catchment boundaries, geological layers and elevations. Furthermore, extensive grid refinement and a transformation from a 'deformed' grid to a rectilinear grid would have been required for numerical stability reasons. At last, a FEFLOW licence is expensive.

It must also be noted here that the model developed for this study does not include variable-density flow to model saltwater movement through the aquifer. However, the model is set up in a way that allows the inclusion of variable-density flow in the next stage of model development without reworking the grid or other features. The current flow model is however able to elucidate some characteristics of the saltwater intrusion.

1.3 WHAT IS NEW?

The model developed for this study is set up for the MODFLOW suite. It includes the lakes north of the borefield as a dynamic and integral part of the hydrology of the subcatchment. This means that the lakes are not used as a head boundary or as a saltwater reservoir with a fixed concentration, yet the head and concentration in the lakes serve as an important calibration feature and are the result of the hydrogeology of the entire system. It must be noted that SEAWAT is not compatible with the lake package of MODFLOW and an alternative way of modelling lakes is devised for this study.

The geology around the borefield is to some extent unravelled by an Airborne Electromagnetic (AEM) survey. The geology of the surrounding area is included by using bore log data. A 3D geological model of the entire subcatchment was developed by combining an interpolated model using kriging geostatistics, on borelogs and AEM data.

The hydrogeology of the Esperance subcatchment was thoroughly investigated by a combination of satellite imagery and literature review. Borehole Salinity observations and Electrical conductivity (EC) measurements from AEM survey made it apparent that the groundwater through flow from the north (inland) to the south (ocean) direction is saline. Furthermore, a part in the southwest of the subcatchment is likely closed off from direct flow to the ocean due to granite outcroppings above sea level.

It is shown that the operation of the borefield in Esperance is linked to the hydrogeology of the subcatchment. By analysing the results of the model, the performance of the bores can be predicted and the location of future expansions can be advised.

Finally, all specialised software used to create the model and visualise the results were freely downloadable.

1.4 LITERATURE

1.4.1 Overview

Various scientific articles describe the process of saltwater intrusion in detail. A small selection of these articles are discussed here.

In an overview article, Werner [5] discusses the general saltwater intrusion process, factors, aquifer management and the areas where the scientific understanding can be improved. Werner identifies a knowledge gap with transient saltwater intrusion processes especially in combination with regional scales, heterogeneities and more complex dynamic systems. Furthermore, thefreshwater/saltwaterr mixing zones, upconing, tides and the effect of pumping is discussed. To close the knowledge gap, intensive measurement campaigns coupled with modelling and calibration with predictive uncertainty analysis is key.

Werner [6] has issued another overview article specifically focussed on Australian coastal aquifers. The Australian coastal aquifers are under increasingly high stress due

to a growing population and below-average rainfall. As a result, some of the Australian coastal aquifers are seriously depleted. The paper aims to evaluate contemporarily investigation and management approaches and provides practical applications of saltwater intrusion management, such as:

- Operational controls (pumping, well construction). The hydrological response to these controls are not well documented
- Engineering works (artificial recharge schemes)
- Trigger level management (abstraction is limited by routinely measuring environmental parameters)
- Water trading (constraints on trading provides incentives to mitigate treats to water supply sustainability)

Future challenges that Werner identifies are the increasing operational costs of desalination plants and rising ocean levels. The need for extensive monitoring of water levels, salinity and chemistry are highlighted.

Most numerical saltwater intrusion computer codes rely on solving variable-density flow coupled with solute transport equations. This algorithm is complicated and computationally expensive compared to the flow equations without variable density or transport. To limit numerical dispersion and obtain accurate results a fine discretisation of the model domain is required. Several authors under which Oude Essink [7], report an upper limit of the Peclet number ($Pe < 2$ for finite difference algorithms) to control numerical inaccuracies due to numerical dispersion. In practice, the element size must be selected much smaller than required for a flow model.

1.4.2 Saltwater Intrusion Modelling - 2D Models

Despite advances in computer power over the last decades, most studies presenting saltwater intrusion with the help of a numerical model rely on 2-dimensional grids (length and height) to gain insights into the saltwater intrusion process. A couple of examples are discussed below.

Costall [8], presents multi-disciplinary research that includes geologists, field hydrogeologists and groundwater modellers. An extensive record of field data of saltwater intrusion in a coastal aquifer north of Perth in Western Australia was analysed. The setting is a highly heterogeneous karstic aquifer used for drinking water.

The drinking water resource is under stress due to a decline in rainfall and a rapid increase in population and sea-level rise. Several findings are reported as follows. It was demonstrated that simple analytical solutions result in errors in the location of the saltwater wedge which is often used as a guide to groundwater management decisions. Heterogeneity in hydraulic conductivity has a large effect on the extent of the saltwater interface. The study also highlights the extremes in fresh groundwater velocities as it flows from inland and discharges in the ocean. The distribution of the flow velocity can identify the location of the fresh and saltwater mixing zones and the location of the saltwater interface. A redesign of saltwater intrusion monitoring wells and systems is proposed that can collect flow velocity data, electric conductivities and pressure heads to more accurately measure the dynamics within the aquifer.

Other examples of seawater intrusion studies that are based on findings a 2-dimensional grid are from Luyun [9] using a numerical model to investigate the effects of recharge wells and flow barriers on saltwater intrusion, Kuan [10] modelling the tidal influence on saltwater intrusion in unconfined coastal aquifers and Badaruddin [11] who investigated the salinization of the (unsaturated) water table. These studies compare the results of the saltwater intrusion in a laboratory-scale testing setup with a numerical model. Luyun showed that water injection at the toe of the saltwater wedge is effective in mitigating intrusion. Kuan modelled the tidal effects on saltwater intrusion and demonstrated that tides can cause a significant reduction of saltwater intrusion in an unconfined coastal aquifer. Tides however cause a more complex mixing pattern in the zone of fresh terrestrial groundwater above the wedge. The research of Badaruddin suggests that salinisation of the water table (and unsaturated zone) is highly likely as a consequence of active saltwater intrusion conditions (hydraulic potential at the landward side is lower than the potential at sea-level).

Colombani [12] reports on a study that includes a man-made saline-brackish lagoon within the coastal setting in Italy. In the ‘60s the land between the lagoon and sea underwent intensive reclamation works to create a recreational area. The 2-dimensional model was run for a period of 1910 to 2017 to model the evolving salinity distribution due to evaporation, recharge and upconing of saline paleo water between the saline boundaries from the lagoon and sea. It was concluded that the majority of salinity originates from upconing from the aquitard immediately below the aquifer and evapotranspiration whereas the sea creates only a limited brackish water wedge.

1.4.3 Saltwater Intrusion Modelling - 3D Models

Examples of studies that cover the 3D modelling of aquifers are discussed below.

Sanford [24] modelled an aquifer in Virginia, USA to reproduce historical water levels and to forecast the potential for saltwater intrusion to 2050. The focus of the study was to explore the challenges in making the model in terms of computing capabilities during the development of the model in 2009. Sanford reports that the regional scale model is computationally prohibitive as the accuracy of the transport equation had to be sacrificed (1,736,040 cells). The model could only be calibrated by PEST++ on flow simulations only due to limitations of computing time. It was acknowledged that numerical dispersion is significant, yet a more finely discretised grid was not feasible. The study area is bounded by a bay and the Atlantic Ocean with a freshwater lens in the centre from which abstraction takes place. Simulations suggested that only a few inland wells would be threatened before 2050.

Siarkos [14] compares constant density solute transport by using the MODFLOW / MT3DMS code with the variable-density SEAWAT code. A coastal catchment in a semi-arid to humid climate with an intensively exploited freshwater lens was modelled by using regularly spaced cells of 100 m x 100 m x 125 m (vertical direction) resulting in a Peclet number equal to 1. Only 2 layers were modelled to avoid computational issues around the 'drying' of cells. When compared, the MT3DMW and the SEAWAT codes give rise to differences in hydraulic head and chloride concentrations distributions in the horizontal and vertical plane. SEAWAT predicts higher hydraulic head variations throughout the domain and higher chloride concentration in the bottom layer of the aquifer.

Lu [24] has developed a 3D density-dependent numerical model (32,990 nodes and 51,140 elements) to predict the future extent of saltwater intrusion. The coastal aquifer is subject to tides of 3m and groundwater abstraction. Lu reports on a maximum sustainable abstraction rate and demonstrates the effect of tides on inland groundwater chloride concentration.

Mohammed [25] presented modelling results of a coastal aquifer that includes 2 well fields and an upstream infiltration dam. The model mesh has 48,160 tri-linear hexahedral elements and 55,990 nodes and represents 80.26 km2, no dimension of the cells or number of layers are reported. The extent of saltwater intrusion is investigated

as a result of the abstraction from the aquifer while running three scenarios. Treated wastewater is infiltrated in the dam, in multiple dams or thirdly no management is applied. It was concluded that the installation of several infiltration ponds is the most effective measure in reducing saltwater intrusion.

Dibaj [17] used a 3D model (947,352 elements and 516,688 nodes, 1,059 km^2, 20 layers) to study saltwater intrusion in all layers of the coastal aquifer system and to predict the future behaviour of the aquifer under different management scenarios such as relocation of bores, reduce abstraction and the sea-level rise. Water abstraction near the shoreline is proven to be the main reason for the inland encroachment of saltwater. A very effective method to avoid saltwater intrusion is the relocation of bores to further inland.

EL Hamidi [24] studied an aquifer in morocco that is representative of the majority of northern Moroccan seashores. The goal of the study was to determine how climate, over-pumping, and sea-level rise affect saltwater intrusion. The surface area of the catchment is 305 km^2 and is represented by 3 layers, 128 columns and 128 rows of 250 m x 250 m. Three different pumping scenarios were tested in combination with sea-level rise and the most likely climatological projections, i.e. an increase in precipitation and an increase in temperature. From the simulations, it was concluded that the saltwater wedge in the northwest of the domain extends some 0.5 km inland while in 2040 the saltwater wedge is further seaward, or 3.5 km to 5.2 km more inland depending on the pumping scenario.

1.4.4 Remarks

In general, from the literature discussed in this section, it can be concluded that saltwater intrusion is mostly dependent on the abstraction rates and the location of the borefield. Climate change and sea-level rise also affect the location of the saltwater wedge. The saltwater wedge is located further seaward if tidal effects are included and a more complex mixing pattern above the wedge develops. Several saltwater intrusion mitigation strategies or engineered designs are effective such as limiting abstraction, flow barriers, relocation of bores, managed aquifer recharge and infiltration ponds.

From the 6 regional scale 3-dimensional modelling studies, only 2 report on the value of the Peclet number or mention numerical stability. From the other studies is not clear whether the numerical dispersion was acceptable or what trade-offs have been applied.

It is expected that the accuracy of the variable-density flow calculation was compromised considering the large grid size used in these models.

Within the studies that resemble 'real' 3D aquifers, only one reported on the methodology to interpolate the geology from borehole data. El Hamidi [24] used the capabilities of the software package RockWorks by supplier Rockware to create a fence diagram from the borehole data followed by a geostatistical analysis based on a kriging interpolation algorithm to obtain the stratigraphic model in 3D.

Finally, an example from the literature of a 3D model with groundwater abstraction between hypersaline water lakes and the ocean has not been found.

1.5 SALTWATER INTRUSION COMPUTER CODES

Numerical computer models are a useful tool to manage or predict future states of the aquifer. There are various options to include solute transport in the aquifer. SEAWAT can be used in combination with the solvers that are issued with the MODFLOW-2005 version, however, the robust Newton-Raphson (NWT) solver in conjunction with the Upstream Weighing (UPW) flow package is not compatible. Alternatively, the Layer Property Flow (LPF) flow package and the Sparse Matrix Solver (SMS) Package with Newton-Raphson formulation developed specifically for MODFLOW-USG can be used instead.

Recently MODFLOW 6 (MF6), the current core version of MODFLOW was extended to include a variable-density package called 'BUY' similar to SEAWAT while it also includes compatible and robust Newton-Raphson based solvers.

A freely available graphical user interface (GUI) is not (yet) available for SEAWAT or the more recently developed BUY package but commercial GUI's may be used instead. The SEAWAT package can also be operated directly in the FORTRAN coding language or with Python (Flopy). Alternatively, the variable-density flow code SUTRA can be used in combination with the GUI called model muse from USGS.

As mentioned before, saltwater intrusion is not included in the groundwater modelling of this thesis as a result of technical difficulties in combination with time constraints. The groundwater flow model that is constructed and findings of the literature review can be used as a starting point for the next stage of modelling which does include saltwater intrusion modelling and aquifer management.

Furthermore, the aquifer and the wetlands in general in Esperance face other challenges than saltwater intrusion alone. In future studies, the computer model that is developed here should be adaptable to suit topics other than saltwater intrusion.

1.6 RESEARCH QUESTIONS

Water Corporation has identified the management of saltwater intrusion in the drinking water aquifer as its highest priority. This study aims to create a numerical model that can quantify the hydrological fluxes and volume of the reservoirs to assist aquifer management. This can be broken down into the following research questions:

- What is the extent of saline groundwater in the system and what are the sources?
- What are the major hydrogeological and hydrological connections and flows; can previous models be confirmed?
- What is the effect of groundwater abstraction on groundwater levels?
- What is the role of the hypersaline lakes on saltwater intrusion?
- How is the borefield designed and operated and how can the borefield be modified to mitigate saltwater intrusion?
- What is the best location for future borefield expansions to limit saltwater intrusion?

The results of the study will be issued to Water Corporation (main client), CSIRO and the Department of Water and Environmental Regulation (DWER).

1.7 REPORT STRUCTURE

Chapter 2 describes the location and the characteristics of the study area and consists of 2 parts. At first, site-specific literature is presented and discussed. Secondly, the data that is used for creating the 3D hydrogeological model is presented together with the fluxes and (ground) water level observations for calibration of the groundwater flow model and the salinity distribution in the catchment.

Chapter 3 describes the methodology that was followed to build the 3D geological model and its transformation to the hydrogeological model. The packages that are used in the finite element numerical groundwater flow model are discussed as well as the calibration and sensitivity analysis tool PEST++.

Chapter 4 shows the results and discussions of the salinity distribution analysis, the geological model, the hydrogeological model, and the results of the calibration. The groundwater flow model that was developed was used to calculate water budgets of the entire domain and of selected areas, the lakes, within the domain. The model was run in two scenarios, with and without groundwater abstraction. The results of the vector flow fields of the two scenarios were compared as well as the difference in the groundwater levels. Finally, borefield abstraction and design features are presented and discussed.

Chapter 5 provides a summary and conclusions and Chapter 6 includes suggestions for future work and recommendations.

Chapter 2: Site Description

2.1 PREVIOUS WORK

2.1.1 Introduction

Site-specific information, literature and data are presented in this chapter to develop a conceptual hydrogeological understanding of the catchment.

Several reports issued by Departments and Water Corporation are discussed to gain an understanding of the water-related issues in the catchment and the constraints on abstraction rates. Two PhD studies that focussed on hydrogeology in Esperance provide valuable insights. Literature is reviewed that focus on the inland source of salinity to form a complete picture of the distribution of salinity. Surface water, previous conceptual models and catchment delineation are discussed. Previous geological studies are presented, followed by specific information on the aquifer in Esperance.

Finally, the input data used to construct the numerical hydrogeological model is presented in this chapter. This data consists of precipitation, evaporation and groundwater levels, lake water levels and groundwater abstraction rates. The fluxes are used as input for the groundwater model, while the water level observations are used to calibrate the model. The dataset needs to cover a relatively long period to properly model the (slow) effect of groundwater abstraction on saltwater intrusion. Therefore the data set that is developed for this study covers a period between 1900 and 2019.

Geological data needed to construct the model and the active domain is also reported in this section. This construction of the model was based on the lithography of bore logs, Airborne Electromagnetic (AEM) surveys and LiDAR data as well as satellite imagery and land use mapping. The active domain of the Esperance Western Lakes Catchment was based on surface elevation delineation (topographic divide).

Finally, data of observed salinity from groundwater bores, AEM data and surface water is collected to visualise the salinity distribution and to develop an understanding of the sources of salinity. This data is not used for groundwater modelling with the density-dependent flow at this stage but is included in the dataset for future work.

2.1.2 Overview

The oldest report on groundwater in the Esperance region stems from 1903 by a geologist called Maitland [19]. It was summarised in a newspaper article, refer to Figure 3. The article states that "The bulk of the underground water is salt but supplies of freshwater may be obtained in isolated localities near the bold granite outcrops in caves in which there is sufficient cover to afford storage. On the whole, the district will continue to depend for water supplies on surface conservation." Before the borefield and the pipeline were installed in the '80s, the town relied upon local groundwater bores and rainwater water collection.

Currently, around 15,000 people are supplied by the borefield. While it is now known that plenty of fresh groundwater is available around the Esperance municipality, a sustainable freshwater abstraction rate and the best location for the abstraction to avoid saltwater intrusion may have to be reassessed.

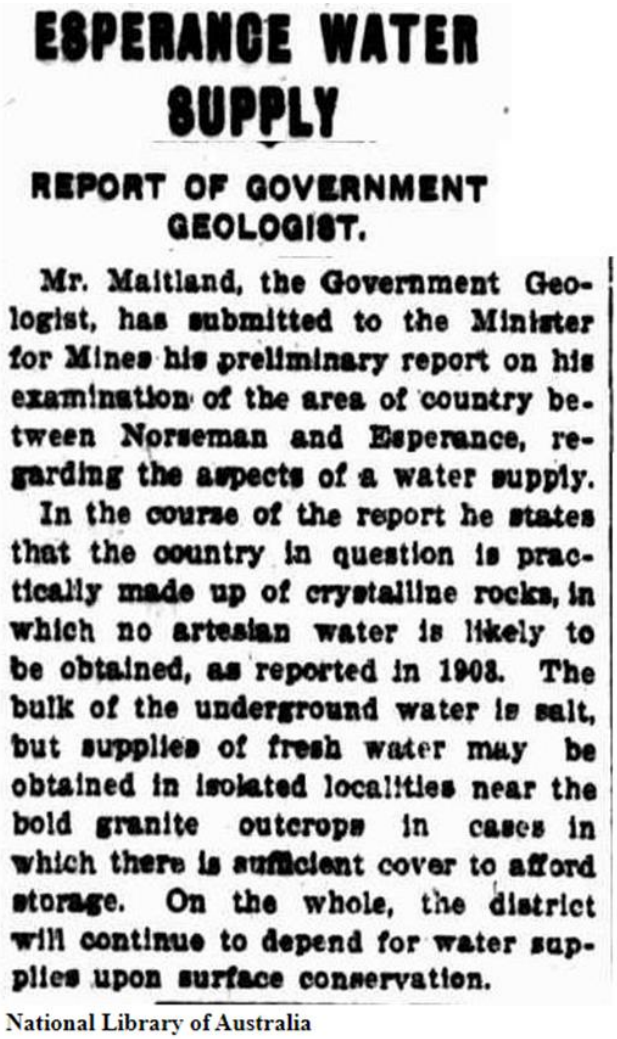

ESPERANCE WATER SUPPLY

REPORT OF GOVERNMENT GEOLOGIST.

Mr. Maitland, the Government Geologist, has submitted to the Minister for Mines his preliminary report on his examination of the area of country between Norseman and Esperance, regarding the aspects of a water supply.

In the course of the report he states that the country in question is practically made up of crystalline rocks, in which no artesian water is likely to be obtained, as reported in 1903. The bulk of the underground water is salt, but supplies of fresh water may be obtained in isolated localities near the bold granite outcrops in cases in which there is sufficient cover to afford storage. On the whole, the district will continue to depend for water supplies upon surface conservation.

National Library of Australia

Figure 3 – Esperance Geology Report Describing Water Supply, 1911

Figure 4 below shows the location of the lakes, creeks relative to the borefield in the Esperance subcatchment. The Department of Water (DWER) allocates an annual volume of water that Water Corporation and other users are allowed to extract from the aquifer. Table 2 in Section 2.4.1 shows the most recent estimate of the volume of water that is available and the volume that is allowed to be abstracted by licenced entitlements.

2.1.3 Reports by Departments and Water Corporation

Saltwater intrusion in the Esperance region has been a focus of the Department of Water and the Department of Agriculture for some time. The departments have issued several reports mentioning the topic: Short [2], Simons [20], DWER [3], Massenbouwer [21], DWER [22], DEC [23] and Lane [24]. These reports cover hydrology and land use information. Groundwater observations are reported by Short [2], Simons [20], DWER [3], Massenbouwer [21] and Lane [24]. Flowtube modelling of the groundwater levels has been performed by Short [2]. The reports are in agreement that salt levels in the wetlands are increasingly threatening the habitat and drinking water aquifer.

An overview article issued in 2015 from the Department of Parks and Wildlife summarises the findings of previous hydrogeological studies, Drew [25]. Readers interested in more details are also referred to this article.

In the report by DEC [23] the hydrology and health of the ecosystem of the Lake Warden Catchment are discussed. Salinity issues and concentrations in surface water are reported. Also, Lane [24] presents plotted time series of groundwater and surface water levels and salt concentrations in the Western Lakes Catchment.

An example of the observations of the saltwater monitoring bores is shown in Figure 5. It is evident that the volume of fresh water in the aquifer is decreasing between 2000 and 2016. The Pink Lake (a hypersaline lake) is one of the main contributors to saltwater intrusion together with Lake Warden and the Southern Ocean.

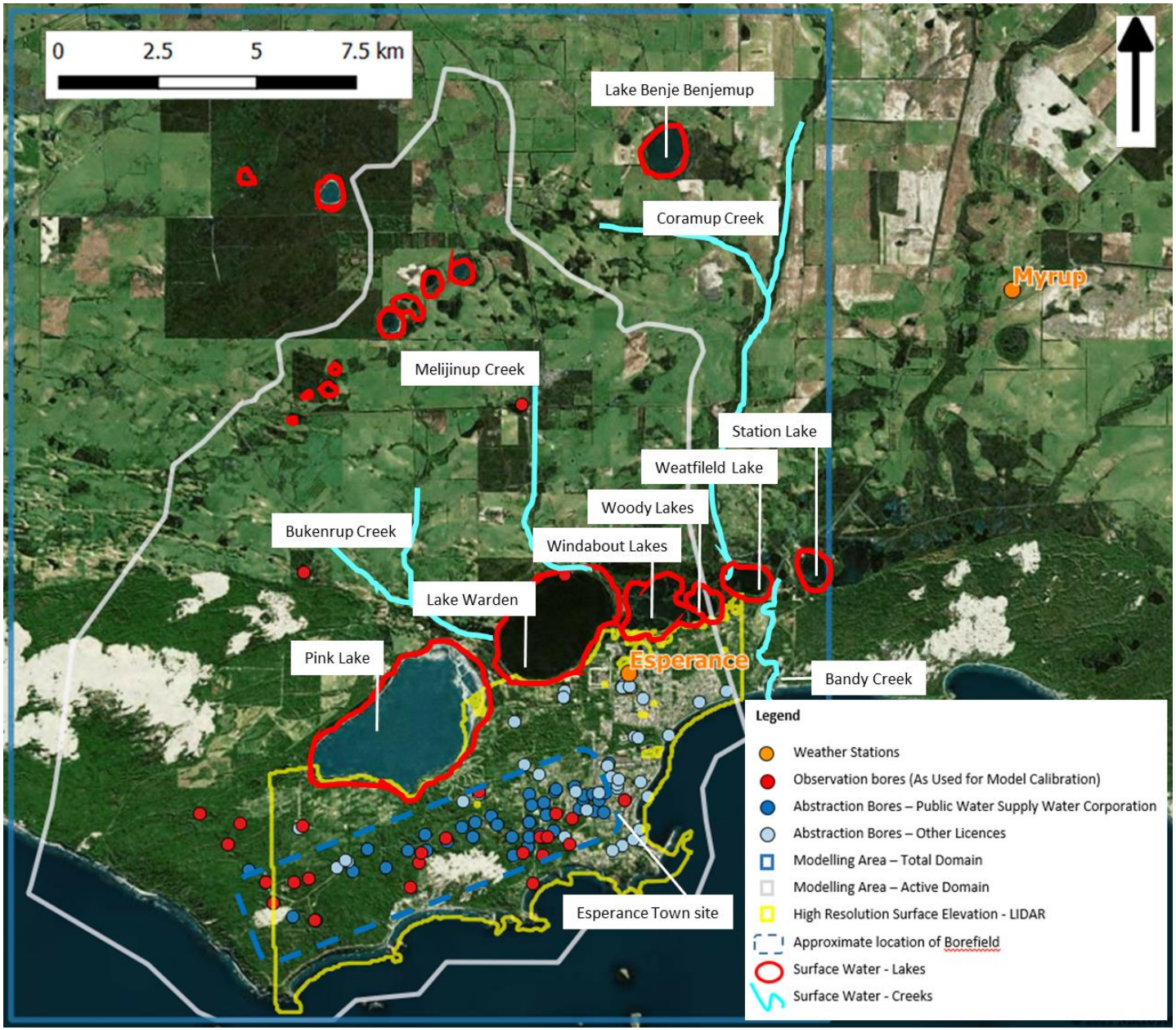

Figure 4 – Esperance Hydrological Field Map

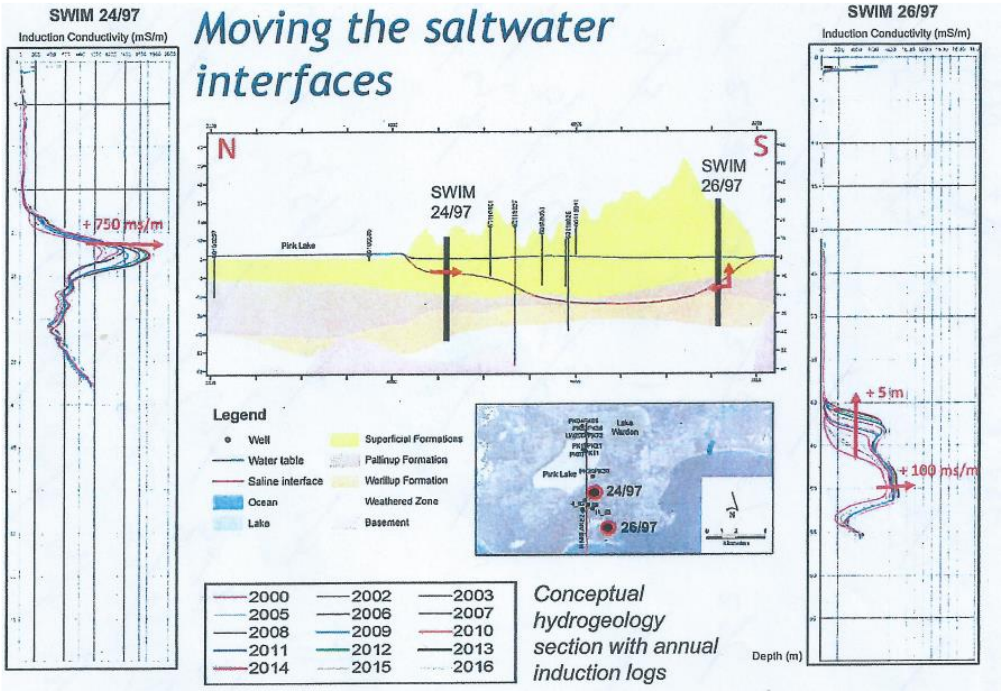

Figure 5: Moving of the saltwater interfaces between 2000 – 2016 [source: unknown]

2.1.4 PhD Studies

The drinking water aquifer is part of the larger Lake Warden Wetlands Catchment. This lake system was the focus of at least two PhD studies. The geohydrology was studied by Marimuthu [4], [26] and [27] and by Abbott [28]. Marimuthu has modelled part of the Esperance Lake Warden Catchment with the finite element software FEFLOW (Finite Element subsurface FLOW). Chemical and stable isotope data were used to provide in addition to head observations to elucidate the hydraulic processes in the wetlands. It was concluded that lakes in the wetlands are flow-through lakes and act as surface water discharge points. Groundwater flow directed towards the ocean also discharges in the lakes. Finally, it is concluded that the Pink Lake (the lake with the highest salinity) is a terminal lake for the north to south and northeast to southwest groundwater flow, Marimuthu [26], [27].

Marimuthu with Reynolds [4] developed a model using FEFLOW of the Lake Warden Catchment which was calibrated using heads, flow-path information, and Deuterium composition together to calibrate the model. This resulted in a flow model that can quantitatively estimate the groundwater fluxes in the Lake Warden wetlands system.

Abbott [28] in his thesis describes the Airborne Electromagnetic (AEM) geophysical methods to elucidate the hydrogeological architecture. The results of flow path

modelling in the Lake Warden wetlands are presented in chapter 4 of the dissertation. A literature review of (hydro) geological studies on the lake system is also covered in the thesis. However, the focus of the chapter is the result of the airborne electromagnetic (AEM) survey carried out with the HoistEM technique.

Figure 8 below shows the main geological formations in the Lake Warden Wetlands. With the HoistEM technique, it was possible to extract the depth and the thickness of the formations for most of the wetland's areas. Technical difficulties, described in Abbott's thesis, prevented accurate results for some areas due to the presence of a radio tower and the undulating terrain. Acceptable accuracy of the collected data was found in the pink area shown in Figure 6.

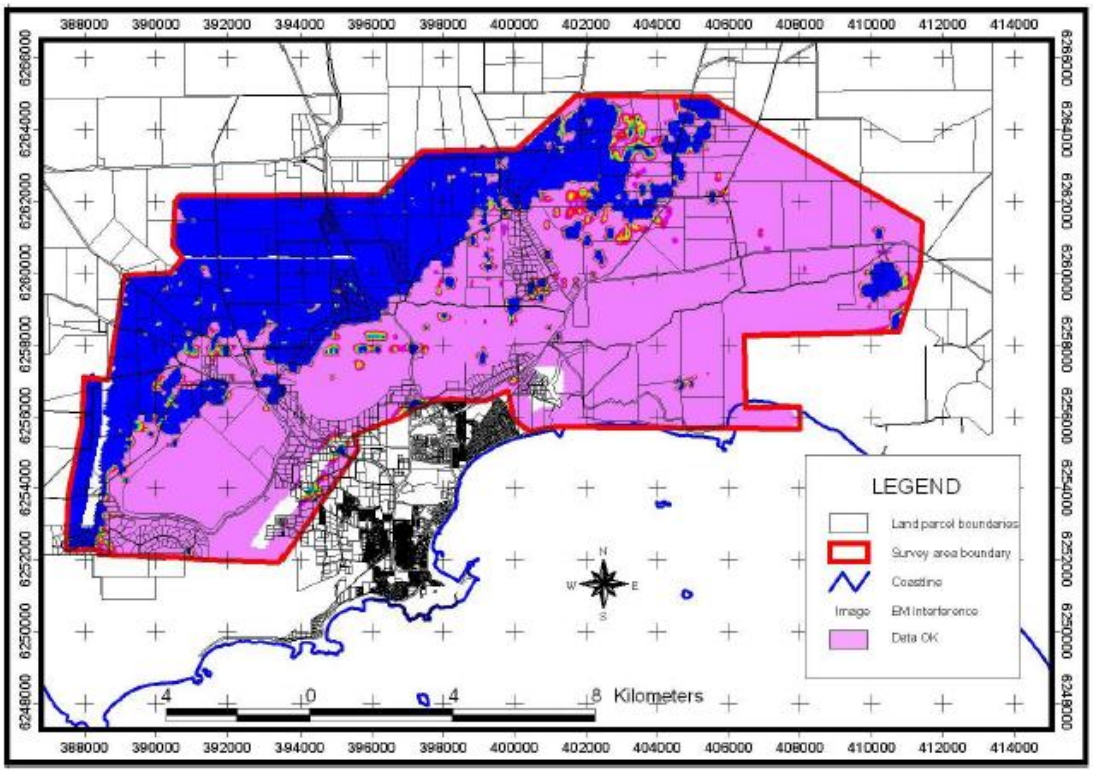

Figure 6 – The pink area identifies reliable HoistEM data (source: Abbott [28]).

From the HoistEM data, it was also possible to extract the flow paths as shown in Figure 9 below. The red flow lines in the figure are determined from studies before the HoistEM survey was undertaken. Abbot is unclear about the data source for the red flow lines but it is assumed here that these originate from the FEFLOW model by Marimuthu [4]. The updated (black) flowlines are mostly in good agreement with the original ones except in the southwest of the area.

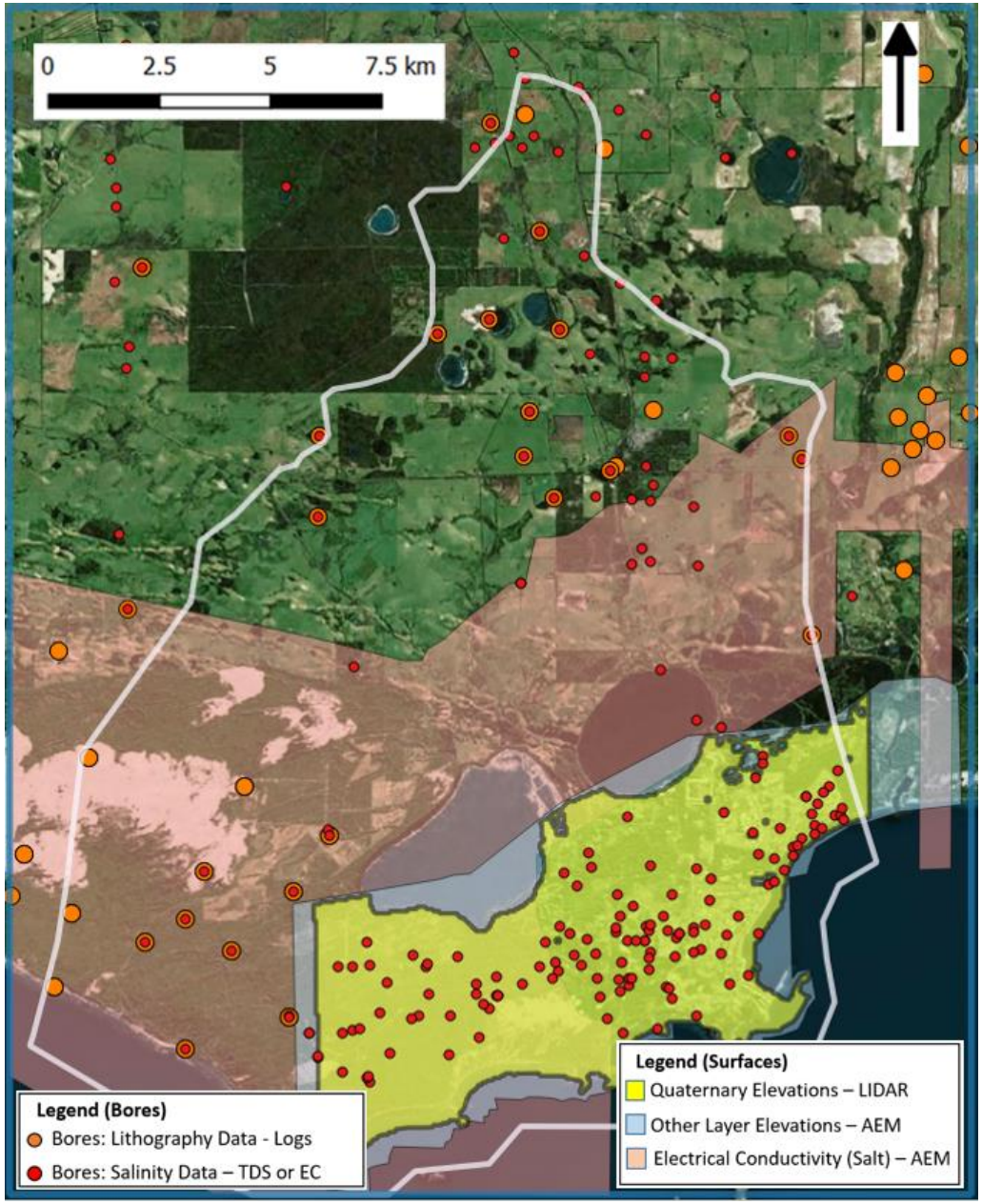

Figure 7: Esperance Lithographic Information Field Map

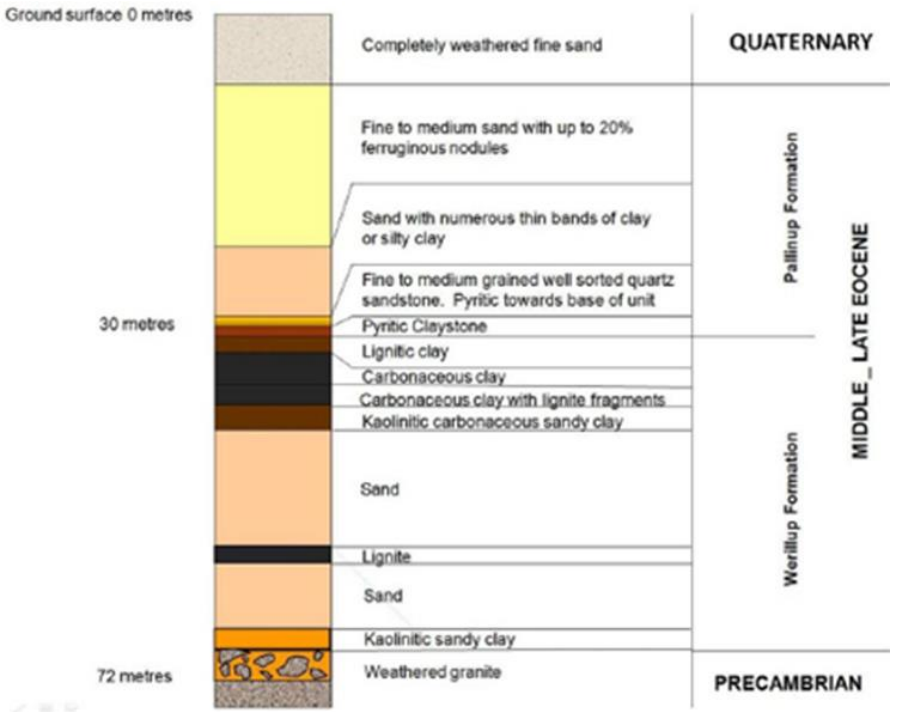

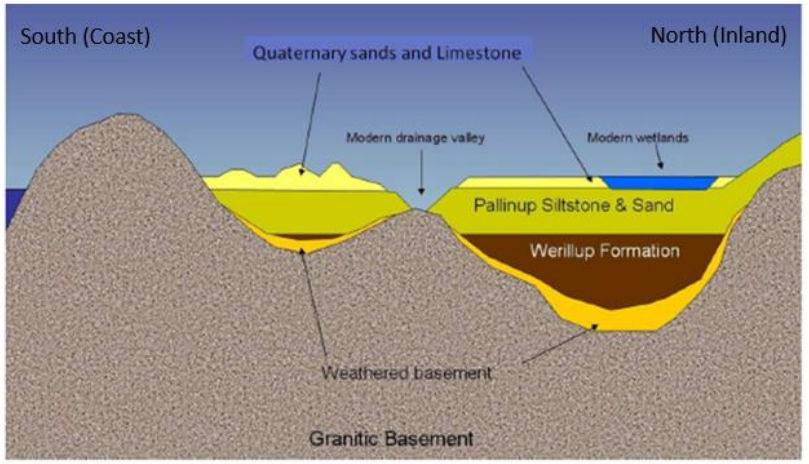

Figure 8: Typical Stratigraphic Column with Geological Formation Notes and Schematic Cross Section (Source: Abbot [28])

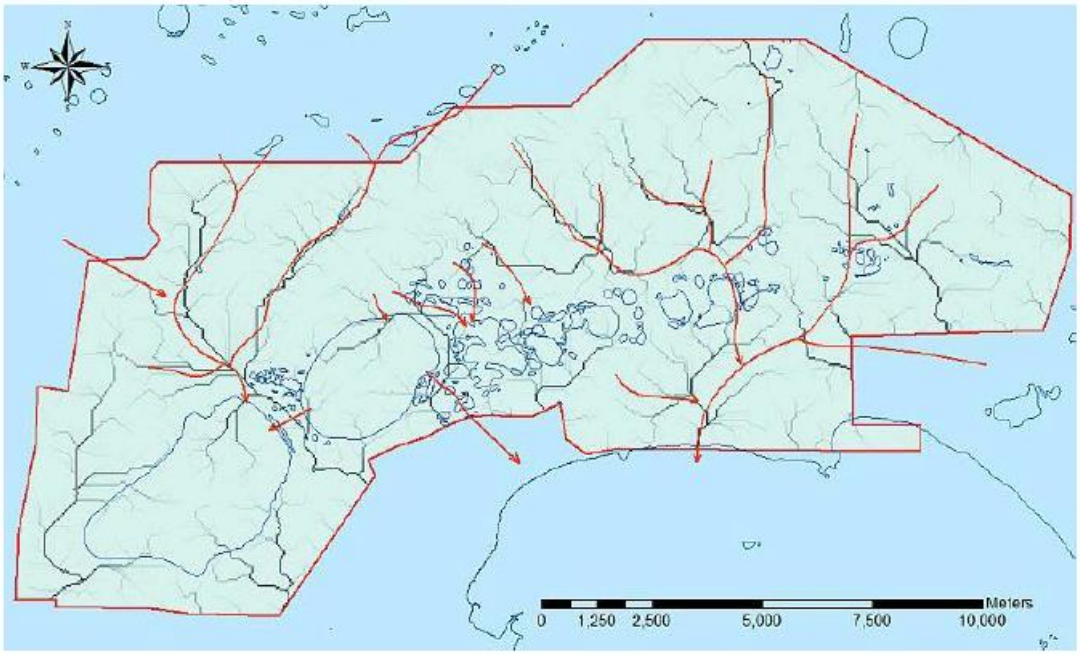

Figure 9 – Original basement flow accumulation interpretation is shown in red for comparison with the revised basement flow accumulation shown in black (source: Abbott [28]).

A TEMPEST fixed-wing airborne EM survey was carried out as part of the survey of the area. The results showed high electrical conductivity in the regolith (weathered bedrock) on the northern shore of Pink Lake and confirmed that saline groundwater is present surrounding the lakes, on some locations at the surface and in groundwater north of the wetlands, see Figure 10 below.

2.1.5 Other Water-Related Issues

Fading of the Pink Lake

The pink lake (the terminal lake in the wetland system) is named after its colour and is, or used to be, a well-known tourist attraction. The pink colour comes from a certain species of algae that accumulate beta-carotene pigment. A reduction of the pink pigment in the water is believed to be a result of decreasing salinity of the lake and the diminishing number of algae as reported by John Lizamore [29].

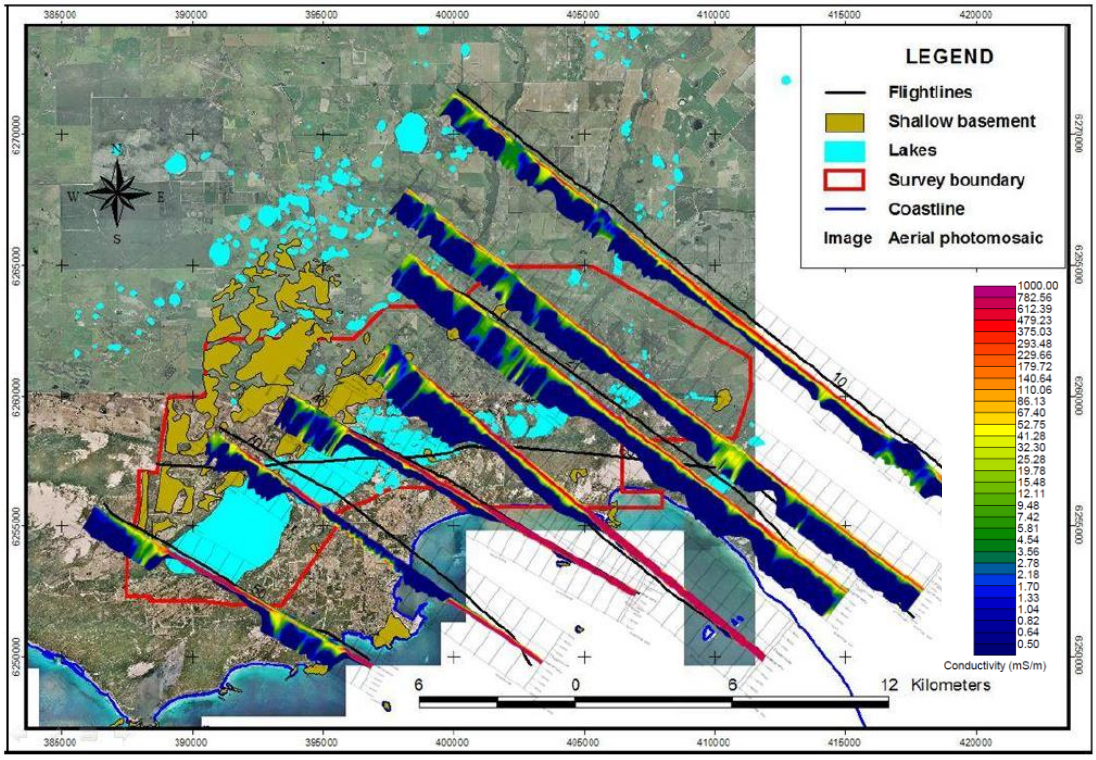

Figure 10 – TEMPEST CDI (Conductivity Depth Images) profiles located on their respective flight lines as a fence diagram (source: Abbott [28]).

Lead contamination

In December 2009 lead as fine dust escaped during the transport, storage and loading processes at the Port, leading to widespread contamination across the town of Esperance. The impact of the contamination was that up to 4,000 birds had died as a result of lead poisoning over a relatively short time period as reported by McCafferty [30]. Elevated lead blood levels above 10 µg/dl (the WHO action level) was detected in approximately 1 % of the population including children [30]. A large clean-up was established to clean houses (both internally and externally), rainwater tanks, publicly accessible equipment, and soil areas as explained by Heyworth [31].

The lead was deposited on areas that are on top of the (unconfined) drinking water aquifer.

PFAS

In 2019 Water Corporation testing detected very low levels of PFAS in three out of 31 active groundwater bores that are used as a source of drinking water for Esperance DWER [32]. It is likely that privately-owned bores in some locations are affected too. Groundwater modelling of PFAS plumes will increase understanding of the current and future extent of PFAS in groundwater and could be used for an impact assessment.

2.2 THE CONCEPTUALISATION OF GROUNDWATER FLOW AND SALINITY

2.2.1 Sources of Salinity

Inland and Seawater

The Pink Lake and Lake Warden, are important features for the hydrology and saltwater intrusion of the aquifer. These salt lakes, as many of the coastal salt lakes in the south West of Australia, are formed during the Holocene marine transgression 8000 to 4000 years before present as described by Hodgkin [33]. Sedimentary processes after the transgression resulted in the Pink Lake and Lake Warden being permanently closed off from the ocean. Permanently closed lakes in (former) estuaries are typical for areas with highly variable seasonal river flows in combination with small tides. The salinity of water in the estuary changes with river flow or precipitation rather than tidally. Figure 11 below provides a schematic sequence of the seasonal hydrology of coastal lakes systems in Western Australia.

Inland salinization in the wheat belt north of Esperance is a widespread phenomenon for as long ago as 2.8 Mya according to George [34]. This is a result of the antiquity, flatness and high evaporation rates compared to precipitation. Evidence suggests that it is most likely that the southern Wheatbelt north of Esperance has been submerged during two marine transgressions the Middle and Late Eocene (48 – 34 Mya). Other sources of salt are from extensive weathering of rocks and from rain originating from the Indian Ocean. Inland salt from these 3 sources eventually accumulates in the weathered bedrock. Climatic changes have caused salts that had been resident in the regolith of catchments to be mobilised as water tables rose in response to groundwater recharge. More recent land clearing has added to the rise of water tables and subsequent (secondary) salinization.

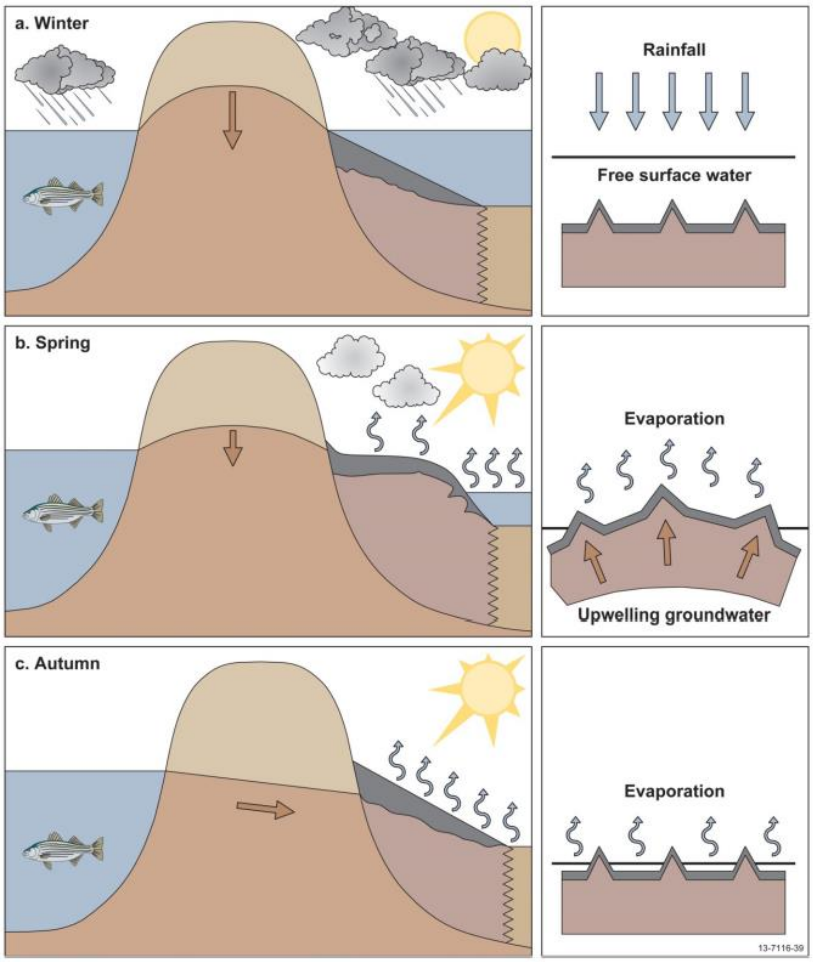

Figure 11 – Typical of Australian coastal salt lakes (after Warren 1982a), (source: Mernagh [40]).

Conceptual models show that groundwater generally flows in the north to south direction from the Wheatbelt to the coast and is measured to be saline or hypersaline as reported by Short [35], Meyers [36] and Overheu [37]. This is also reported by Timms [38] who studied the saline lakes in the Esperance Hinterland. The study included lakes that are situated 20 km to 100 km directly north of the Esperance subcatchment. Some of these lakes are subject to occasional large overland flows and have low salinity. Most of the lakes however are groundwater controlled and are saline (mostly hypersaline) and may fill and dry over periods of years. It is assumed in this study that the small lakes in the north of the Esperance Western Lakes Catchment boundary are hydrologically comparable to the lakes studied by Timms [38]. Aside from saline groundwater entering the Western Lakes Catchment, the most obvious source of salt is directly from the ocean, i.e. from saltwater seepage, saltwater spray and precipitation.

Water tables are generally rising in the Esperance region as reported by Raper [39] which increases the risk of salinity issues. Figure 12 below shows a map of the groundwater salinity in the ~3 billion-year-old Yildarn Craton catchments, Mernagh [40].

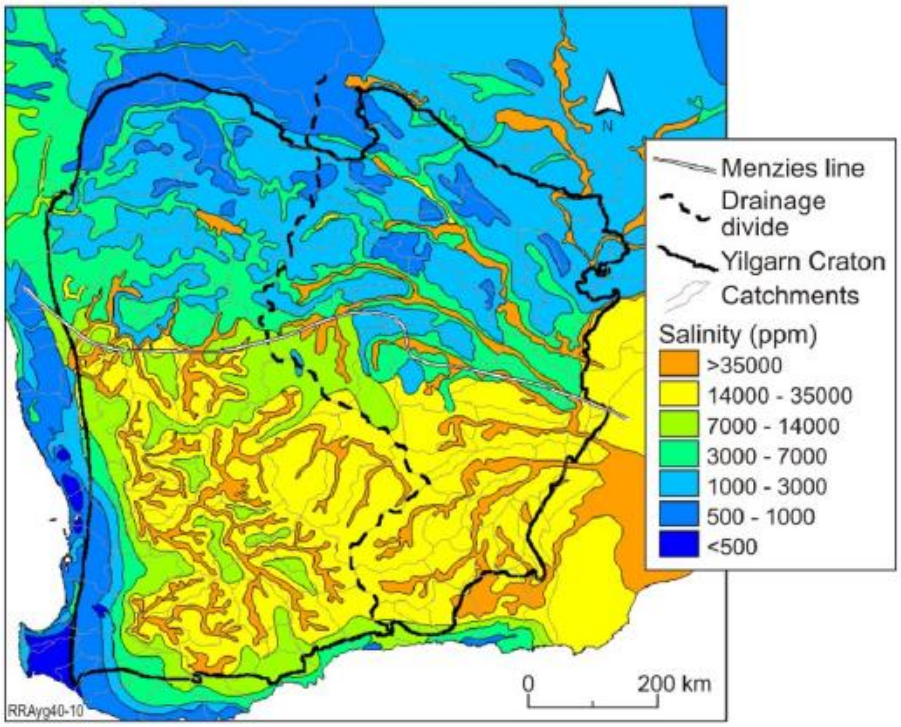

Figure 12 – Groundwater Salinity Distribution in the Yilgarn Craton (Source: Mernagh [40]

As reported in the overview article from the department of Geoscience Australia by Mernagh [40], salt inflow into the Pink Lake is conservatively estimated to be about 800 tonnes per year from surface streamflow, and approximately 5,500 tonnes per year from groundwater flow. An estimated 1.1 million tonnes of salt occurs on the surface of the lake as halite. Drilling indicates that up to 18 million tonnes of salt could be contained in the subsurface sediments, after Galloway [41]. A recent study by Massenbauer debates this value and states that 18 million tonnes are significantly overestimated [42].

Surface Water

Several small creeks drain into the coastal wetlands system within the Esperance subcatchment. On the East just outside the subcatchment boundaries is Coramup Creek, which discharges in the wetlands in the east of the boundary of the

subcatchment. Bandy Creek, further east delivers flow to the wetlands as well and has the potential to discharge in the ocean. Coramup Creek discharges in the wetlands in Lake Wheatfield which is dissected by the Esperance subcatchment boundary. All the lakes in the wetlands are interconnected by groundwater flow.

The Coramup Creek and the Bandy Creek are mostly fed by groundwater and discharge year around as concluded by Marimuthu [26]. Other creeks in the system are fed by mainly surface runoff. Figure 4 above outlines the location of the lakes and the creeks.

2.2.2 Conceptual hydrological models

Groundwater Flow in Lake Warden Catchment

At least three studies have presented conceptual hydrological models of the Lake Warden Catchment, i.e., by Marimuthu [4], [26], [27], by Abbott [28] and by short [2]. A new conceptual model for this study was not developed as the existing models are in good agreement.

Short [2] reports on groundwater levels through a series of transects using borehole observations. The conceptual results of these three studies are compiled and presented in this subsection. The main findings of the studies are:

- The lakes in the study area (the subcatchment) are connected to the regional groundwater system
- Groundwater flow enters the subcatchment with a general flow from East to West in the wetlands.
- The lakes are acting as flow-through lakes and terminate in the Pink Lake in the west.
- The water level in these lakes is higher in winter and lower in summer than groundwater level. This suggests that the lakes are recharging to the groundwater system in winter and groundwater discharges in summer.
- Groundwater measurements indicate that water is entering the subcatchment in the elevated areas from the northeast. Some seepage from sub-artesian systems probably feeds into the Pink Lake according to Street [43].

The figures below are extracted from reports and studies and provide a good overview of the flows in the Lake Warden District. Flow paths are shown in figures from Marimuthu [26], Street [43] and Abbott [28].

Figure 13 below shows a schematic of the basement topography including the flow paths from northeast to southwest (coastal plain). A 3-dimensional view was issued by Street [43] and is shown in Figure 14.

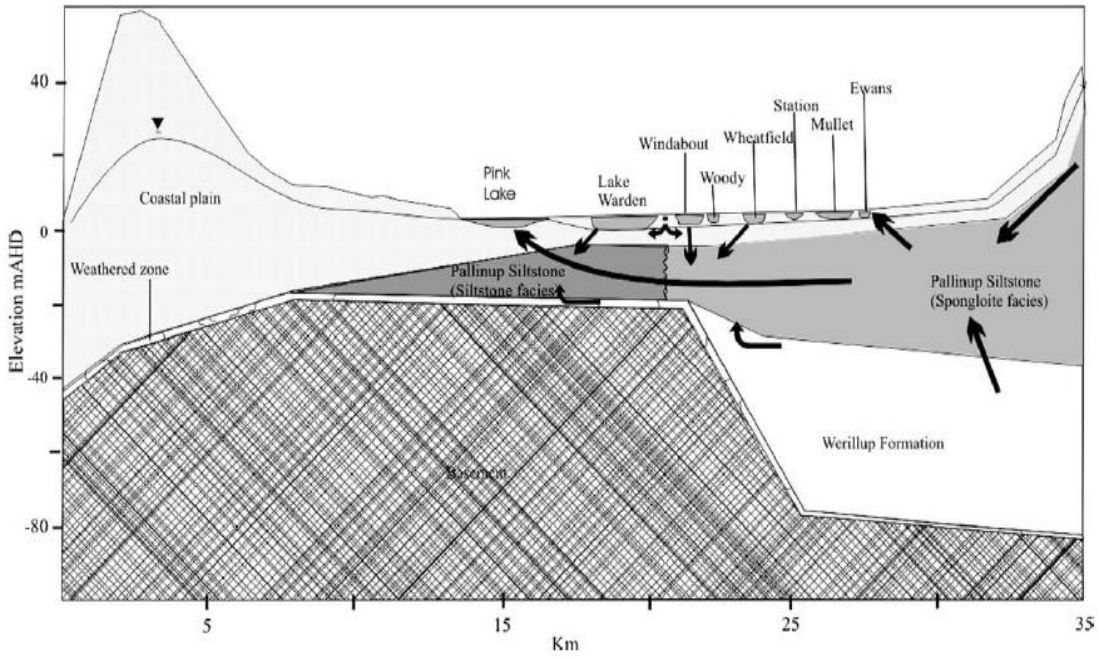

Figure 13 – Conceptual model of the interaction between the regional groundwater and groundwater discharge zone. Arrows denote groundwater flow (source: Marimuthu [26]).

Saltwater Intrusion in the Lake Warden Catchment

The Esperance Groundwater Allocation Evaluation Statement 2012–2020, DWER [44], presents a map of the area showing the known areas of saline groundwater that exists under fresh water in Figure 15 below.

A conceptual understanding and diagram of saltwater intrusion and saline upcoming in Esperance townsite are shown in Figure 16 below. Abstraction of fresh groundwater will decrease the groundwater flow towards the ocean. As a result, the saltwater interface will extend further land inwards. Reduced rainfall, as expected due to climate change, will further intensify saltwater intrusion.

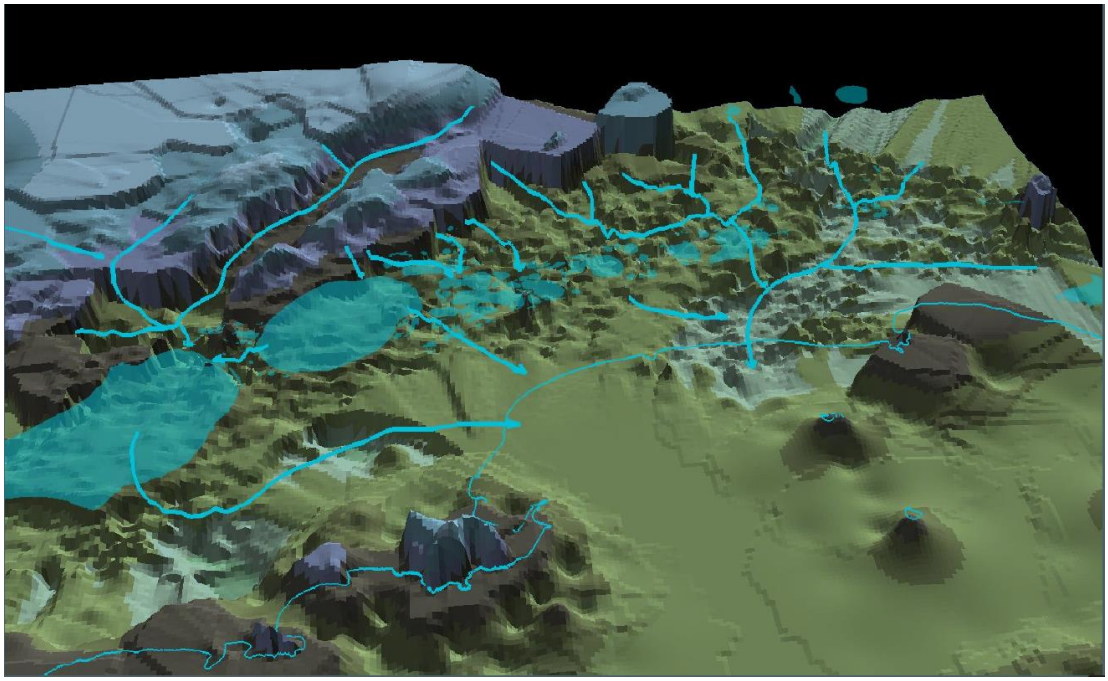

Figure 14 – Basement topography with lakes, coastline and interpreted subsurface drainage paths superimposed (source: Street [43]).

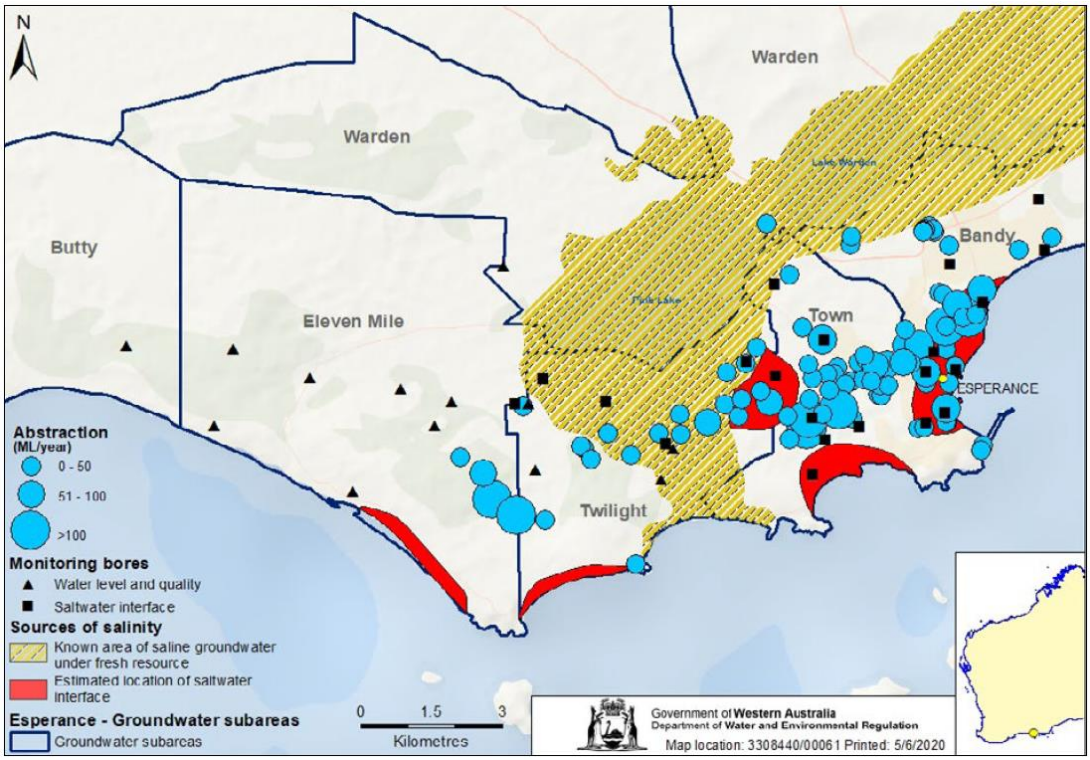

Figure 15 – Current salinity risk areas (source: DWER [44]).

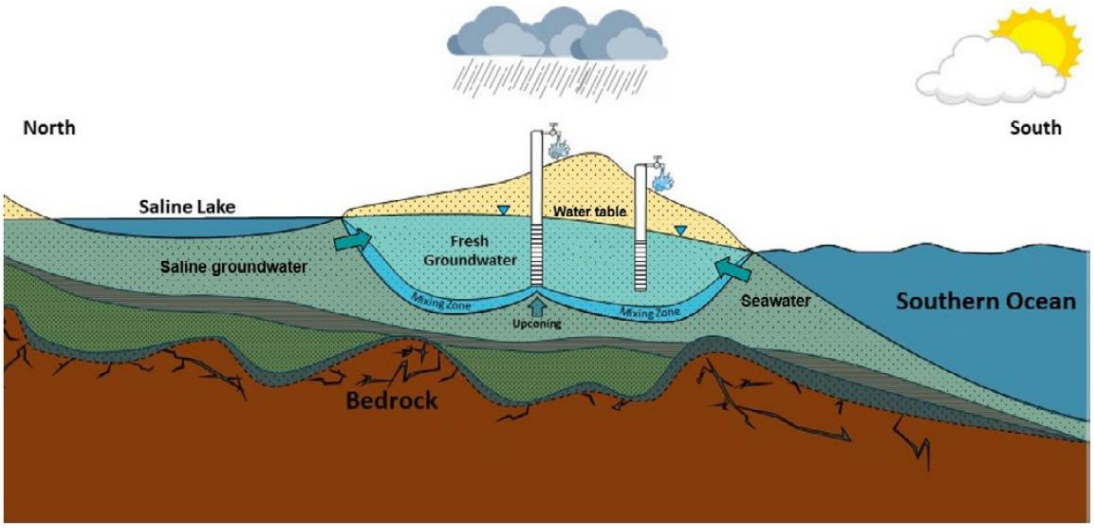

Figure 16 – conceptual understanding and diagram of saltwater intrusion and saline upcoming in Esperance Townsite (source: DWER [44]).

2.3 DATA USED FOR MODEL INPUT

2.3.1 Subcatchment Delineation

Gee [45] issued a map of the Esperance Western Lakes Catchment (in this study referred to as 'subcatchment') refer Figure 17 below. The map is based on surface elevation delineation (topographic divide). The subcatchment boundaries were used to define the model boundary developed for this report and is already shown in Figure 1, Figure 4 and Figure 7. The area of the subcatchment is approximately 190 km^2.

It is assumed that any precipitation that is collected within this boundary has the potential to recharge groundwater. The justification is based on the assumption that underneath the relatively conductive quaternary top layer a far less conductive Pallinup layer is present which is partly comprised of siltstone. Secondly, the top of the Pallinup layer is expected to follow similar elevation contours of the quaternary layer. Using model boundaries based on surface profile delineation is expected to produce a more accurate groundwater response to annual precipitation cycles than a randomly selected geometric boundary.

The land surface elevation correlates less with the elevation of the basement. Groundwater is likely lost and/or gained from the subcatchment in the deeper formations such as the Werillup or the weathered base rock layer (regolith). The occurrence of natural lakes in the Esperance hinterland discussed by Timms [38], are mainly fed by groundwater flow along a north to south direction. A similar set of small

lakes are located north of the boundaries of the subcatchment. At least one of them is perennial. It is therefore likely that (saline) groundwater enters the subcatchment boundary.

Another source of discharge into the subcatchment originates from the Coramup Creek and, to a lesser extent, the Bandy Creek. Both creeks are running in the north to south direction at the east of the Esperance subcatchment. Coramup Creek discharges in Lake Wheatfield and the Bandy Creek in the east of the wetlands and the ocean. Water levels in the wetlands fluctuate seasonally with an amplitude of approximately 1 m.

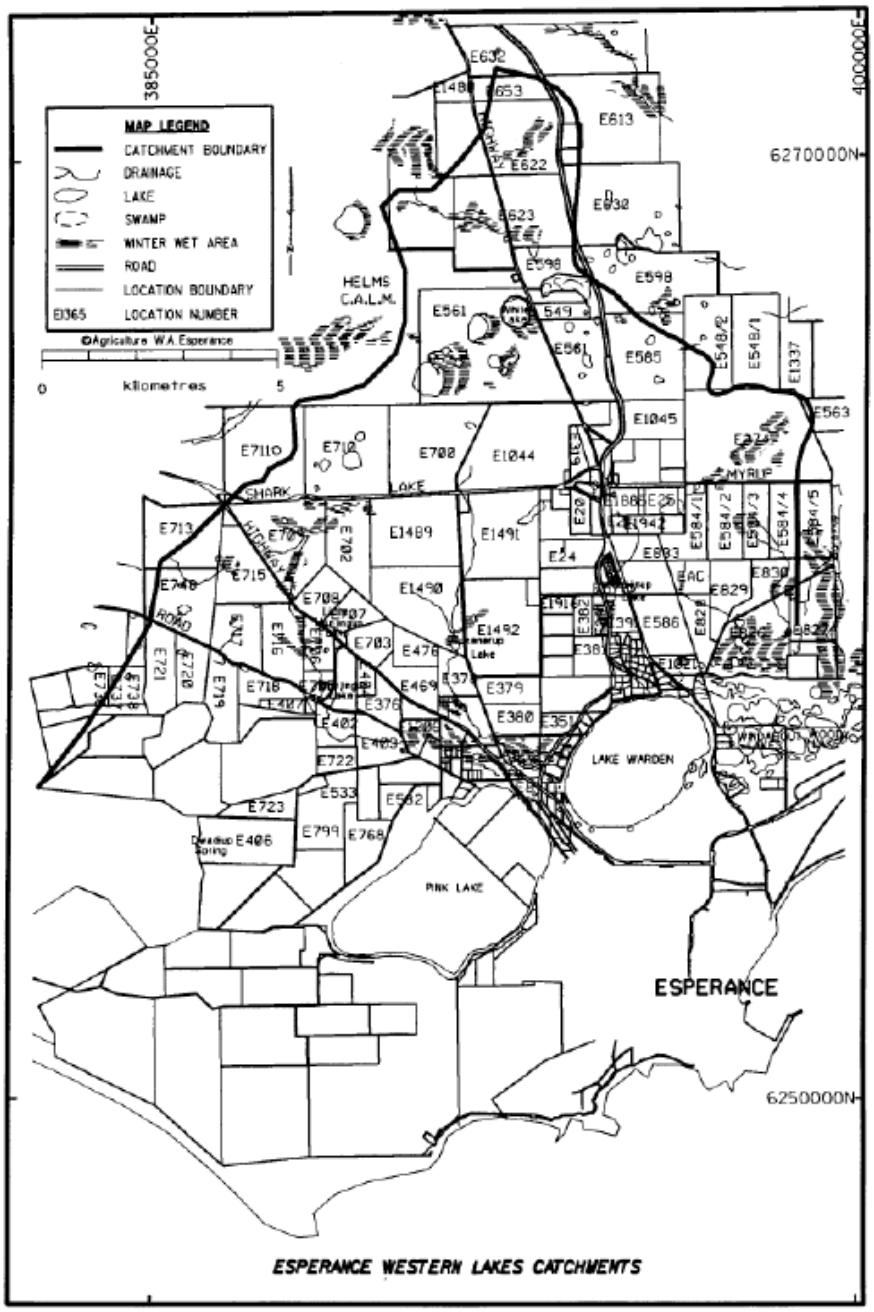

Figure 17 – Esperance Western Lakes 'Subcatchment' (source: Gee [45]).

2.3.2 Geology and Soils

Various reports provide details on the soil formations and its physical properties in the Esperance region for example from Johnson [46], Marimuthu [4] and Short [2]. The relevant findings of these reports are shown in Table 1 below. Conductivities of pump tests reported by engineering consultancies Rockwater [47] and Talis [48] are included if the data is available.

The data from Table 1 below has been used to estimate the parameter boundaries of the hydraulic conductivity of the geological layers in the model. Figure 8 shows a typical stratigraphic column with the geological formations.

Table 1 – Stratigraphy and Soil Properties (Hydraulic Conductivities)

Age	Formation	Lithology	Conductivity (m/d)
Quaternary	Alluvium Coastal Sand Eolian Dune	Silt, sand, and gravel Sand Limestone Fine Sand	10 [46]
Tertiary – Eocene	Pallinup - Shoreline facies - Spongelite facies - Siltstone facies	 Fine Sand, Silt, Clay Spongelite, Clay Siltstone,sandstone, claystone	'low hydraulic conductivities' and 0.05 [2] Pump test [47]: 1.65 and 2.6 Pump test [48]: 0.38 Measured: 0.1 to 0.5 [4] Siltstone Measured: 1 to 5 [4] fine quartz
Tertiary – Eocene	Werillup	Sand, gravel, lignite, and carboneous clay	Measured: 6 to 10 [4]
Proterozoic (Basement and regolith)	Albany Fraser Orogen	Gneiss, Granite, Sandy Clay	5.5 'gritty' [2] 0.05 'kaolinite clays' [2] 0.1 to 10 [2] 'good hydraulic conductivity ' [46]

2.3.3 Environmental Fluxes

Rainfall Data - BOM

Precipitation data was obtained from the website of the Bureau of Meteorology (BOM), Australia's official weather bureau. The monthly average rainfall data of two weather stations Esperance (station 9789) and the nearby Myrup (Station 9584) was downloaded. The Myrup precipitation data goes back to October 1901 and is patchy, whereas the first available monthly rainfall observation from Esperance was recorded in July 1969 and is continuous since.

Monthly precipitation data to include in the data set between 1900 and 2019 was selected as follows:

1. The Esperance weather station data is preferred (if available)
2. Myrup data was selected when Esperance data is absent
3. If both were missing, the monthly average from the existing data was included

Average rainfall in Esperance varies between less than 0.5 mm per month in summer months to 5 mm per month in the winter months.

Evaporation - BOM

The Bureau of Meteorology provides downloadable evaporation data for the Esperance Weather Station based on the Penman–Monteith equation, FAO paper 56, Allen [49], from February 2009 to 2019. The Evaporation data covers a period of 10 years. The average evaporation rate for each month was determined from the existing data and was used to fill in the unknown open water evaporation rates in the months prior to February 2009. The open water evaporation rate was used as input of the numerical groundwater flow model.

Annual Precipitation, Evaporation and Long Term Trends

The bar plot in Figure 18 below shows the monthly average between January 2009 and January 2019 of the Penman-Monteith open water evaporation and the precipitation recorded by Esperance Weather Station. This plot indicates that the evaporation exceeds precipitation except for in the winter months July and August. December and January are the driest months with the evaporation rate exceeding the precipitation with a factor of approximately 6½.

The 12-month rolling average precipitation in Myrup was plotted (figure not shown) to investigate the long term trend using a period of 117 years. The trend line did not provide any indication of a change in annual precipitation.

The evaporation rate shows a slight decline however, it cannot be concluded that this trend is statistically significant due to the limited period of data available (10 years).

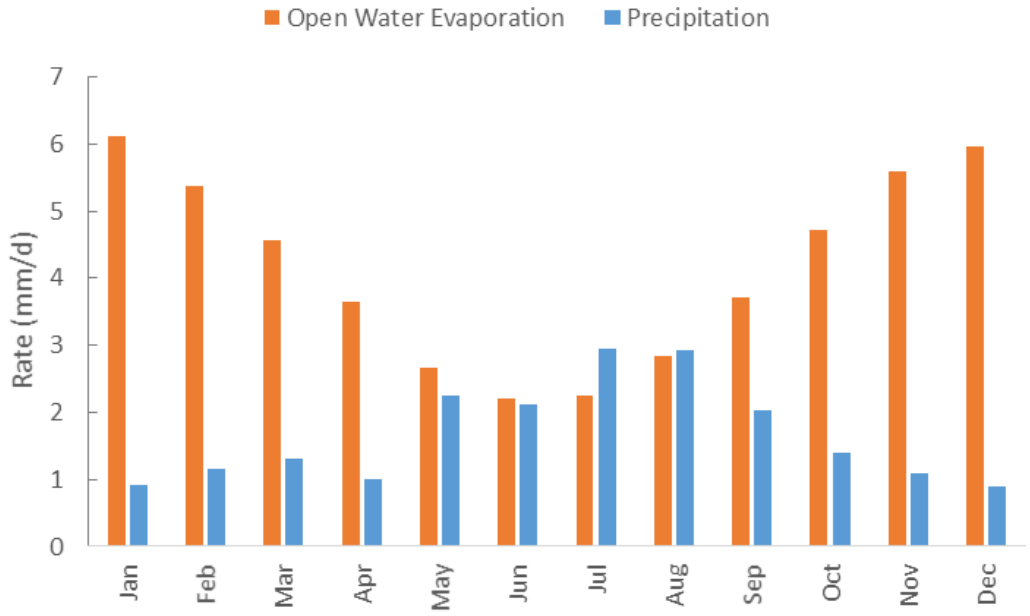

Figure 18: Open Water Evaporation and Precipitation in Esperance

Landuse Maps – Geoscience Australia

A map with land use for the period from January 2014 to December 2015 in a resolution of approximately 250 m x 250 m was obtained from Geoscience Australia [50]. This map was used to estimate evapotranspiration and groundwater recharge from the soil (saturated zone). The map was saved in a resolution in the horizontal plane of 96 m. Figure 19 below shows the land use in Esperance. The data is applied to coefficients that model recharge and evapotranspiration. The magnitude of the coefficient depends on the land use and needs to be calibrated. Four classes have been used in this study; open water, sparse vegetation, dense vegetation and urban areas.

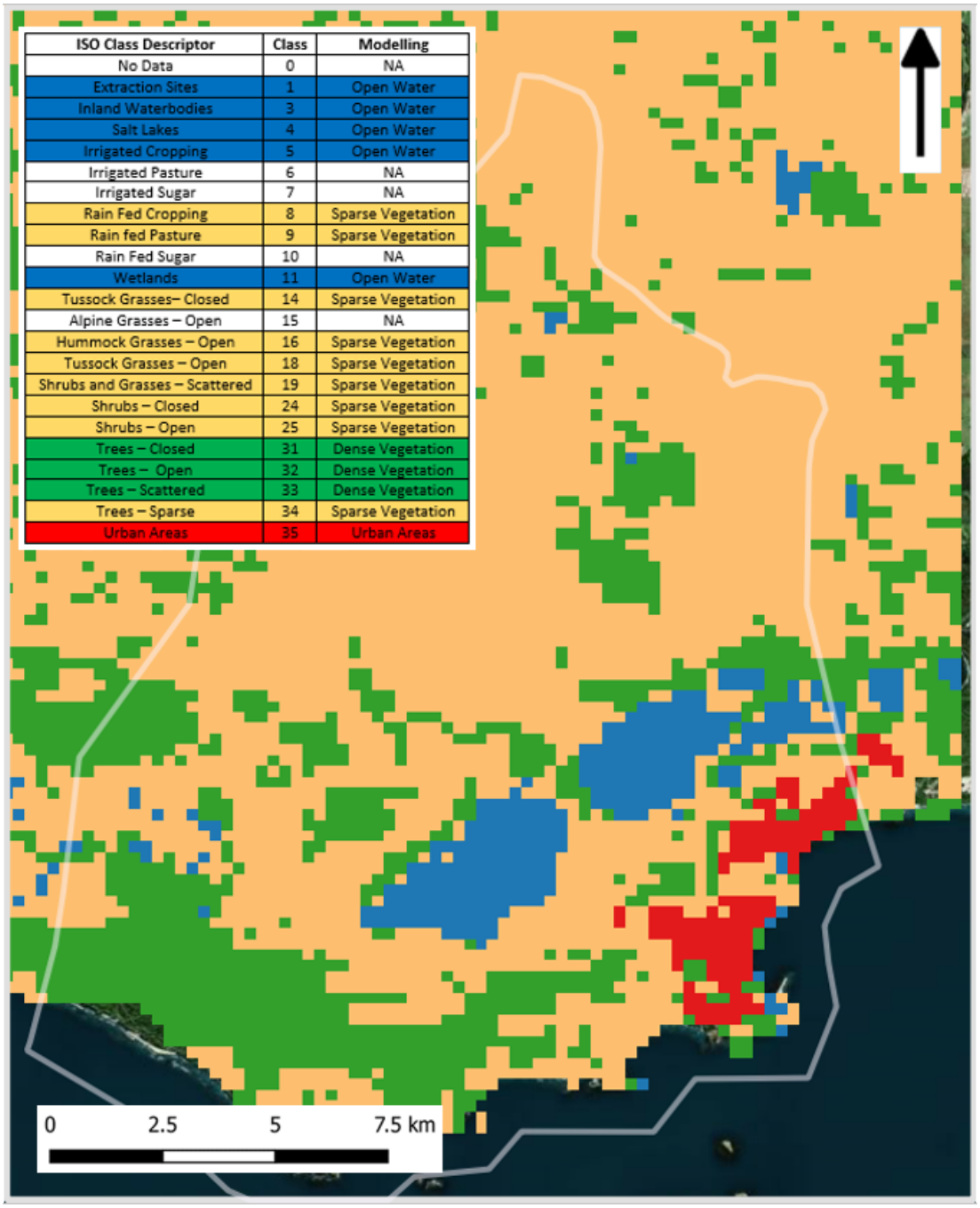

Figure 19: Land use Map Esperance (Blue: Open Water, Orange: Sparse Vegetation, Green: Dense Vegetation, Red: Urban Areas)

a) Bore far-west: Bore (43)

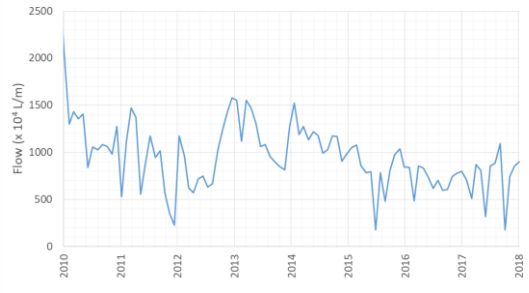

b) Bore mid-west: Bore (32)

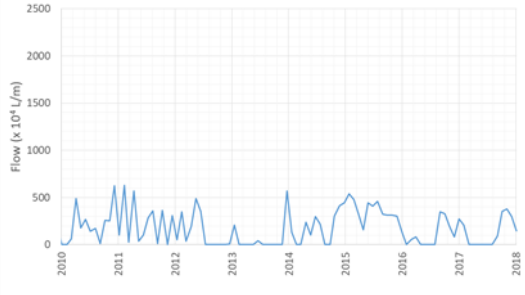

c) Bore mid-east: Bore (28)

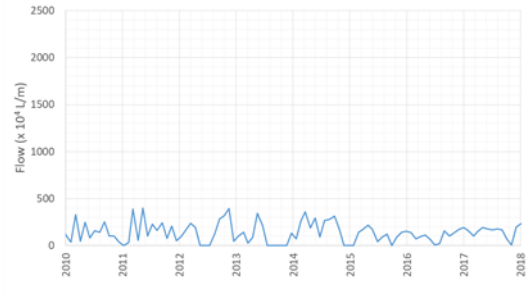

d) bore far-east: Bore (38)

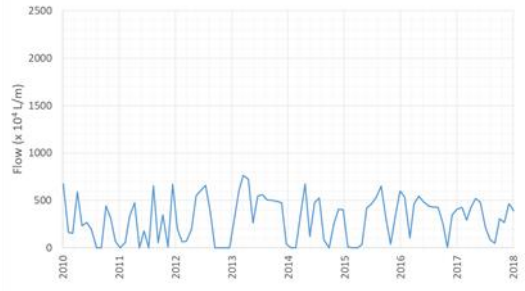

Figure 20: Typical Operation of Groundwater Bores in Esperance 2010 to 2019

2.3.4 Geology and Topography

Bore Lithography - DWER

The Department of water provides publicly available downloadable bore logs. Data from stratigraphic units from bores within the extent of the area shown in Figure 7 were collected. In some cases, the classification was done by experts and was directly used as input for the 3D Kriging algorithm to create a geological model. If the classification was missing, the logs from the drilling crew were compared to the stratigraphic features described by short [2] and to the stratigraphic column from Figure 8 to classify the logs. Most of the bores were not drilled into the basement material whereas approximately half of the bores were deep enough to penetrate weathered bedrock.

AEM data - DWER

Airborne Electromagnetic (AEM) data was obtained in March 2004 by the Department of Conservation and Land Management (CALM) [43] and later in 2013 by DWER and Geoscience Australia, Brodie [51]. For this study, the data obtained in 2013 is used although reference is made to the 2004 survey. It is not known what the source is from the stratigraphic layers that were issued by DWER for this study, the 2004 survey, the 2013 survey or both combined.

AEM involves a low altitude aircraft equipped with a device that emits a pulsed magnetic field. The magnetic field induces an electrical current in the soil which in turn induces a pulsed magnetic field that is detected by the receiver in the aircraft. The strength of the induced magnetic field depends on the conductivity in the soil. From the magnetic signal, a conductivity map of the subsurface is created and the depths of specific soil types can be resolved. The penetration depth is more than 100 m provided that the aircraft flies low enough [52].

Figure 21 below shows the layer reconstruction as collected in the Esperance region during the 2004 or the 2013 survey (or both). The resolution was approximately 190m x 190 m in the horizontal plane. DWER issued the AEM data as point shapefiles which was converted in a GeoTiff format and saved in a 96 m x 96 m resolution in the horizontal plane. Manually deleting spurious points, replacing data at surface water locations and deleting basement outcrops from the quaternary surface layer was required. The elevation relative to AHD of the 5 soil layers is shown in Figure 21. Several locations where the basement material outcrops the land surface are shown in Figure 21 a (marked red). Note that the Esperance harbour at the southeast of the domain was included in the (impermeable) basement layer.

The layers were directly used in the 3D geological model of the subcatchment which resulted in a numerically unstable groundwater flow model and were used to create data points for geostatistical analysis to create the 3D geological model.

Seabed Depth

The seabed elevation was estimated from nautical maps available online and used as input for the 3D Kriging algorithm to create the geological model. The shape of the seabed can be of importance for saltwater intrusion.

a. Basement

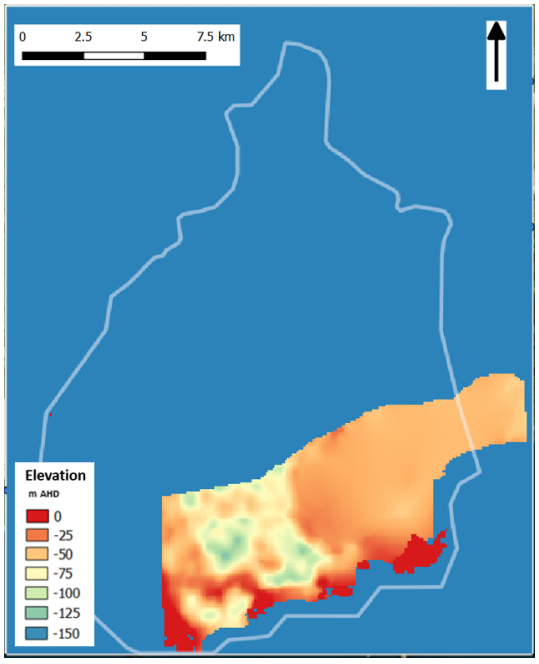

b. Weathered Bedrock

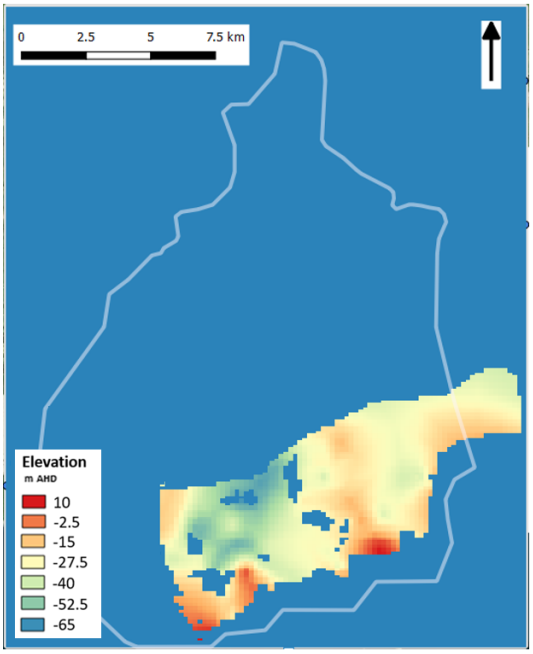

c. Werillup Formation

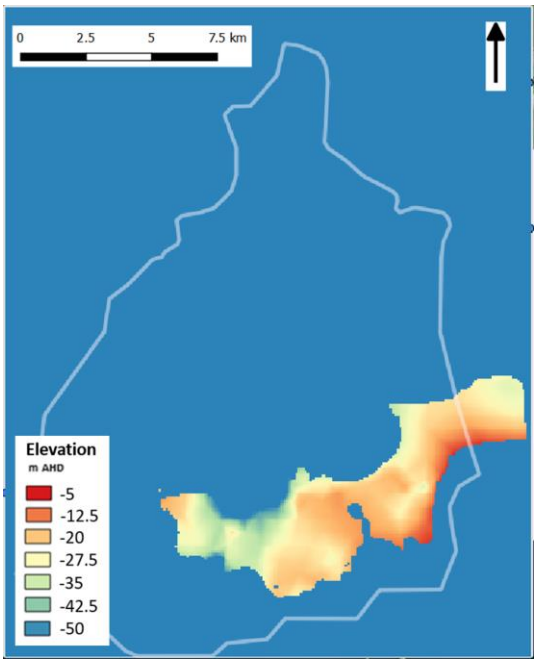

d. Pallinup formation

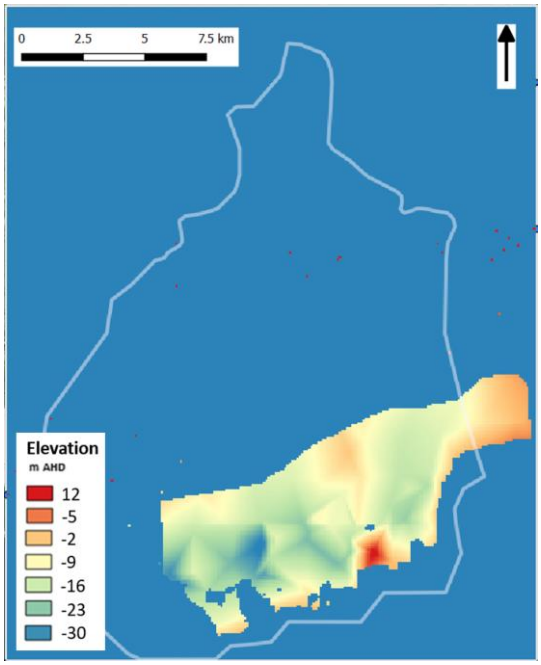

Figure 21: AEM data showing the elevations of the dominant 4 soil formations in Esperance. The top soil (Quaternary) overlays the Pallinup formations and the elevation is shown in Figure 22

LiDAR and Satellite data – DWER and Geoscience Australia

During the AEM surveys (2004 and 2013), Light Detection and Ranging (LiDAR) data of the land surface was collected at a resolution of 50 m x 50 m as issued by DWER for this study. The data was transformed from a point file to a GeoTiff in a 96 m resolution in the horizontal plane. The result is shown in Figure 22 below. The area where LiDAR data was collected is outlined in black.

The area outside the black outline originates from Landsat (1s) with an approximate resolution of 30 m in the horizontal plane Gallant [53] with a standard deviation of elevation change due to smoothing less than 1.5 m in 84% of tiles. The two Digital Elevation Models (DEM) were combined creating a high resolution (LiDAR) area within the black outline and the lower resolution (Landsat) elsewhere.

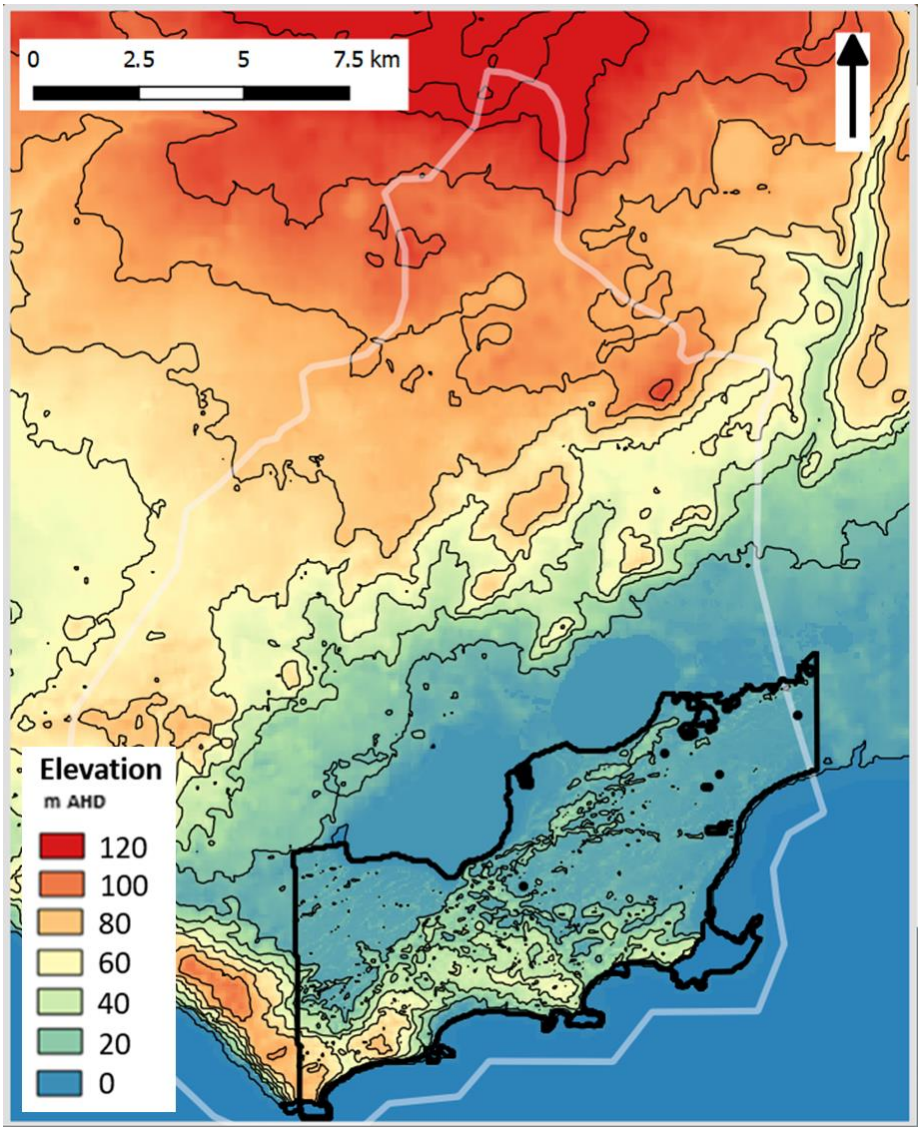

Figure 22: DWER - DEM LiDAR and Landsat in Esperance, 15m contour lines

2.3.5 Groundwater Abstraction

Production Bore SCADA Data - WC

Water Corporation has made production bore data available for this study for a period from 1 January 1993 to 21 June 2019. This includes a total of 42 production bores of which 7 are decommissioned. The production bore GIS coordinates and abstraction rates were used for this as input for the numerical flow model. The bore groundwater level relative to Top of Casing (TOC) was not used due to suspected inaccuracies from incomplete recovery after drawdowns.

Bore production data (SCADA data) is frequently sent to the central database of Water Corporation. Yet only data points are saved in the database when changes of the measured values occur. As such, the SCADA data is stored in irregular time intervals.

The transient groundwater model will run in stress periods of one month. To be able to extract values for each production bore in the correct time interval a Python script was written to interpolate the database values and save the interpolated data in monthly time intervals suitable for groundwater modelling. This way the time-weighted average of the data points was applied. Figure 23 below shows a schematic overview of the measured SCADA data, saved database values and the modelled values that are used as input for the groundwater model.

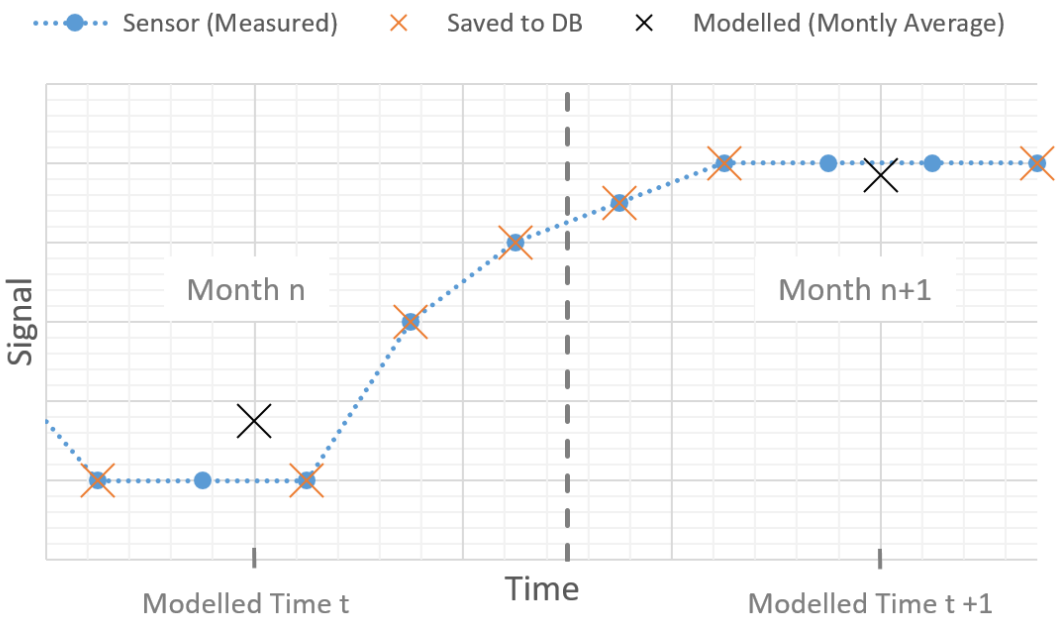

Figure 23: Measured SCADA data, Saved Database Values and Modelled Values

Abstraction Data - WC

The production bores are equipped with groundwater pumps on Variable Speed Drives (VSD) to adjust the flowrate. Analysis of the SCADA data shows that operators frequently, on weekly timescales, adjust the discharge from each production bore. Bores are typically online for periods of several months while on the other hand, the recovery time of bores can be lengthy as shown in Figure 20 b. Bores situated in the west of the borefield generally run continuously without recovery periods and with a greater production rate compared to the rest of the borefield. Abstraction rates are manually decreased or stopped to adjust the flow to the demand or to prevent upconing. It is likely that in many instances operators shut down bores when the electrical conductivity (EC) of the abstracted bore water is found to increase.

2.3.6 Population and Monthly Water Abstraction Rates

Assumed Abstraction from Public Water Borefield

Various sources reporting on the history of Esperance (non-scientific websites) [54], [55], [56] as well as the Australian Bureau of Statistics (ABS) [57] were used to piece together the population size in Esperance from 1900 to 2019. If drinking water abstraction data was absent the population size was used to estimate the groundwater abstraction rate. It is assumed that the population size and the total volume of water abstracted from the aquifer are linearly correlated.

The SCADA production borefield data suggests that 378 L/d water is used per capita in Esperance based on averaging the SCADA data from 1993 to 2019. This rate is applied for the years where extraction data is absent (before 1993).

Figure 24 below presents the population size and the (estimated) water abstraction rates from the drinking water aquifer between 1900 and 2019.

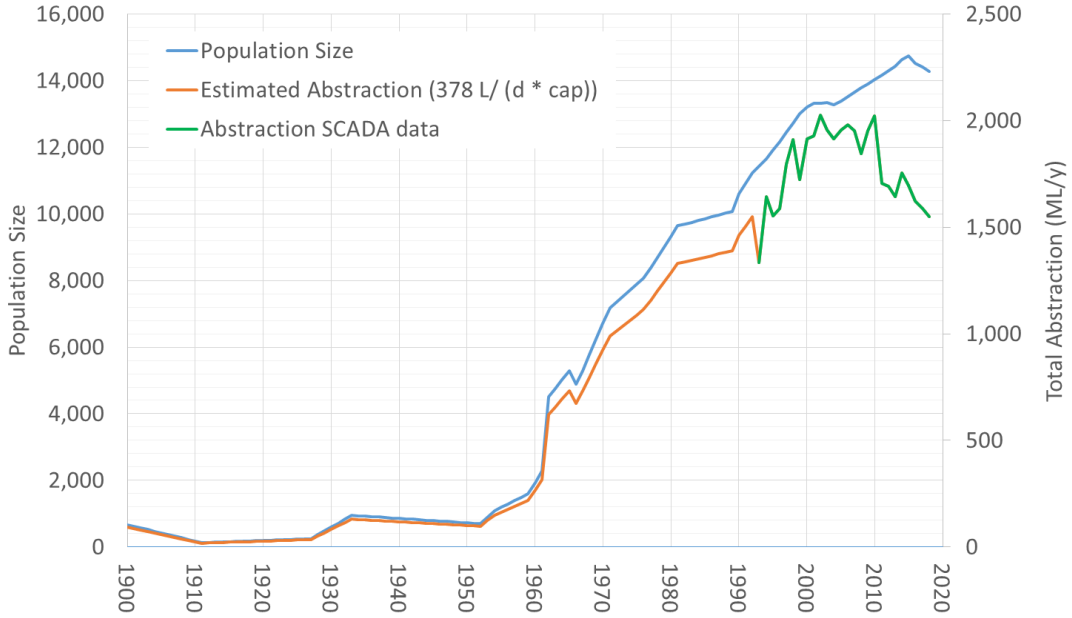

Figure 24: Population Size and Drinking Water Abstraction Rate

The SCADA data for each production bore later than 1993 was used to approximate the abstraction at that location for years prior to 1993. The abstraction rate for each production bore was scaled to population size for each month.

Figure 25 below illustrates how the assumed production prior to 1993 for Bore 01-00 (15) Town Mtr 109402 was calculated. Although the majority of the borefield was installed in the ’80s, it is assumed that groundwater was abstracted from the aquifer in a similar manner as before borefield installation.

Assumed Abstraction from Private Bores

A list of allocated individual annual abstraction volumes for 40 private bores (35 for irrigation and 5 industrial bores) was received from Marimuthu. It was assumed that 80% of the annual allocated volume (462,322 kL/year, refer to Table 2) is effectively abstracted on an annual basis. As such, the allocation volume of each private bore was scaled up so that the total volume matched 80% of the allocated total in the peak year for public water bores in 2014.

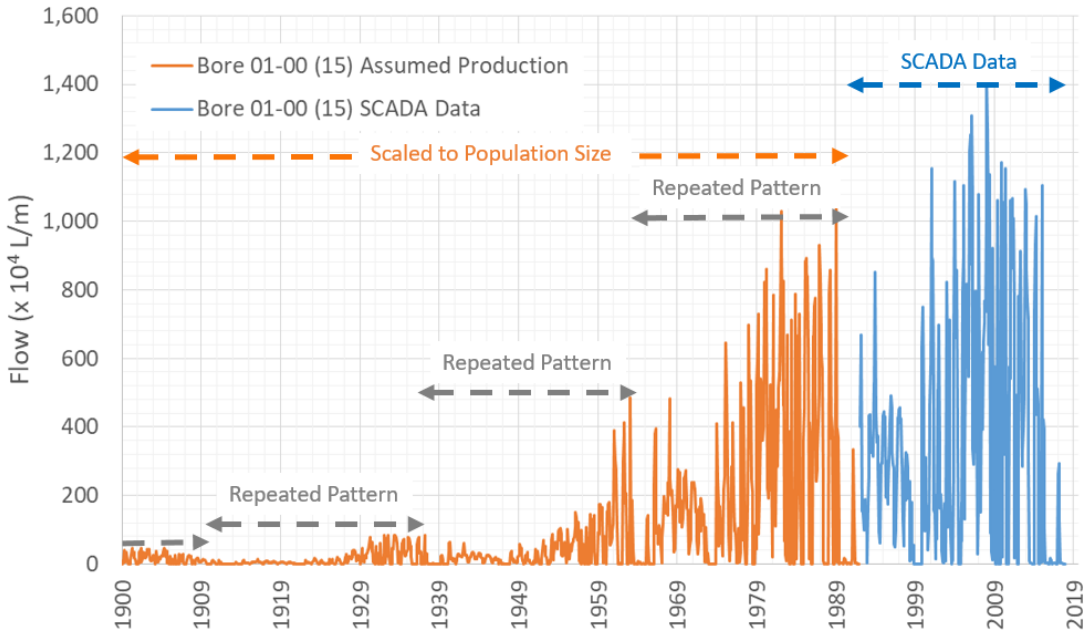

Figure 25: Assumed Abstraction for Production Bore (15). Orange: Prior 1993 (Assumed Rate), Blue: Post 1993 (From SCADA data)

A normalised annual usage pattern was assumed for the 35 of the 40 private bores that are used for irrigation, see Figure 26 below. The population size is shown in Figure 27, and the normalised annual pattern was applied to scale the abstraction rate to estimate the monthly abstraction for each irrigation bore from 1900 to 2019. The population size without a normalised annual pattern was applied as a factor to scale the abstraction rate of the industrial bores.

The monthly abstraction rates of the public water supply bores, the privately-owned bores and the total monthly abstraction is plotted in Figure 28 below.

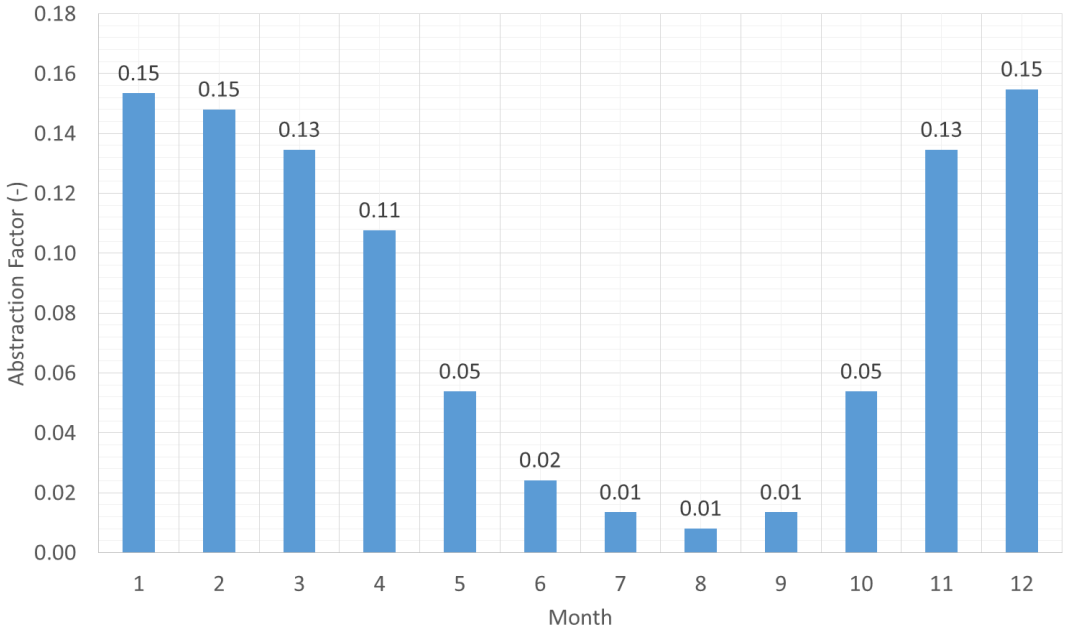

Figure 26: Assumed Normalised Annual Abstraction Pattern for Private Irrigation Bores

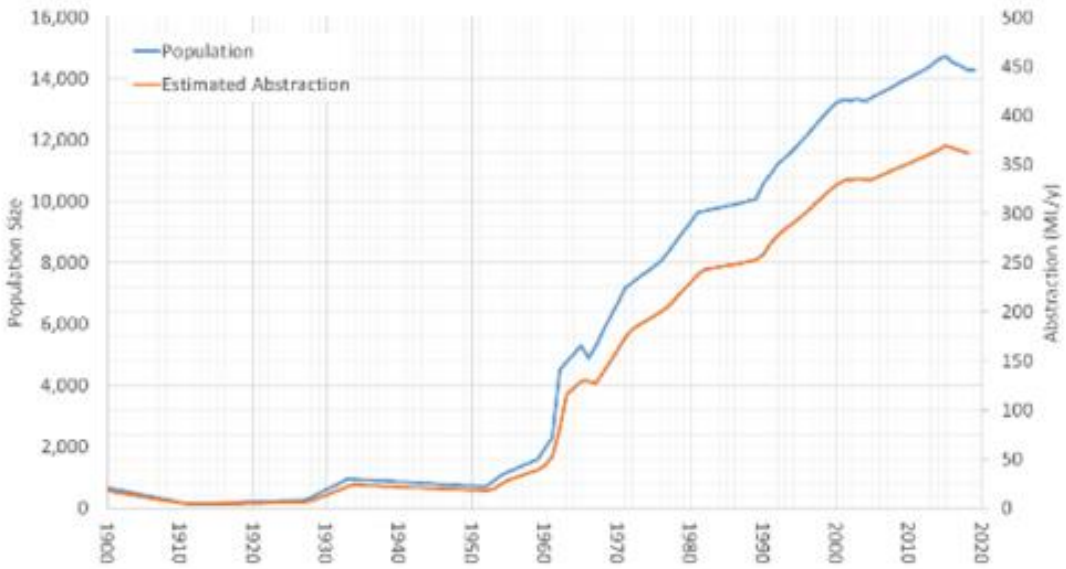

Figure 27: Population Size and Assumed Annual Water Abstraction Rate by Private Bores

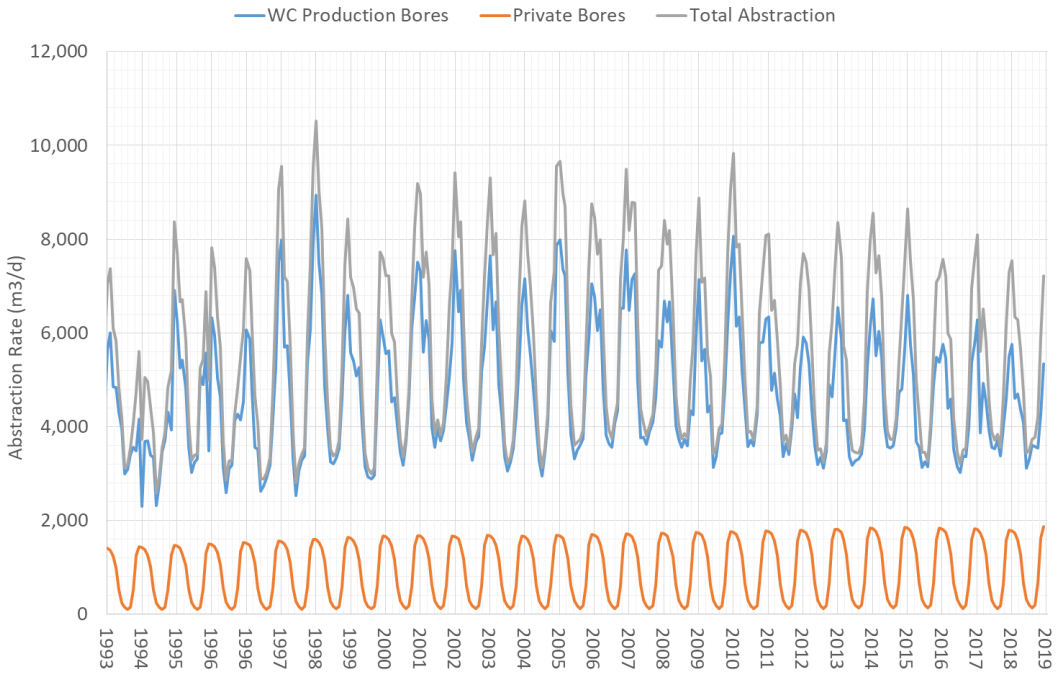

Figure 28: Assumed Monthly Groundwater Abstraction Rates from 1993 to 2019

2.4 DATA USED FOR MODEL EVALUATION

2.4.1 Public Water Aquifer

Groundwater Monitoring in the Subcatchment

Esperance's drinking water is supplied from 33 production bores located within the town boundaries and to the west of the town. These bores draw freshwater from an unconfined aquifer, with depths ranging from around 6 m to 70 m. The borefield also has 15 monitoring bores and five saltwater interfaces monitoring (SWIM) bores Figure 29 below shows the location of the drinking water aquifer with the location of the boreholes.

The Esperance drinking water aquifer has been an area of extensive monitoring due to the saltwater intrusion and salinisation issues, refer Section 2.1. This resulted in groundwater data covering a period of over 30 years. A multitude of boreholes were logged to determine the lithography. Furthermore, 7 SWIM bores measure conductivity along the vertical axis at various locations along the coast. The drinking water company 'Water Corporation' is operating the groundwater production borefield. SCADA production data from each bore (e.g., flow and groundwater head) is stored in a database as well as observations from the SWIM bores and groundwater observation bores.

Water Allocation

The Department of water allocates the volume of water that may be abstracted from the various subareas of the drinking water aquifer, refer to Table 2. As mentioned before, the estimated annual sustainable yield has been based on per cent of total recharge, DWER [3]. Aside from the 33 drinking water production bores that are currently online, another approximate 40 private bores are in use. Five of these are used for the mining industry whereas the others are used to irrigate golf courses, sports fields and parks.

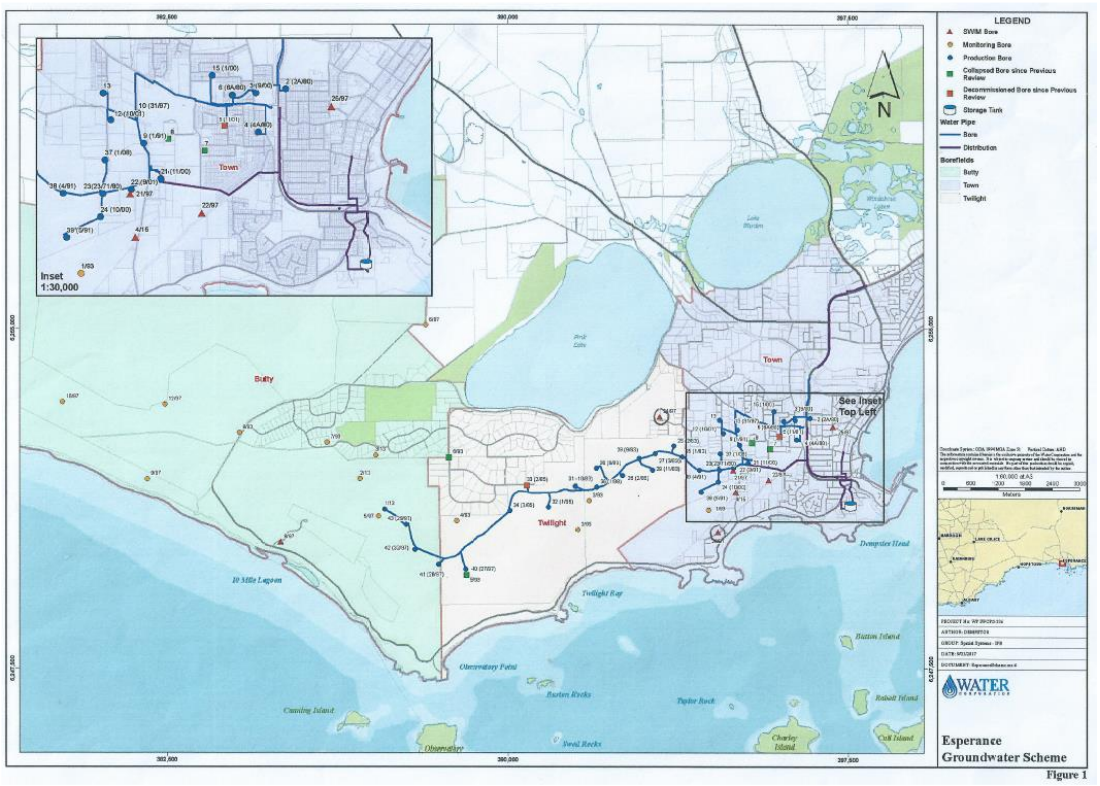

Figure 29 – Location of the drinking water aquifer and of Water Corporation's boreholes. Sub regions, Butty: Light Green, Twilight: Pink, Town: Purple (source: unknown)

Table 2 – Water Availability in the Esperance Groundwater Area (source: DWER [3])

sub-area	Allocation Limit (kL/yr)	Public water supply[1] licensed entitlements (kL/yr)	Other licensed entitlements (kL/yr)	Groundwater Availability (kL/yr)
Town superficial aquifer	1,900,000	1,150,000	394,722*	126,278
Twilight superficial aquifer	700,000	600,000*	67,600	31,200
Butty superficial aquifer	4,200,000	950,000*	0	3,250,000
Warden fractured rock aquifer	1,000,000	N/A	223,570*	776,490* Low yields

*Includes applications under assessment, up-to-date figures are indicated in aquifer allocation report.
All figures are current to 26 May 2006.

Data Collection

Data were collected from several sources but mainly from, Water Corporation, the Department of Water, the Bureau of Meteorology, Geoscience Australia and Marimuthu's database. Table 3 below provides an overview of the data used for this study. The data presented in sections 2.3.3 so Section 2.3.5 below was used for building the hydrogeological model or as input for the groundwater flow model. Section 2.4.1, describing the salinity in the subcatchment, is applied in a more qualitative way.

2.4.2 Water Levels

Groundwater Head Data - WC

Groundwater heads are measured and stored by Water Corporation in several observation bores, in Saltwater Intrusion Monitoring Bores (SWIM) and all production bores. This data is largely shared with the Department of Water. An overview of the groundwater head data is discussed in the subsection below.

Table 3 – Overview of Data Sources

Owner	Type	Number	Comment
DWER	Observation Bores (Includes Production Bores)	100	51 DWER Observations. Only Head Data of Observation Bores Used (26 bores usable for calibration)
DWER	SWIM Bores	7	Saltwater Intrusion and Heads
DWER	Lithography	64	136 Soil Elevations points
Water Corporation	Production Bores	42	Flow Data Used Only (7 decommissioned)
Water Corporation	Observation Bores	40	Head Data
Water Corporation	SWIM Bores	7	Saltwater Intrusion Monitoring
Bureau of meteorology	Precipitation	2 weather stations	Esperance and Myrup
Bureau of meteorology	Evaporation	1 weather station	Esperance (Penman–Monteith)
Geoscience Australia	Map Land DEM	1	1 s Resolution Map
Geoscience Australia	Land Cover map	1	ISO Class Land Use
S. Marimuthu	Lake Water Levels	6	Pink, Warden, Wheatfield, Woody, Windabout, Station
S. Marimuthu	DWER Private Bores Water Allocation and GIS Coordinates	40	Irrigation and mining industry-related bores
DWER	Borehole Salinity data DWER	212	Latest TDS or EC observation (converted to TDS) used
DWER (owner) Geoscience Australia (custodian)	AEM lithographic layers (2004 and/or 2013 survey)	5 soil layers, EC data (2013)	Layers delivered by DWER, EC data downloaded from dataset, Brodie [51]

Groundwater Head Data - DWER

Groundwater heads were collected by the department of water and Water Corporation and both data sets were combined for this study.

The DWER data goes back more than 25 years and is patchy with occasionally a couple of head readings in one bore. The data was used for calibration of the groundwater flow model. Overlapping data points from both sets were merged or used if data points from one of the sets were absent. Head data collected at locations very close to production bores were not used for model calibration.

Lake Water levels - Marimuthu

Lake levels from the five lakes (4 located in the subcatchment) from west to east are shown in Figure 30 below. The level of the three lakes, the central hydrological suite, in the east typically fluctuate between 4 and 5 m AHD. Lake Warden is less predictable and the level in the pink lake (the terminal lake) is between 1.15 and 1.8 m AHD. Note that the bottom level of the pink lake is only slightly below 1.15 m AHD and pooling occurs in some summers.

The level in Lake Warden dropped in the years 2009 and 2015. It is assumed that a decreased inflow was a result of the installation of a gravitational pipeline in May 2008 in Lake Wheatfield which is hydrogeologically connected to the lakes in the subcatchment, Department of Environment and Conservation (DER) [24].

The level almost completely recovered in 2016 which cast doubts on the assumption. Either the pipeline is not functioning properly after 2016 or other hydrogeological reasons are causing the rise in water level. For example, the discharge in Coramup Creek for some periods in 2016 and 2017 is much greater than average, refer Figure 35. Other lakes seem to follow a similar trend as Lake Warden although the drop and recovery are less pronounced. The natural state of lake Warden is lower than the period before 2011, the increase since the mid-‘80s is assumed to be a result of land clearing and intense rainfall, DER [24].

a) Pink Lake (bottom 1.15 m AHD)

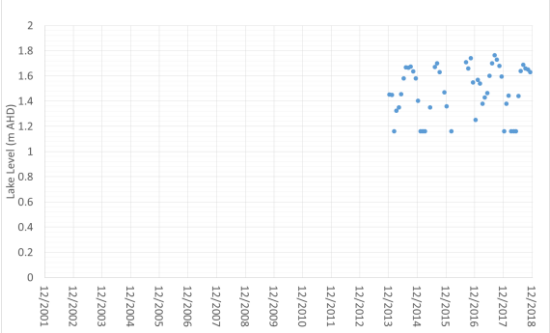

b) Lake Warden

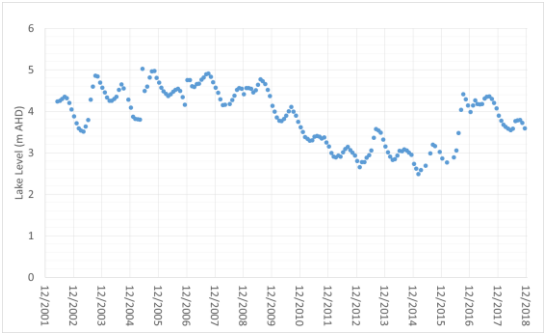

c) Lake Windabout

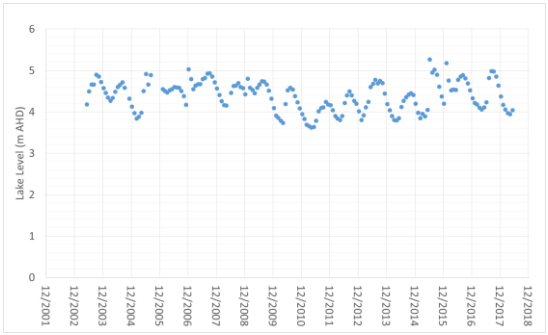

d) Woody Lakes

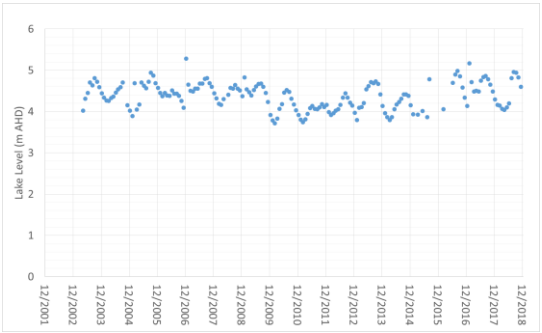

e) Weatfield Lake

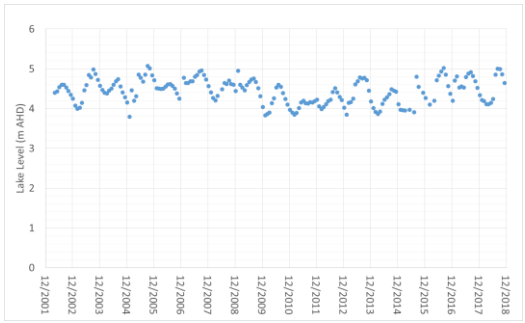

Figure 30: Lake Levels from 2001 to 2019, from west a, to east e

2.4.3 Salinity Data

Overview

Borehole TDS or Electrical Conductivity (EC) data and AEM Electrical Conductivity data from the 2013 survey was used to investigate the salinity distribution in the Esperance region as discussed below as well as a brief methodology applied to visualise the data. As mentioned before, salinity data has not been used for numerical modelling at this stage.

Salinity levels in this study are grouped in line with the classification from the Department of Environment and Conservation [23] as shown in Table 4 below.

Table 4 – Salinity Levels Classification

Classification	**TDS (mg/L)**
Freshwater	≤ 2,000
Hyposaline	> 2,000 – 5,000
Saline	> 5,000 – 35,000
Hypersaline	> 35,000

Groundwater Salinity Distribution - Bore Hole Observations

A total of 212 borehole salinity measurements from DWER water information were processed to produce a salinity distribution map of the region. Salinity was either reported as Total Dissolved Solids (TDS in mg/L) or as Electrical Conductivity (µS/cm). The measurements that were reported in µS/cm were multiplied by 0.65 to obtain an approximate value of the TDS in mg/L. The TDS for each borehole location was plotted in QGIS and points between the bores were interpolated with Inverse Distance Weighing with a distance coefficient of 5 to obtain the most representative results. The newest observation was used if a borehole had multiple observations. Observations from the Saltwater Intrusion Monitoring (SWIM) bores were selected at a depth of approximately 20 m relative to the land surface.

Groundwater Salinity Distribution - AEM Data (2013)

The data set from the 2013 AEM survey by DWER [51] contains Electrical Conductivity measurements with intervals of 5 m in the vertical direction relative to ground level. Flight lines were separated by approximately 300 m or 650 m (in the west of the domain) and EC measurements were taken every ~10m to ~15m along the line. The raw data was plotted in QGIS and each layer was interpolated with Inverse Distance Weighing with a distance coefficient of 3 to obtain a resolution over the domain of 96 m x 96 m x 5 m (same as the groundwater flow model). The results were adjusted relative to m AHD and plotted as a fence diagram in Paraview.

Surface Water Salinity of the Lakes and Coramup Creek

The salinity levels TDS calculated from the EC of the Pink Lake and Lake Warden between 2016 and 2020 have been reported by Lizamore [29]. The relevant plots are shown in Figure 31 and Figure 32 respectively. The hydrology of the coastal lakes and the connections between them are described by the report from DEC [23], using the findings from Marimuthu [4], [26] and [27].

To summarise, Coramup Creek discharges into Lake Wheatfield and connects with Lake Windabout. In wet years Woody Lake can overflow into Windabout Lake, which in even wetter years has overflowed into Lake Warden. Salinity levels in Lake Warden will decrease as a result of mixing with the less saline water from the lakes. No overflow from Lake Warden to Pink Lake is reported.

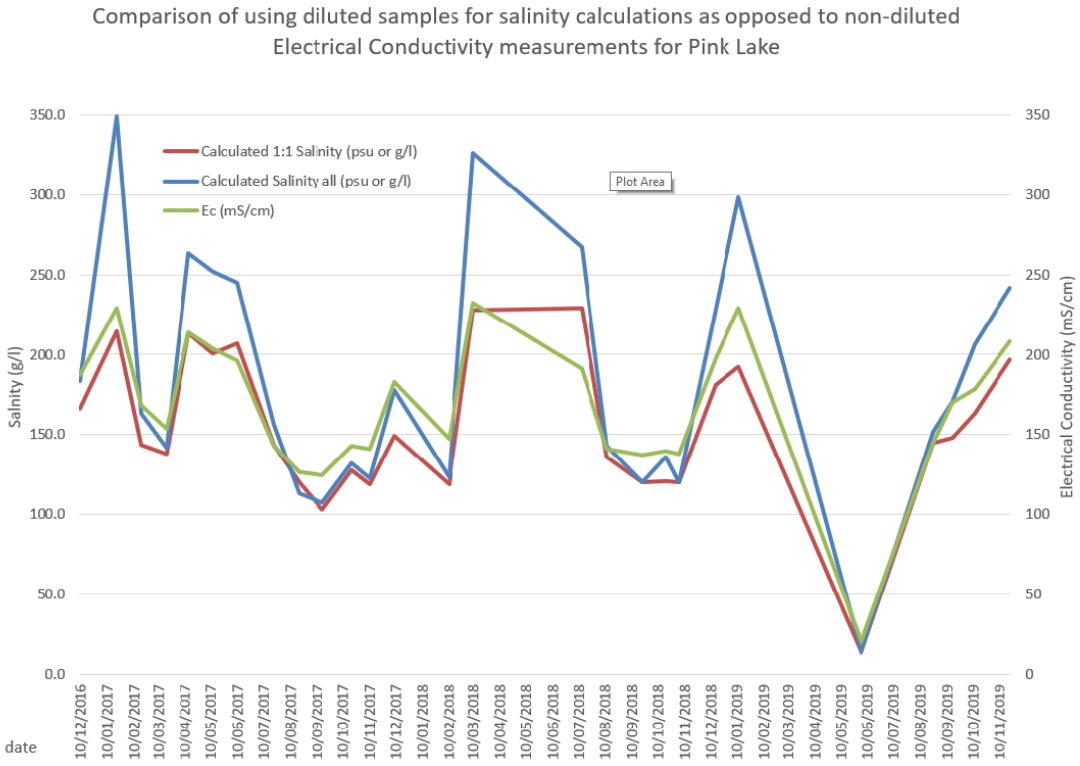

Figure 31: Calculated Salinity (TDS) and Measured Electrical Conductivity (EC) of the Pink Lake Between 2016 and 2020 (source: Lizamore [29]).

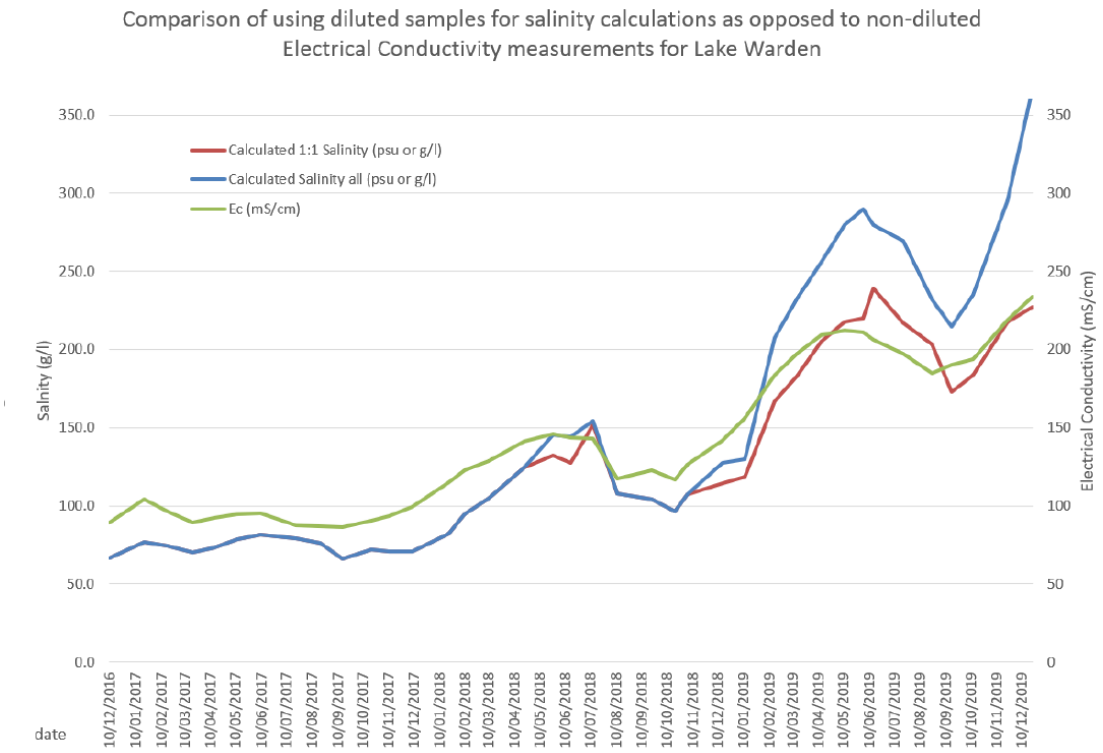

Figure 32: Calculated Salinity (TDS) and Measured Electrical Conductivity (EC) of Lake Warden Between 2016 and 2020 (source: Lizamore [29])

Longer-term salinity measurements of the Lake Warden are reported in DEC [23] and shown in Figure 33 below. The maximum salinity (~225,000 mg/L) is approximately 4 times the average and presumably the result of a sequence of dry years without overland flow from the less saline Windabout Lake. Fewer precipitation events leading to the overflowing of Lake Windabout into Lake Warden may also explain the rising salinity in Lake Warden between 2017 and 2020.

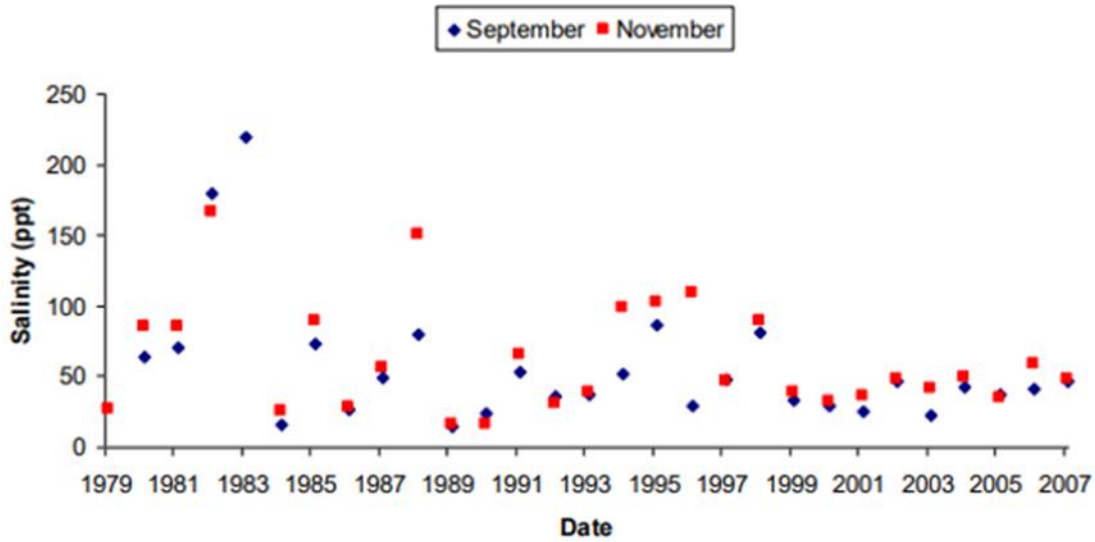

Figure 33: Salinity measurements (TDS) of Lake Warden between 1979 and 2007 (source: DEC [23]). Note: 1 ppt (part per thousand) ≈ 1,000 mg/L

Lake Wheatfield, the Woody Lakes and Lake Windabout (the Central hydrological suite in the Lake Warden System [23]), records one order of magnitude less salinity than Lake Warden and the Pink Lake, see Figure 34 below. The salinities of the lakes in the central hydrological suite are comparable due to the open surface water connection between the lakes. Lake Windabout, most downstream of the three lakes, has a slightly higher salinity due to longer exposure to evaporation.

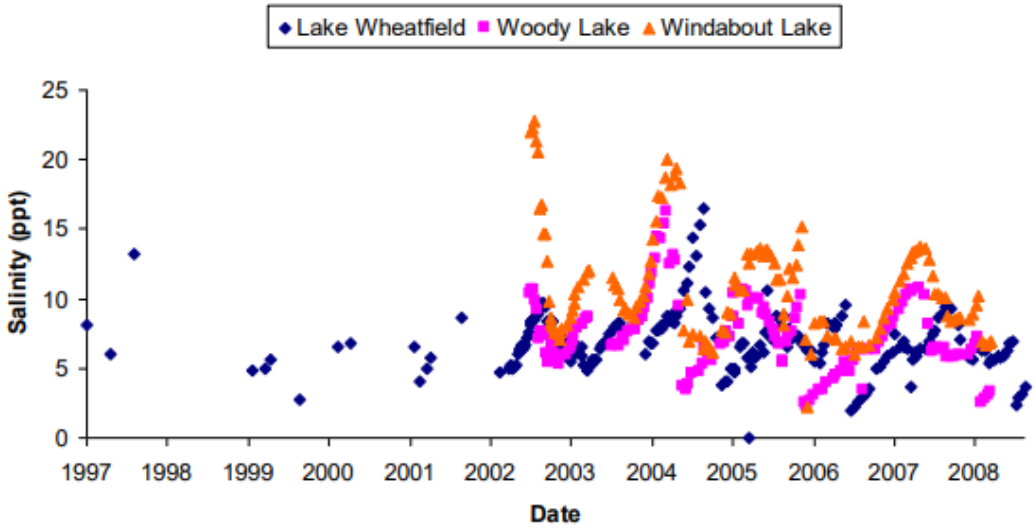

Figure 34: Salinity (TDS) of Lake Wheatfield, Woody Lakes and Lake Windabout between 1997 and 2009 (source: DEC [23]). Note: 1 ppt (part per thousand) ≈ 1,000 mg/L

A time series of EC observations and flow in Coramup Creek was downloaded from the DWER website and is shown in Figure 35 below. It discharges into Lake Wheatfield, the most eastern lake in the central hydrological suite. The Coaramup Creek station (ref: 601008) is located approximately 10 km inland and salinity in the creek cannot be attributed to saltwater intrusion effects. Coramup Creek is fed by groundwater for most of the time and the EC observations suggest that the TDS is commonly between 3,000 mg/L and 6,000 mg/L (factor 0.65 x EC (µS/cm)) with excursions to greater than 15,000 mg/L.

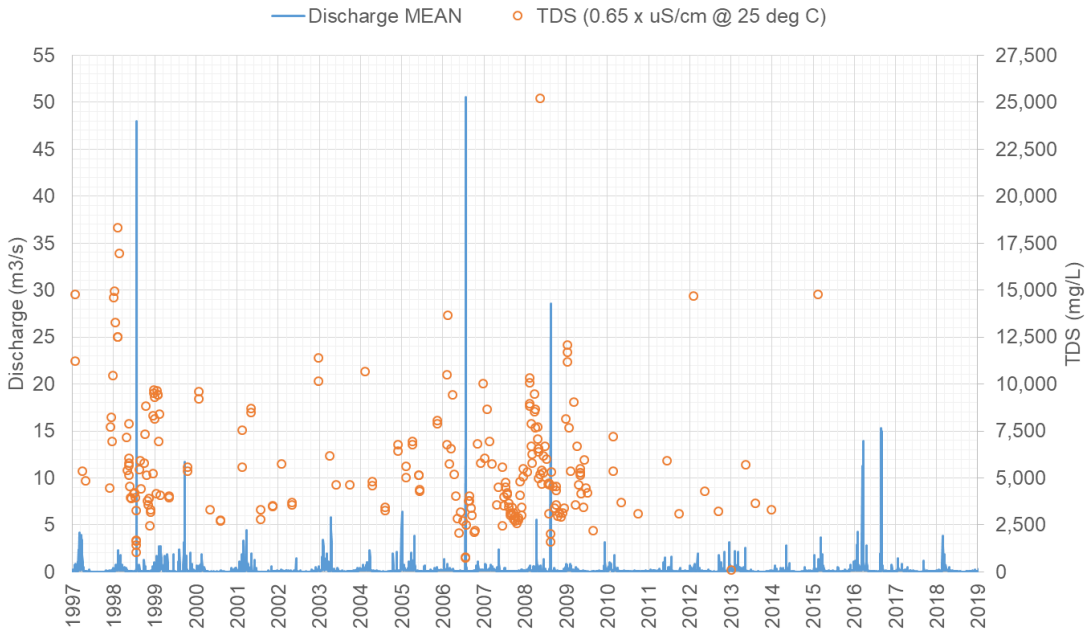

Figure 35: Discharge and EC Observations in Coramup Creek. Calculated from EC Measurements by applying factor 0.65 to µS/cm obtain TDS in mg/L

To summarise, the surface water in ranges from hyposaline to saline in the Coramup creek, saline in the lakes of the central hydrological suite (Weatfield, Woody, Windabout) to hypersaline in the last 2 lakes of the chain (Lake Warden and Pink Lake). The salinity increases in the direction of flow due to evaporation. The well-connected lakes in the east of the subcatchment central hydrological suite are saline, while hypersalinity is prevalent in the terminal Pink Lake and Lake Warden.

Chapter 3: Methodology and Model Setup

3.1 INTRODUCTION

This chapter explains the methodology that was applied to develop, run and calibrate the model. At first, the creation of the 3D model grid is explained by using a combination of geological inputs from AEM data, bore log data, LiDAR and DEM and geostatistical techniques.

Land use, model boundaries and geological data in the form of maps were compiled, processed, and discretised to the desired resolution (96m x 96m) by QGIS. Once digitised the maps were saved in the GeoTiff format which could then be loaded as python arrays. The python arrays formed the basis for creating the geological model and the input files for MODFLOW.

The lakes were created in a way that is compatible with SEAWAT. Note that the LAK package that is normally used for modelling a lake stage is not compatible with SEAWAT version 4, USGS [59]. At lake locations, a layer of cells underneath and surrounding the lakes is introduced with a lower hydraulic conductivity to represent the lakebed. This way, the lake stage and salt concentration (to be included in the next model upgrade) is a result of the hydrogeology and not a boundary condition.

The selection of the subcatchment boundaries is presented based on hydrological features.

The finite-difference groundwater model software MODFLOW-NWT is discussed including the packages that are used to model the fluxes and boundaries. Finally, automatic calibration and parameter sensitivity analysis with PEST++ is discussed.

As explained earlier, the goal of the modelling is to investigate:

- The hydrology and water balance of the aquifer
- Indication of areas at risk of saltwater intrusion
- Locating the most sustainable area for groundwater abstraction
- Preferred location of future borefield upgrades
- Increase understanding around the interaction of the hypersaline lakes, the superficial groundwater aquifer and borefield.

3.2 GRIDDED RECTILINEAR APPROACH

The Hydrogeological model was developed using a gridded or rectilinear approach. This means that each model cell has the same vertical and horizontal dimensions within the entire domain as opposed to the 'deformed grid' where model cells (typically the elevation) follow the geological layering. The advantages and disadvantages of both approaches are provided in Section 'Conceptual Aspects of Vertical Discretization' of the USGS report presenting MODFLOW-2005, Harbough [61]. In addition, a rectilinear superposition has the following advantages, Harte [62]:

- Suitable for steep slopes in the landscape
- More suitable to model Anisotropy
- More suitable for modelling significant contrasts in horizontal hydraulic conductivity

Finally,

- Better suitable for SEAWAT in terms of numerical stability

Considering the above, the rectilinear approach was found favourable for this research.

3.3 GEOLOGICAL MODEL

The 3D geological model was created from the bore logs from the DWER, from AEM data (refer to Figure 21) and from combining LiDAR and satellite DEM (Figure 22).

3.3.1 3D Kriging Introduction

Kriging is a statistical technique commonly used in geoscience to interpolate data at a location where the true value is unknown. There are many types of kriging (simple,

ordinary, universal, etc.) of which the universal Kriging is applied here to interpolate the geological model from borehole information and the Digital Elevation Map (DEM).

Equation 1 below forms the basis of all types of kriging.

$$Z^*(\boldsymbol{u}) - m(\boldsymbol{u}) = \sum_{\alpha=1}^{n(u)} \lambda_\alpha [Z(\boldsymbol{u_\alpha}) - m(\boldsymbol{u}_\alpha)] \qquad \text{Equation 1}$$

Where,

- Z*(**u**) is the basic linear regression estimator (at location u)
- **u** and $\mathbf{u}_\alpha$ are the location vectors for estimation point and one of the neighbouring data points, indexed by alpha
- n(**u**) number of data points in the local neighbourhood used for estimation of Z*
- m(**u**), m($\mathbf{u}_\alpha$) are the expected values (means) of Z(**u**) and Z($\mathbf{u}_\alpha$)
- λ_α (**u**) kriging weight assigned to datum z($\mathbf{u}_\alpha$) for estimation location u; the same datum will receive different weight for different estimation location

The problem is to determine the weights λ_α for each location in the domain that minimises the variance of the estimator Z* at that location. For simple Kriging the mean is assumed constant and known over the entire domain. In Ordinary Kriging, the mean is assumed an unknown constant (a global mean) in the local neighbourhood of each estimation value Z*(**u**) so that the sum of the weights is constrained to be 1.0. In Universal Kriging (equivalent to regression Kriging, Hengl [63]) the mean is fitted to a trend (drift).

Goovaerts [64] provides a methodology of solving the equations for the three different Kriging methodologies. Detailed information on Kriging can also be found in Hengl [63]. Note that the algorithm applied in 3D Kriging is essentially the same as in 2D Kriging yet with one more dimension in the location vectors **u**.

3.3.2 3D Kriging Algorithm Selection

Hengl [63] in Section 2.2.2 outlines a decision tree that can be applied to select the most suitable interpolation technique. In the domain in Esperance, the variable Z is correlated with environmental factors while the residuals are spatial auto-correlated

(areas close together have similar values characterised by a small nugget, i.e., the intersection with the y axis, in the variograms). As such, regression Kriging is the most suitable type of Kriging for solving the geology in Esperance.

A geological model was created by applying a 3D Universal Kriging statistical algorithm with the Python-based PyKrige code [65]. Ideally, all AEM data points would be applied in their entirety to solve a 3D geological model by Kriging statistics. However, this is not possible due to the computationally heavy algorithm and a large number of data points from the AEM data set.

Instead, 'virtual bores' were applied along the boundaries of the AEM data and at randomly selected locations along the blue shaded area shown in Figure 7. These non-existing bores use the AEM data points to define the depth of the geological layers at 151 locations. 1235 surface elevations from the top layer (all quaternary lithography) were included as input to the Kriging algorithm. Including more data points would cause the available working memory of 64 GB RAM to overflow.

The geostatistically obtained model covering the entire extent of the domain was (initially) combined with a rendered model from the superior AEM data. Furthermore, the 'virtual bores' around the outline of the AEM data section make the transition from the rendered AEM part to the Kriging part of the model as smooth as possible. Table 5 below presents the algorithm and parameter settings applied to obtain the 'best' model.

Due to the spatial variability of the terrain and the lithography, and the few data points (relative to the variability), the best model was obtained by trial and error. Variograms were created from the existing borehole and 'virtual' borehole data to select reasonable estimates of the slope and the nugget using a linear variogram model. Eventually, the 'best' model was selected based on user judgement by visually comparing the output of the model produced by Kriging to the geological layering produced by the AEM survey.

Table 5 – Selected PyKrige [64] Parameters and Algorithm

Input	Total: 2000 points 1235 surface points (Quaternary) 151 'Virtual bores' (AEM data) 46 Actual bores (bore logs)
Algorithm	Universal 3D Kriging
Variogram Model	Linear
Variogram Parameters	Slope: 0.003 Nugget: 0.01 m
Drift Terms	Regional Linear
Number of Rows	275 (~ 9.78 m)
Number of Columns	223 (~ 96.2m)
Number of layers	30 (~ 9.78 m)

The geological model was used to create the hydrogeological model that forms the input for MODFLOW. Hydrogeological features such as lakes, ocean, and cells representing water levels (Dirichlet boundary or first type boundary) or flows (Neumann Boundary, second type boundary) were included refer 3.4.3.

Subsections 3.3.3 and 4.3 below explain how the part of the domain that was unravelled by AEM was merged in its entirety in the model created by Kriging. However, the merged model resulted in convergence errors with MODFLOW. Resolving this issue is suggested as future work.

3.3.3 AEM Data Rendering

The AEM data was received as point shapefiles that represented the elevation of the top of each lithography type. After data cleaning and digitising to 275 rows x 223 columns with QGIS, the layers were transformed to create a 3-Dimensional model. A Python script was written to insert the correct number of cells according to the rectilinear approach between the layers in the domain where the AEM data exists (on top of basement cells). The algorithm accounted for the fact the particular soil types are missing at some locations.

After the rendering step the, 3D rendered AEM model was merged into the model derived with Kriging at locations where AEM data existed.

3.3.4 Construction and Manual Adjustments

The model derived with Kriging was overlaid with a layer of quaternary material with a thickness of at least one cell representing the surface elevation. Gaps between the Kriging model and the overlaid quaternary cells, if present, were filled with quaternary cells. Cells were deleted from the model that was derived with Kriging if the elevation was too high.

Finally, layers were manually adjusted to include areas with marine sand, removal of isolated cells, inserting no flow boundaries and clearing the connection to the ocean where required.

3.4 HYDROGEOLOGICAL MODEL

3.4.1 Introduction

Several hydrogeological features are added to the geological model. The transformation of the geological model to a hydrogeological model suitable for MODFLOW involved adding lakes with lakebed and water cells, ocean water cells modelled as fixed heads, Coramup groundwater cells as fluctuating heads, cells representing regional groundwater inflow (‘regional inflow’) and production bores. Most of these features do not require a detailed explanation. However, special attention should be paid to the construction of the lakes in the hydrological model.

3.4.2 Lakes

The method used to include lakes is shown in Figure 36 below. Lakebed cells are included and have a larger hydraulic resistance than aquifer cells. This is to regulate the in- and outflow of groundwater in the lake. The magnitude of the hydraulic conductivity was calibrated with PEST++. The lake cells have a very high hydraulic conductivity and an effective storage coefficient of (nearly) 1 to approximate the behaviour of water.

It was mentioned before that MODFLOW’s Lake Package (LAK) is not supported by SEAWAT [59] and that the method to create lakes described here is a suitable workaround. To correctly model density-dependent flow, the lakes should not be modelled as a forcing. Rather, the lake water levels are a result of the hydraulic behaviour of the entire system. One of the main driving forces of the formation of saline or hypersaline lakes, such as Lake Warden and the Pink Lake, is evaporation followed by a density-driven episodic convection. This mechanism is numerically

modelled in detail by Nield [60]. It is suggested that the future upgrade of the flow model, which includes density-dependent flow is set up in a comparable way.

The lakes have been modelled using a Python script by adjusting the top and bottom elevation of the cells matching the lake bottom and water levels. Cells on the lake bed and lakeshore were assigned a separate hydraulic conductivity to model a semi-confined 'leaky' layer see Figure 36. Cells with lower conductance are also applied around the lake water cells so that flow in or out of the lake must go through a 'leaky' layer cells.

a) Geological Model as Produced by PyKrige [64]

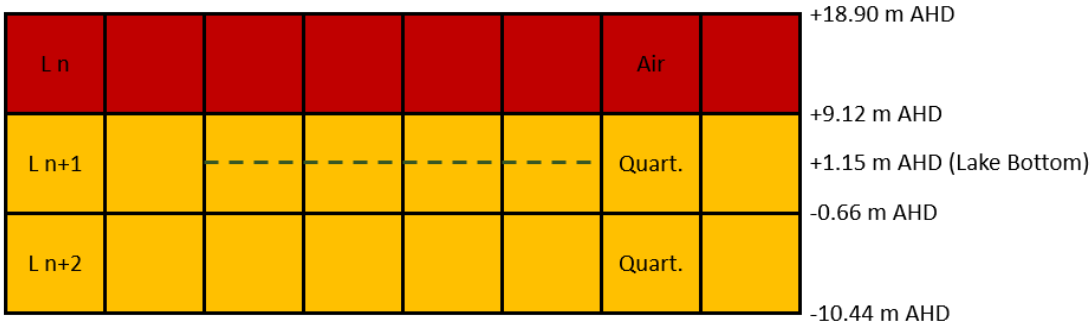

b) Hydrogeological Model after Including Lake Cells

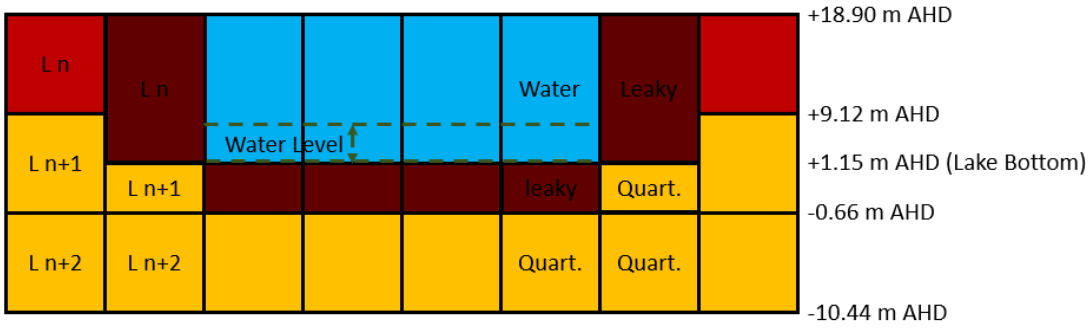

Figure 36: Representation of the Inclusion of Lakes in the Hydrogeological Model

3.4.3 Topological Features

Figure 37 below shows topological features that are implemented as boundaries in the hydrogeological model. A groundwater flow is expected to enter the subcatchment in the north as is explained earlier in Section 2.2.2. The small natural lakes inside the north of the subcatchment indeed point to the existence of a general groundwater flow field in the north to south direction. Some of these lakes are filled throughout the year, see Figure 38 indicating that groundwater must contribute to the lake water. Perennial

lakes can otherwise not exist in the semiarid environment of Esperance. Section 3.5.2 provides more details on the modelling of the individual boundaries.

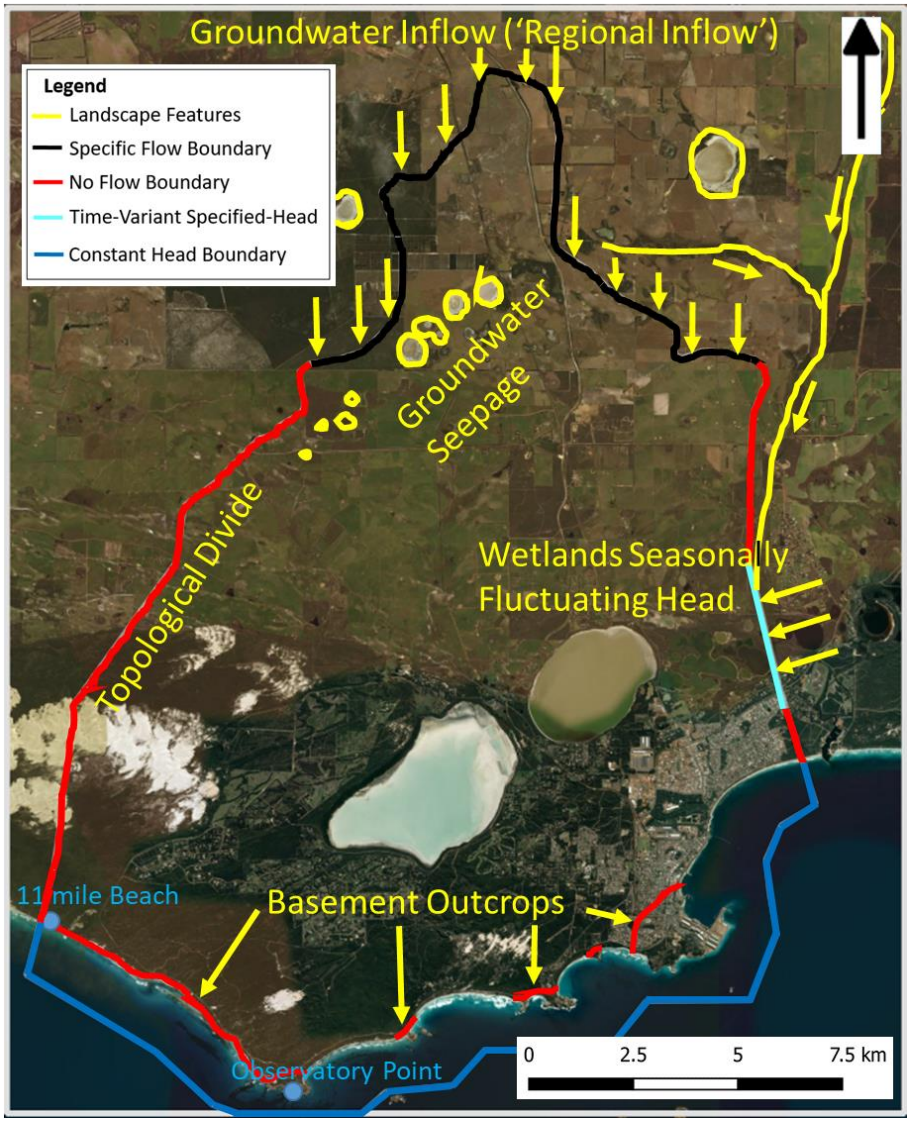

Figure 37: Landscape Features Used to Determine Boundary Conditions. The Resulting Model Boundaries Outlining the Subcatchment are Shown

Lake Benje Benjemup is a similar perennial lake that is researched in more detail and is located at 6 km to the northeast from the lakes shown in Figure 38 and its hydrological features are described by Lizamore [29]. This lake is situated just outside of the Esperance subcatchment and is visible on the image in Figure 37. It is mostly fed by fresh to brackish groundwater containing mainly sodium chlorides. It is expected that groundwater through flow with similar or less saline properties enters the Esperance subcatchment in the north.

These observations are useful for calibration of the flow model and also suggests that saline groundwater flow is a source of salinity in the borefield of the Esperance aquifer, the Pink Lake and Lake Warden.

a) July 2005 (Winter: All Lakes Filled)

b) January 2012 (Summer: Only Northern Lake Filled)

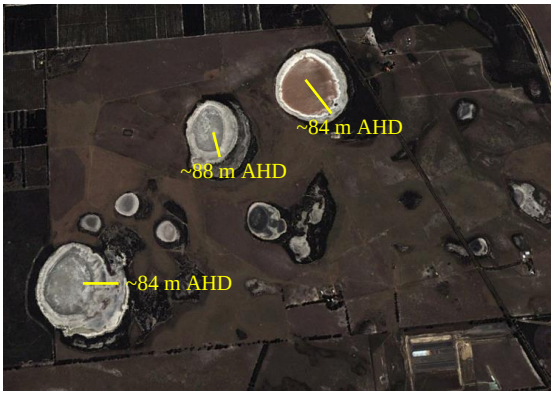

c) November 2016 (Early Summer: All Lakes Filled)

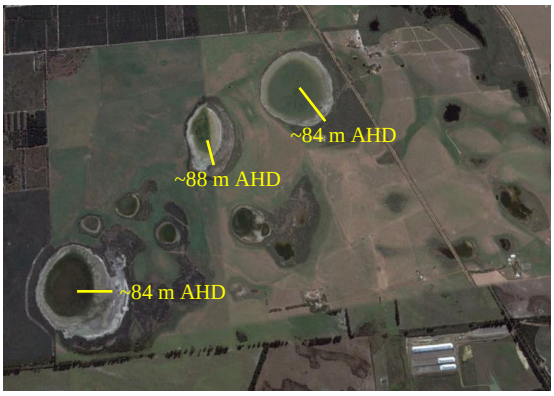

d) December 2018 (Summer: All Lakes Filled)

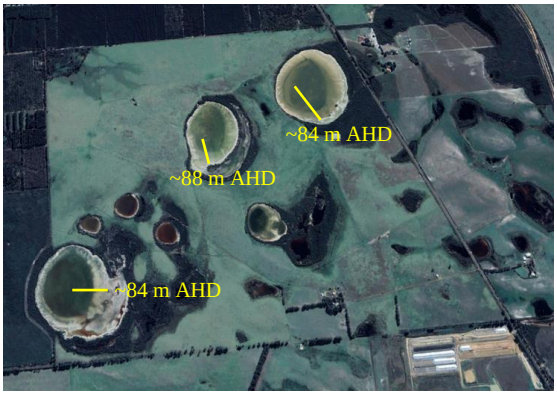

Figure 38: Historical Aerial Imaginary of the Small Lakes North in the Subcatchment. These Lakes Arise through Groundwater Seepage. Perennial Lakes, Like the Lake Most Northeast, Indicate Good Groundwater Connection

The seasonally fluctuating groundwater level of the wetlands near the lakes on the east of the domain (the Woody Lakes) are used as a forcing. Basement outcrops, where the elevation of the basement exceeds the ocean water level, are modelled as no-flow boundaries. The ocean itself is considered a constant head, tidal fluctuations are neglected.

3.5 MODFLOW

3.5.1 Software

MODFLOW is 3D numerical modelling software based on the finite difference method. In the case of groundwater, flows through cell faces and heads within cells are calculated. A multitude of cells is connected to approximate the shape of a (realistic) domain. Each cell is provided with hydraulic conductivity.

A 3-dimensional flow of groundwater through porous media is given by the partial-differential equation, Harbough [61]:

$$\frac{\delta}{\delta x}\left(K_{xx}\frac{\delta h}{\delta x}\right)+\frac{\delta}{\delta y}\left(K_{yy}\frac{\delta h}{\delta y}\right)+\frac{\delta}{\delta z}\left(K_{zz}\frac{\delta h}{\delta z}\right)+W=S_s\frac{\delta h}{\delta t} \qquad \text{Equation 2}$$

Were,

- K_{xx}, K_{yy}, K_{zz} (L/T) are the values of hydraulic conductivity along the x, y, z coordinate axes,
- h (L) is the potentiometric head,
- W (T^{-1}) is the volumetric flux per unit volume representing sources and sinks of water, with W < 0 for flow out of the groundwater system and W > 0 for flow into the system, S_S (L^{-1}) is the specific storage of the porous material and,
- t (T) is the time.

Equation 2 is describing an infinitesimal portion of porous material for an infinitesimal small duration of time. The finite difference method applies a discretised version of Equation 2 to cells with a finite volume and with finite time steps.

For unconfined flow, relevant for this study, the specific storage S_S is substituted by the specific yield, S_Y, using the relationship $S_S = S_Y / H$ and assuming the Dupuit-Forchheimer approximation. The specific yield is related to the effective porosity, a soil property representing the pores space that is available for fluid flow.

3.5.2 Model Boundaries

Several features in the landscape in Esperance point to the application of specific model boundaries. These features are outlined in Figure 37 above.

Constant Head Boundaries

Constant head cells in the discretised model are applied at locations that represent the ocean in the south.

Specific Flow Boundary

The perennial lake in the north of the subcatchment and the nearby Benje Benjenup Lake suggest a good connection with the groundwater table. Groundwater inflow in the subcatchment from the northeast has been suggested in earlier studies, refer Section 2.2.2 and is included in the model.

Time-Variant Specified-Head Package

A line of model cells with time-variant heads represent the seasonal groundwater fluctuations observed in the central hydrological suite at the eastern border of the domain which includes the Woody Lakes (refer Figure 37).

No Flow Boundaries

The subcatchment delineation is based on the topographic elevations of the ground level, refer Section 2.3.1. The delineation boundary is assumed to be a no-flow boundary. It is hypothesised that the contribution of precipitation and evapotranspiration fluxes within the subcatchment boundaries can be modelled with the delineation. However, the slope of the basement is not known and therefore the location of the in- and outflow of groundwater in deeper layers cannot be determined without more accurate hydrogeological data.

Basement outcrops in the south of the subcatchment act as no-flow barriers between the ocean and the groundwater. The existence of the relatively long no-flow boundary in the southwest of the model domain (between Observatory Point and 11 Mile Beach) is assumed due to a gap in the local geological data. It must be noted that Marimuthu [4], [26] and [27] did not apply a no-flow boundary in this region and instead modelled an open connection to the ocean.

Whether basement outcrops exist along the coastline can have far-reaching consequences for drinking water abstraction and saltwater intrusion. Saltwater intrusion can be haltered by no-flow boundaries as was also shown by Luyun [9].

For the following reasons the basement outcropping above the saltwater level between Observatory Point and 11 Mile Beach is likely:

- The elevation of the basement at the most western part of the AEM data is greater than saltwater level ~ 40 m.
- The elevation of the land surface is high (between ~50 m and ~100 m) which often relates to a high basement elevation in the Esperance subcatchment.
- Basement outcrops at ~0 m AHD are visible in the ocean between Observatory Beach and 11 Mile Beach as well as granite boulders.
- The flows in the southwest of the FEFLOW model does not agree with the findings of Abbott [28]. It is postulated here that this may be a result of Marimuthu's assumption [4] of direct groundwater access to the ocean.

Other considerations

The Pallinup layer underlying the Quarterly top layer has a relatively large vertical resistance due to the presence of a silt layer and various other poorly conducting clays in the top of the Werrilup layer as shown in Figure 8. Artesian pressure is observed in some locations in the field according to Marimuthu [4]. The vertical resistance within the Pallinup is modelled as a separate parameter that is calibrated.

It is assumed that groundwater inflow in the subcatchment exists in the north. The inflow of groundwater is simulated in the model by the application of cells producing flow in the north of the subcatchment.

3.5.3 Packages

MODFLOW is modular in structure and hence packages that describe flows additional to the basic cell to cell flows can be added. In this study, the following packages have been applied. Variable-density and transport modelling was not included.

MODFLOW-NWT

To avoid issues with drying and wetting and non-linearities MODFLOW Newton (NWT) was used, Niswonger [66]. MODFLOW-NWT is a standalone version of MODFLOW 2005 but has the same functionalities. MODFLOW-NWT must however be used in conjunction with the Upstream Weighing Package (UPW) which is the equivalent to the Layer Property Flow (LPF) package of MODFLOW 2005.

The UPW package uses an alternative approach to calculate the heads and the resulting conductance between adjacent cells. Dry cells remain active with MODFLOW-NWT unlike MODFLOW 2005. Furthermore, the horizontal conductance and storage

function is smoothed in the UPW package. The Jacobian Matrix of partial derivatives to the finite-difference approximations of the groundwater-flow equation is solved by the NWT solver.

MODFLOW-NWT is not compatible with SEAWAT to model variable-density Flow and Dispersion. Since December 2020 MF6, the newest core version of MODFLOW can be used in conjunction with variable-density flow and dispersion in conjunction with an inbuilt newton solver. Alternatively, the Sparse Matrix Solver (SMS) Package from MODFLOW-USG can solve the flow matrix produced by the LPF package and can deal with cell drying and rewetting problems.

Discretisation Package (DIS)

In the Discretization File the following specific data was entered:

- Number of Layers, Rows, Columns (30, 275, 223)
- Cell Dimensions are typically: delr = 96.2 m, delc = 96.1 m, delz = 9.78m. At locations of the lakes the delz is variable so that the bottom of the lake is matched to the approximated bottom of the lake
- Time discretisation parameters: number of periods: N months, period length = 30.44 days, time steps per period: 1

Note that the input of all forcing's of the RCH, EVT, CHD and WEL packages is supplied as monthly time series.

Basic Package (BAS)

The domain of the model is entered in the basic package and includes the model boundaries shown in Figure 37. All cells are active except:

- Cells outside of the subcatchment delineation boundaries
- Cell that represent the basement
- Cells that represent air
- Ocean cells within the subcatchment domain (marked as constant heads).

Upstream Weighing Package (UPW)

The Upstream Weighting package is used to specify properties controlling flow between cells in MODFLOW-NWT. The hydraulic conductivities of each cell are defined in this package and are calibrated with the PEST++ procedure. All cells in the domain are marked as convertible. The vertical conductivity is assumed to be $1/6^{th}$ of the horizontal conductivity based on the average reported in Freeze [67]. The magnitude of the specific storage (~ effective porosity) of the soil is a parameter that is calibrated with a coming magnitude of around 0.15.

Time-Variant Specified-Head Package (CHD)

The seasonal fluctuation of the head in the wetlands (in Woody Lake and Windabout Lake) is modelled by using the Time-Variant Specified-Head package.

Recharge Package (RCH)

The recharge package is used to describe precipitation and subsequent recharge of the groundwater in the saturated zone. Recharge is the fraction of the precipitation reaching the groundwater table also referred to as deep percolation. The recharge of each surface cell was calculated by multiplying the precipitation with a factor depending on the land use (i.e. sparse vegetation, dense vegetation, urban areas) of the cell shown in Figure 19. These factors are calibrated using the PEST++ procedure, refer to Section 3.5.4. Monthly rainfall data was used from 1900 to 2019 and was assumed uniform over the entire subcatchment.

The recharge of lake cells is equal to the precipitation (i.e. precipitation multiplier = 1) and does not need to be calibrated, refer to Table 6 below for details. A calibrated surface runoff/quickflow factor multiplies the precipitation rate to account for the areas around lakes that contribute to additional flow that the lake receives. This flow is added to the direct precipitation of the lakes.

A review of the digital elevation map reveals various creeks and catchment areas that feed the lakes. Surface runoff/quickflow from these features contribute to the lake volume. The seasonal fluctuation in the lakes in the subcatchment cannot be reproduced unless a runoff/quickflow factor is added to the direct precipitation into the lake.

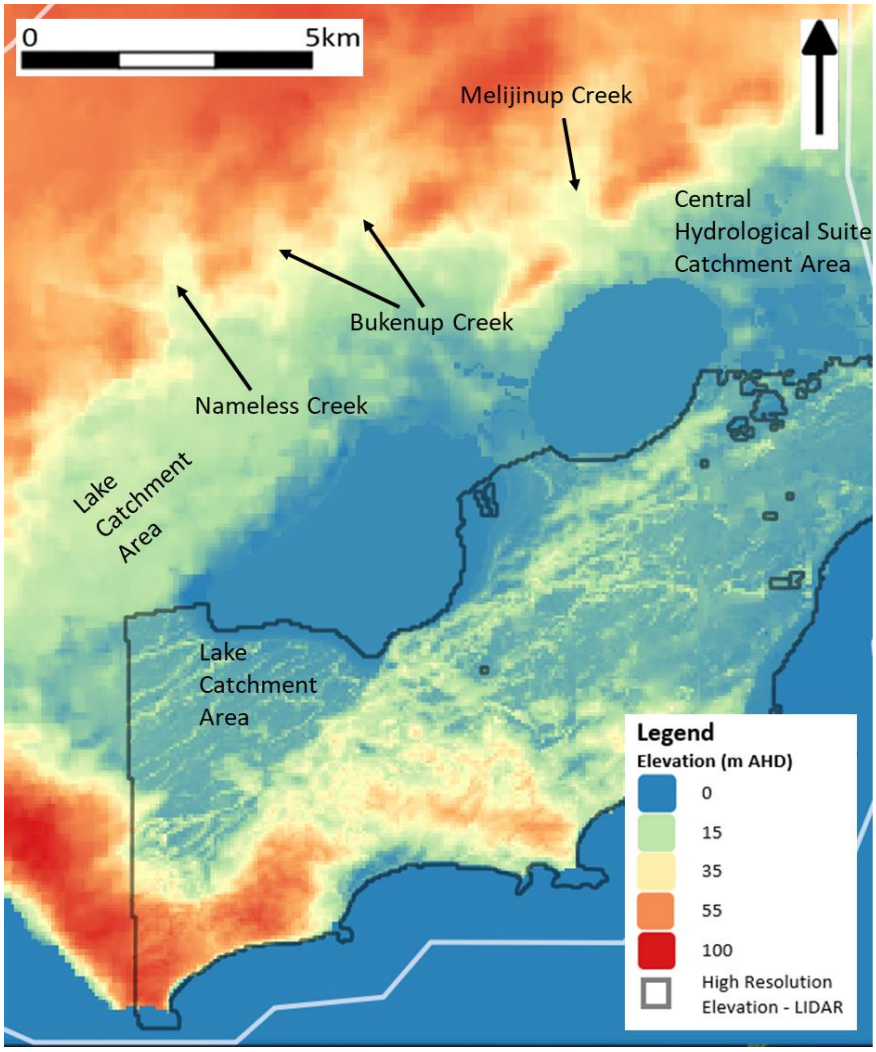

Figure 39: Digital elevation mapping showing drainage patterns and catchment areas surrounding the lakes

Evapotranspiration Package (EVT)

Monthly Evapotranspiration is directly applied to the main lakes in the model. The land cover map is used to select the areas (cells) where open water is present. The open water evaporation rate is directly applied to the lake areas. At this stage, adjustments to account for a decreased evaporation rate due to hypersalinity is not included. Open water evaporation directly from the lakes does not require calibration. Future updates of the model may require that the evaporation rates depend on (hyper) salinity level of the lake.

The evapotranspiration is also dependent on land use, refer to Table 6 below. An important difference between the recharge and the evapotranspiration is that the evapotranspiration rate is dependent on the groundwater level relative to the land surface. This is the reason that evapotranspiration and recharge are both included in the model and not only the recharge as a fraction of the precipitation.

Table 6 – Multiplier (Recharge = Multiplier x Net Precipitation. Evapotranspiration = Multiplier x Open Water Evaporation)

Land cover type	ISO Class	Assumed Min. RCH Multiplier	Assumed Max. RCH Multiplier	Assumed Min. EVT Multiplier	Assumed Max. EVT Multiplier	Calibration
Open Water [3]	0, 3, 4	NA (= 100% Precipitation)	NA (= 100% Precipitation)	NA (= 100% Precipitation)	NA (= 100% Precipitation)	NO
Open water Surface Runoff Factor [3]	0, 3, 4	1	4	NA	NA	YES
Wetlands [3]	11,5	NA (= 100% Precipitation)	NA (= 100% Precipitation)	NA (= 100% Evaporation)	NA (= 100% Evaporation)	NO
Dense Vegetation	31, 32, 33	0.05	1	0.3	1.2	YES
Sparse Vegetation	8, 9, 14, 16, 18, 19, 24, 25, 34	0.05	1	0.3	1.2	YES
Urban Areas	35	0.05	1	0.5	0.5	YES / NO

Large areas in the domain, especially where rain-fed agriculture is practised north of the wetlands (> 35 m AHD), have groundwater levels below the selected extinction depths. Typically, the water table of crops (wheat, grain, barley etc.) and shrubs is below the rooting zone of the vegetation.

Justification of the selected extinction depths can be found in FAO paper 56, Allen [49] and in the article from Schenk [68]. Table 7 below shows the selected extinction depths based on typical root zone depths.

The root zone depths were multiplied with a factor of 2 as the EVT package from MODFLOW NWT does not allow segmentation. The EVT package models

3 Open water in the model is treated different than the other classes in the model. Recharge in open water lake cells equals precipitation + a factored precipitation to model the runoff/quickflow. Evapotranspiration in open water cells equals open water evaporation (see Evapotranspiration Package below).

evapotranspiration linearly from the maximum value to 0 from the land (or EVT) surface to the extinction depth. The estimated root zone depths reported in the literature for dense vegetation, sparse vegetation and urban areas (approximately 6 m, 2 m and 1 m respectively) were multiplied by a factor of 2 to obtain extinction depths of 12 m, 4 m, and 2 m, respectively. Note that the root zones are not the only force causing a vertical flux from the water table. Capillary rise causes an upward flux of several meters above the saturated zone in clay soils. It is assumed that the evapotranspiration flux from within the root zone is greater than the capillary rise. Evapotranspiration from below the root zone is included in the model as shown in Figure 40.

Table 7 – Selected Root Zone Depths

Land cover type	ISO Class, Refer Figure 19	Selected Extinction Depth	Extinction Depth Calibration
Open Water [4]	0, 3, 4	NA	NO
Wetlands [4]	11,5	NA	NO
Dense Vegetation	31, 32, 33	12 m	NO
Sparse Vegetation (i.e., crops and shrubs)	8, 9, 14, 16, 18, 19, 24, 25, 34	4 m	NO
Urban Areas (turf grass)	35	2 m	NO

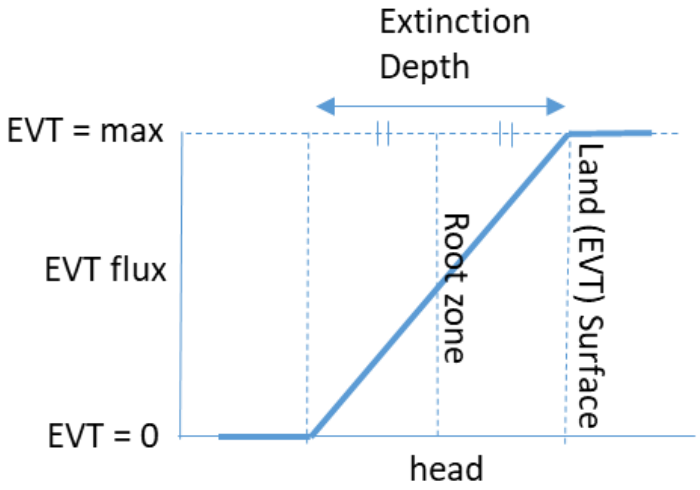

Figure 40: Schematic plot of Evapotranspiration Flux

4 Open water in the model is treated different than the other classes in the model. Recharge in open water lake cells equals precipitation rates. Evapotranspiration in open water cells equals open water evaporation (see Evapotranspiration Package below).

Recharge and evapotranspiration are antagonists and as a result, the value of the extinction depths will affect the (calibrated) evapotranspiration factors and, in return affect the (calibrated) magnitude of the recharge factors.

Well Package (WEL)

Monthly flow from wells extracting groundwater from the aquifer are included with the WEL package. Screened depths provided by DWER in the drinking water source protection plan [22] are used to determine from which cell water is extracted. If the screen crosses more than one cell, the total extraction flow was divided by the number of cells that the screen crosses. The resulting flow was applied to each of the cells that was crossed by the screen.

The screens for the private irrigation wells are all assumed to cross in layer 16, equivalent to approximately 1.4 m AHD to -8.2 m AHD.

3.5.4 FLOPY

The model was developed, run and post-processed with Flopy. This allows the user to enter the input of the variables in the MODFLOW packages with Python Script without the use of a Graphical User Interface (GUI) or coding of MODFLOW directly in FORTRAN. A more detailed description of the code is given by Bakker [69].

3.6 PARAMETER ESTIMATION (PEST++)

3.6.1 Introduction

Numerical groundwater modelling is inherently an inverse problem, i.e., observations such as heads are measured while the factors that produce the heads such as hydraulic conductivities are unknown. Unique solutions (a unique parameter set) will not exist as a result of the non-linearity and the complexity of the system. Thus, the problem of finding a ‘best’ parameter set is an ill-posed inverse problem, i.e. the solution does not depend continuously on its parameters and more solutions are equally valid. Regularisation is the procedure that aims to obtain one unique solution to an ill-posed inverse problem. In groundwater modelling, this equates to finding the best performing parameter set.

PEST++ is freely available software that automatically executes Parameter Estimation by running a model many times with different parameter values. In each run, the model results are compared observations and new parameter values are calculated as input

for the next run. The final parameter settings are found when the behaviour of the model is improved within the acceptable limits set by the user or if a maximum number of iterations is reached.

PEST++ is a model-independent parameter estimation and uncertainty analysis program. It can be used to calibrate any model and conduct uncertainty analysis as long as the model reads in and prints out in ASCII format. In this case, the model is created in Flopy. After each MODFLOW model run, the output is saved in the binary file containing the head of each cell for each time step (.hds extension in case of heads). Another Python script is called to run to read out the binary file and to produce the output files in the ASCII format. PEST++ then reads the modelled output for comparison with the observations and the model is run with updated parameter settings to obtain a better fit with the observations as explained in more detail below.

3.6.2 PEST++ Algorithm Overview

The purpose of the PEST++ algorithm is to determine the optimal parameter values by comparing observed values by modelled values with an objective function Phi Φ, where Phi is the sum of squared residuals (see Equation 3 below), Dorothy [70]. Phi is a measure used to objectively quantify the difference between model results and observations. As such, minimising Phi results in a model that best matches the observed values. The weight of each observation (heads only) was set to 1 in this study.

$$\Phi = \sum (w_i r_i)^2 \qquad \text{Equation 3}$$

Where,

- Φ is the sum of squared residuals,
- r_i is the *i*'th residual and,
- w_i is the weight associated with the *i*'th observation

First the model is run as many times as there are parameters to compute a Jacobian Matrix by approximating partial derivatives around parameter values. The N x M shaped Jacobian contains the parameter set (M) and all observations (N). The Jacobian indicates how sensitive the model is in response of changes of the parameters and provides direction to the parameters to minimise phi.

For this study, the PESTPP-GLM 4.2.16 version from the PEST++ suite was used. The Gauss-Levenberg-Marquardt algorithm is a robust method to solve non-linear least squares problems using the Jacobian. At each iteration, the algorithm is performed to determine new 'best' values for each parameter to minimise the objective function Phi.

Furthermore, the PEST++ algorithm determines if the objective function phi has converged to an acceptable value. If not, the Jacobean matrixes are calculated with the new 'best' parameters and the iterations steps are performed.

Parallel computing using multiple processing cores offers a great computational advantage due to a large number of model runs that are required for a PEST procedure. PEST++ utilities have been applied to perform parallel computing. Detailed information on PEST++ and its capabilities can be found in documentation such as manuals and scientific articles issued by Dorothy [70], [71], [72], [73], [74], [75] and [76].

The maximum number of iterations of PEST++ was set to 7 due to the limited number of cores (11) that were available and the runtime of the model. All parameters were log-transformed throughout the regularisation problem. The total calibration data set contained a total of 1,326 groundwater head observations.

3.6.3 Sensitivity Analysis with PEST++

As mentioned above, parameters are not uniquely estimable, meaning that the same model can produce results that are equally acceptable or accurate with different sets of parameter values. Models inherently have a limited set of parameters and are only a simplified representation of real-world systems.

The difference between the simplified parameterised model and the complex real hydrological system is generally the largest source of error of model predictions. The error can be estimated as part of the PEST++ calibration with the software that is supplied with the PEST++ suite.

In this study, the error of the best parameter set was explored with regularised inversion using linear uncertainty analysis with GENLINPRED (GENeral LINear PREDictive uncertainty/error analyser). Doherty and Hunt [73] provide the derivation of these statistics.

GENLINPRED executes other PEST++ utilities to produce metrics that indicate the following:

- Identifiability
- Relative parameter error variance reduction
- Relative parameter uncertainty variance reduction
- Additionally: parameter contributions to predictive uncertainty/error variance

A model parameter is identifiable if its value can be uniquely recovered from the observed data set. Identifiability varies between zero and one in PEST++, with zero indicating complete non-identifiability and one indicating complete identifiability, Dorothy [73]. It can beforehand be noted that some parameters in groundwater models are correlated, for example, recharge and hydraulic conductivity, while they are estimated together by PEST++.

Relative error reduction indicates the extent to which the calibration process reduces error in the estimation of a parameter from its pre-calibration level where its value must be assigned purely based on prior expert knowledge. Error reduction has a maximum value of one (which can only be achieved if there is no measurement noise), Dorothy [73].

Relative parameter uncertainty variance reduction is slightly different to relative error reduction: While the error is the absolute difference between the posterior expectation and the true value, uncertainty relates to the width of the associated credible interval of the prediction.

In general, large reductions in parameter uncertainty or identifiability of certain parameters indicate that they may be reliably determined by the model.

The following procedure was followed to execute the linear uncertainty analysis:

- The model was run with PEST++ in estimation mode with the best-calibrated parameters as the starting values
- The observation weights were adjusted (PWTADJ2) so they are the inverse of measurement noise.
- A sensitivity analysis to obtain the Jacobean.
- GENLINPRED was run (running the required set of programs from the PEST++ suite).
- Singular values were decomposed and the mutual relationships were identified by running IDENTPAR.

Chapter 4: Results and Discussion

4.1 INTRODUCTION

This chapter presents the results and discussions of the salinity distribution, the construction of the hydrogeological model and the calibration with uncertainty analysis with PEST++.

Simulations with the calibrated MODFLOW model were conducted for the following scenarios:

- With groundwater abstraction.
- Without groundwater abstraction.

The outputs in the form of heads in the entire domain are compared and discussed.

Secondly, the water budgets of the entire model and in some key areas are presented and discussed. Only the scenario with groundwater abstraction is included.

Finally, the operation and some of the design aspects of the borefield are discussed and locations for future expansions are suggested.

4.2 SALINITY DISTRIBUTION ANALYSIS

4.2.1 Groundwater Salinity - Borehole Observations

Groundwater salinity observations in boreholes have been plotted in QGIS to visualise the salinity distribution in the domain. Points between the bores were interpolated with Inverse Distance Weighing with an inverse distance power of 5. The result of the analysis is shown in Figure 41 below.

Due to a large number of observations a general salinity distribution appears even though the depth of the screens are unknown for approximately half of the bores. Besides, the date of the observations varies from 1947 to 2021. In general, salinity is more prevalent in the eastern part of the domain. Directly south of the lakes higher TDS values are found compared to the southwest where a freshwater mound is present.

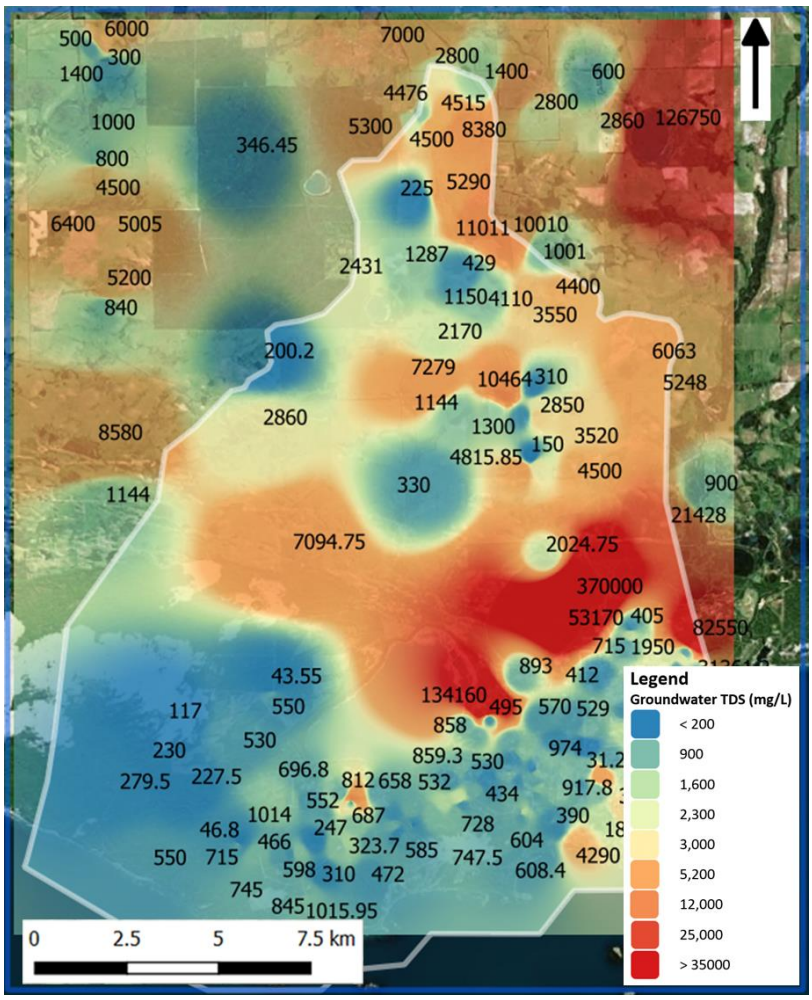

Figure 41: Groundwater Salinity in TDS (mg/L) indicated in Numbers and Colours, based on bore observations. IDW Interpolation carried out with inverse distance power of 5

4.2.2 Groundwater Salinity - AEM Data (2013)

EC data as part of the dataset from the AEM survey by DWER in 2013 was used to create a 3D view of the salinity distribution in the Esperance model domain, see Figure 42 below. The slices of EC data are pictured on top of the granite basement. The surface area over which the AEM survey was carried out is shown in Figure 7.

The results are in line with the groundwater salinity observations from boreholes. The groundwater salinity values are higher in the eastern half of the domain and again, the presence of a freshwater mound in the southwest is observed. In the lower-lying areas, particularly south of the Pink Lake, higher levels of salinity are observed. The area in the coastal region south of the Pink Lake where the surface level is elevated contains fresh groundwater. Note that the EC data south of Lake Warden and around the town was not collected during the AEM survey.

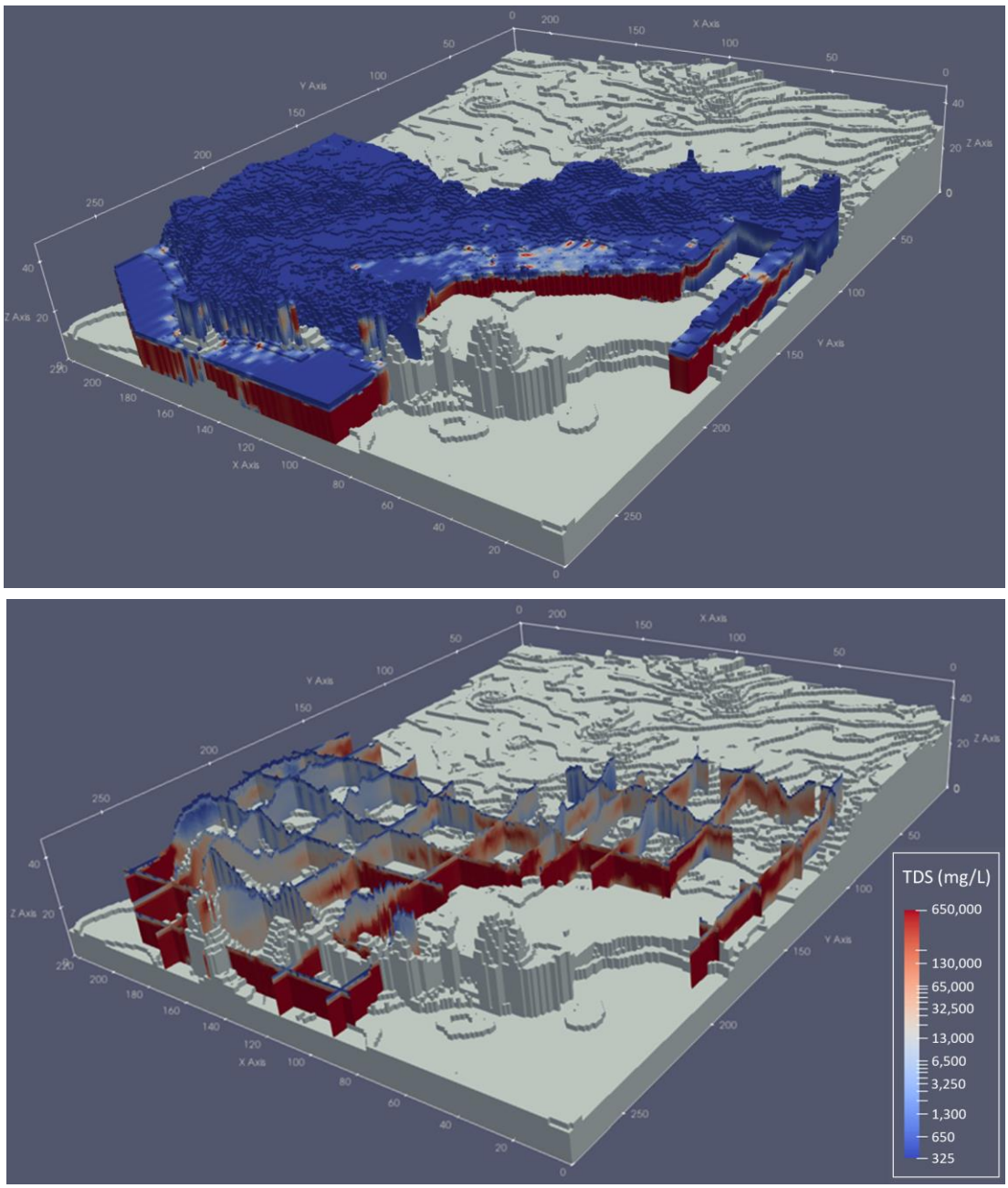

Figure 42: Groundwater Salinity distribution in TDS (mg/L), based on AEM survey (2013). Values are populated in a model grid (Row x Column x Layer: 275 x 223 x 60 or 96m x 96 m x 5m), slices are pictured on top of the basement material from the geological modelling.

4.2.3 Groundwater Salinity Discussion

Noticeably, the groundwater around Coramup Creek is relatively saline with TDS ~ 5,000 mg/L based on borehole data, AEM EC data and surface water measurements (Figure 35). As discussed, Coramup Creek is mostly groundwater fed and discharges into the wetlands on the east of the domain.

It is demonstrated in previous studies, and in this study in coming sections, that groundwater connects the central hydrological suite (wetlands), Lake Warden and the terminal Pink Lake. Accumulation of salinity in the lakes and the soil occurs due to evaporative action and shallow groundwater tables.

The general groundwater flow from north to south distributes salinity towards areas south of the lakes. Groundwater abstraction reinforces this effect as shown later in this study.

Likely, the clearing of the land for agriculture in the north of the Lake Warden Catchment has contributed to the groundwater salinity of the coastal wetlands. This would have caused the groundwater levels to rise and resulted in an increased recharge of Coramup Creek. Previously deposited salts were mobilised and discharged in the wetlands. Likely, the new equilibrium of groundwater levels and salinization (post land clearing) has not been reached.

Unfortunately, the AEM survey did not collect data in the coastal region southeast of the domain which is most susceptible to saltwater intrusion due to the geological setting and groundwater abstraction. Data from monitoring bores however indicate that salinity values in this part of the domain are indeed higher than in the southwest which may originate from both inland and the ocean.

4.3 GEOLOGICAL MODEL

4.3.1 Observations

The 3D geological model was built using geostatistics using bore logs and AEM data. The layers constructed directly from the AEM data were inserted (merged) in the model derived with geostatistics. Some observations of the resulting geological model are outlined below:

- The feature that the Quaternary layer overlays the other layers as a veneer (at least in elevated areas of the domain) is reproduced by the model.
- The part of the model solved by Kriging geostatistics, due to its algorithm, mostly consists of 5 lithography's while in reality some lithography's, particularly werillup, are absent in some regions in the domain.
- The soil thickness is relatively uniform throughout the part of the model solved by geostatistics while soil thicknesses tend to show more spatial

variety. This feature may have been captured better if more bore logs had been available and more bores were drilled to the basement.

- Sand (Quaternary) should be more prevalent at the elevated areas (dunes) on the southwest side of the model. This has been manually corrected.

The two bullet points below are particularly applicable to the model where the AEM data and the model derived from Kriging are merged:

- Transitions between the Kriging derived domain and the AEM domain are generally smooth except for an area in the southwest of the model
- The weathered material layer is thicker in the AEM data than calculated by the kriging algorithm. The AEM data suggests that the weathered material has filled the local depressions in the geological past and is absent at locations where the basement is locally elevated.

As mentioned, the model created by combining the AEM and Kriging data caused significant convergence issues when used as input as flow model in MODFLOW. The irregularity of the geological layers and basement at various locations is likely to result in the numerical issues that were encountered.

4.3.2 Cross Sections

The model derived with the Kriging algorithm only, proved to be suitable for MODFLOW after manual adjustments such as changing the number of topsoil cells (quaternary) to match the surface elevation. Other manual adjustments aimed to connect or block the direct connection to the ocean to match aerial imagery or geological interpretations. Figure 43 below shows an overview of the steps that were followed. Figure 43 c is the most accurate geological model in the region between the lakes and the ocean where layering is directly based on AEM data. However, due to numerical instabilities, the model depicted in Figure 43 d was used as the basis for the layers loaded in MODFLOW.

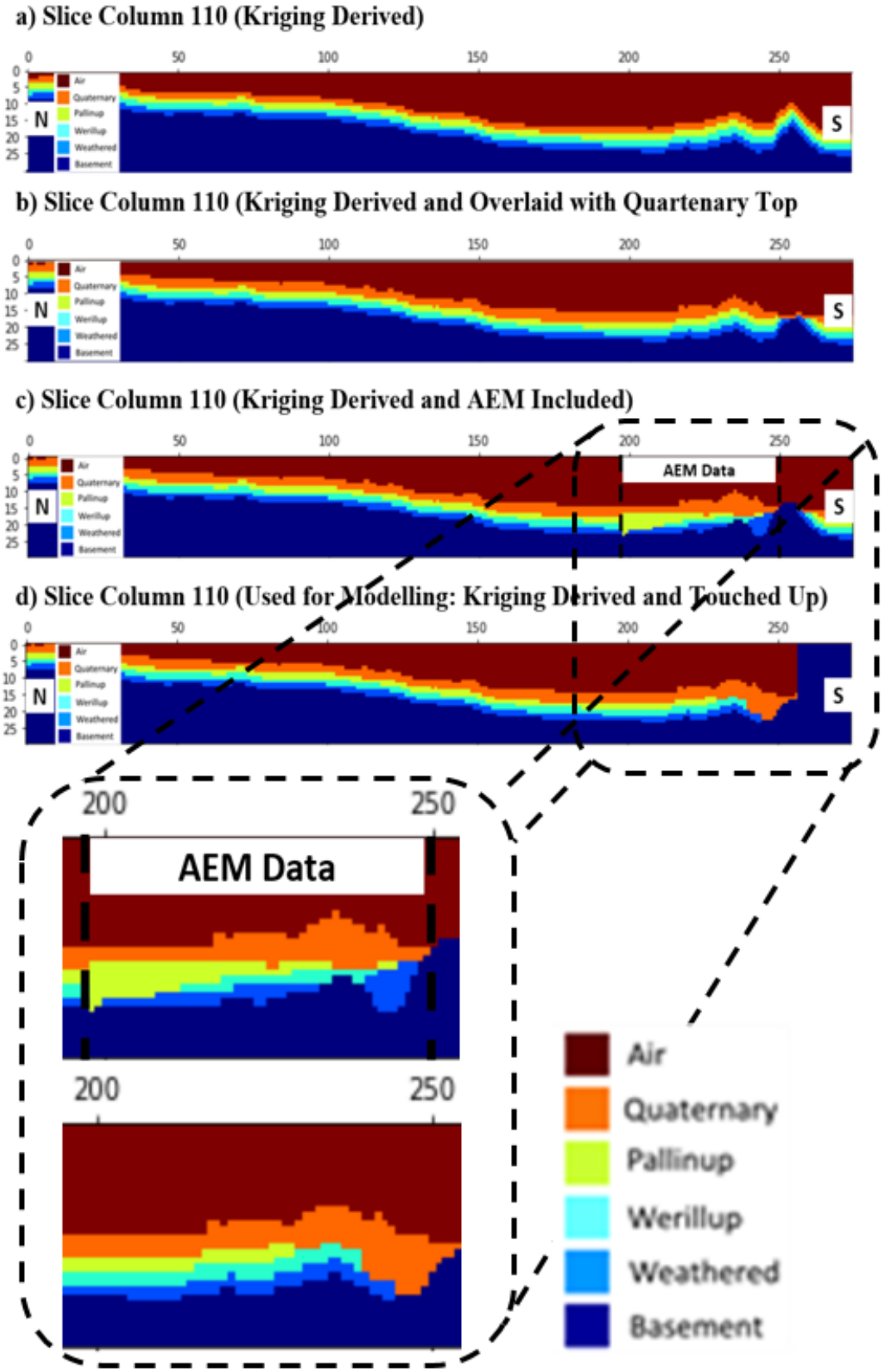

Figure 43: 3D Geological Layers (30 layers x 275 rows x 223 columns) and Slices through Column 110 indicating the Sequence of Development of the Geological Model a, b, c to d. Model b was selected for transformation to the Hydrogeological Model d

4.4 HYDROGEOLOGICAL MODEL

4.4.1 Overview and Boundaries

The geological model was adjusted to include the hydrological features and boundaries. In the areas representing dunes and areas with a low elevation along the coast, a zone with properties representing marine sands was included. The active domain of the hydrogeological model only allows for flow inside the subcatchment, cells outside the subcatchment are made inactive. Furthermore, the basement and air cells are made inactive. The end result of the model is shown in Figure 44 below.

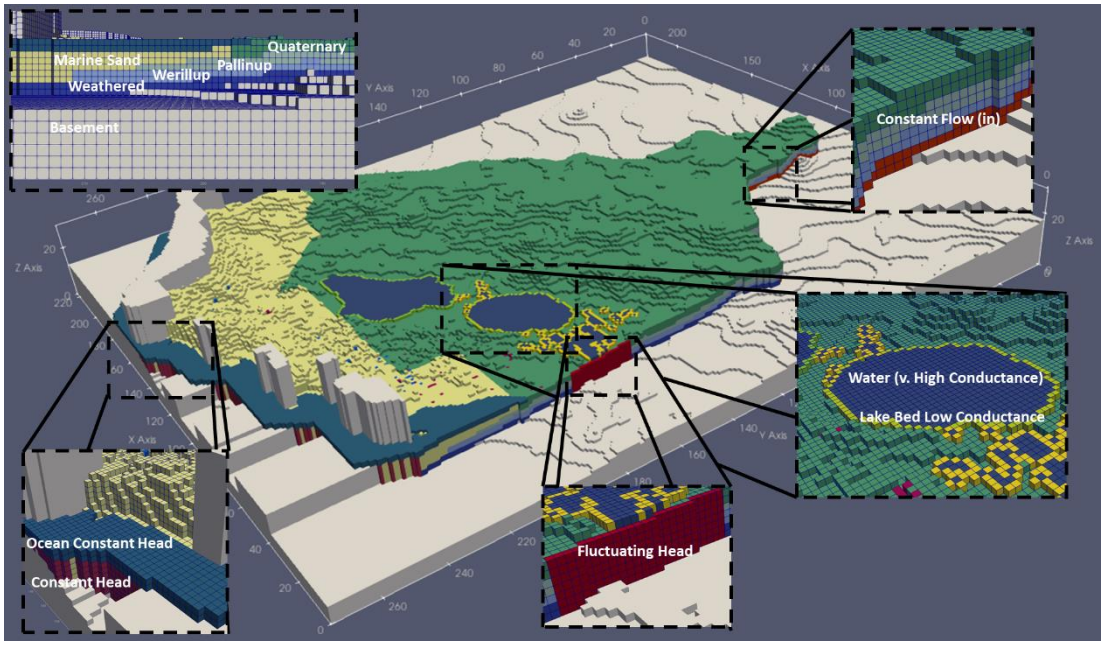

Figure 44: 3D Overview of Hydrogeological Model, 10 x Vertically Exacerbated. The Axis Shows the Number of Layers (30), Rows (275) and Columns (223)

No numerical issues were encountered after the inclusion of the boundaries and the MODFLOW consistently reports a water balance discrepancy of close to 0 per cent for each time step. In the following section, the results and discussion of the calibration is presented and some details of some of the properties of cells and boundaries are highlighted.

4.4.2 Lakes

Lakes are commonly modelled with the special LAK package which is not compatible with SEAWAT. Therefore, the water cells in the lakes are modelled with a very large hydraulic conductivity and a storage coefficient of 1. The water cells are surrounded by cells with a lower hydraulic conductivity to simulate a lake bed resulting in a

delayed response in the hydraulic head difference between lakes and the aquifer. This setup is compatible with SEAWAT and, as a secondary advantage, the heads within the water cells of the lake are faster to compute. A disadvantage is the reduced accuracy of the head calculations.

For example, the head in water cells in the north of the Pink Lake can be up to ~ 0.20 m higher than in the south of the lake. However, this difference is deemed acceptable for the purpose of this model.

4.5 CALIBRATION RESULTS

4.5.1 Running PEST++

22 parameters were part of the PEST++ calibration cycle. All parameters had the same weighing factor and all observations were groundwater head measurements or lake stages. The model was run for 600 months (from January 1969 to including December 2018) which included a ~300-month (= 300 timesteps) spin-up time to adjust the starting heads to the new parameter set of each calibration. Phi decreased from 31,922 before the PEST++ calibration cycle to 1,855 after.

4.5.2 Calibrated and Selected Parameters

The PEST++ procedure was not entirely successful in calibrating the model due to a combination of time constraints and the available computing power. The process required 27 model calls per iteration, with a 7 iterations total resulting in a runtime of ~4 hours for each iteration. The following factors contributed to long PEST++ run times:

- A single model run time of ~35 min (3.79 GHz core clock Processor, 64 GB RAM)
- 22 parameters are selected for calibrating with 11 processing cores available
- Long model spin-up times are required for hydraulic heads to stabilise (preferably ~900 months)
- PEST++ attempts to match a couple of hydrographs (see Section 4.5.7) that follow a declining trend. The parameters for hydraulic conductivity adopt values from the calibration that are too large to match the trend. Subsequently running the model after calibration and using the parameters

directly calculated by PEST++ with the final heads as new starting heads, resulted in unrealistically low simulated groundwater levels.

Realistic parameter values were found by manual parameter adjustments, running the model and visually comparing the results with observed hydrographs. Long PEST++ calibration cycles were omitted and the model behaved more realistic as a result.

Table 8 below shows the initial bounds of the parameters before calibration and the estimated parameter value after calibration and manual adjustment. The reduction of the standard deviation showed that the uncertainty in approximately half of the estimated parameters has been notably reduced upon calibration.

Some of the parameters, namely the hydraulic conductivities of the quaternary, Werillup and Weathered layers, reach the upper bounds of the initial estimation based on the observations shown in Table 8. As the starting heads are slightly too high compared to realistic values, PEST++ directs these model parameters to the upper bounds so that the calculated hydraulic heads fit the observations of the last 300 months, post 300-month spin-up. As discussed, the relatively high hydraulic conductivities cause the model to end with hydraulic head values that are unrealistically low if the model is run is extended. A stable model is achieved when the values of the hydraulic conductivities are manually adjusted by trial and error. The hydraulic conductivities then fall within the boundaries that were initially estimated.

The value of the runoff/quickflow parameter to the Windabout Lake and Woody Lakes also reached the upper bound. It must be noted that these lakes are in proximity of a fluctuating head boundary (wetlands of the central hydrological suite) which locally dominates the groundwater head. Nonetheless, the correlation between observed and calculated head was acceptable and no changes to the parameter value were made.

The other parameters stayed within the set boundaries. Some of these parameters are highly sensitive, others are not identifiable. The sensitive parameters show a large drop in standard deviation most notably the runoff/quickflow, the recharge parameters and the hydraulic conductivities of the marine sands and quaternary layer. The values of the insensitive parameters did not deviate much from the initial estimate and the values could not be optimised.

The recharge factor of the dense vegetation is higher than expected but slightly lower than the upper bound after calibration (0.49). It may be that the modelled groundwater

flow is too small towards the areas with a lower elevation where the dense vegetation is more abundant. The recharge factor for dense vegetation may have compensated for the low groundwater inflow with a high recharge coefficient.

At this point, it must be mentioned that a local variation of hydraulic conductivities is not incorporated in the model. Only one hydraulic conductivity value was allocated to the distinct soils layers following the layers that resulted from the AEM survey. However, local variations in hydraulic conductivity may be large. This effect can be captured by the inclusion of zones with varying hydraulic conductivity and/or with the application of pilot points [75] and [76] at locations where a large spatial variation is expected.

Table 8 – Parameter Selection and Calibration Overview

Parameter	Initial Value	Lower Bound	Upper Bound	Prior Standard deviation	Parameter value post PEST++	Post Standard deviation	Manual Adjustment
Lake Bed HC Pink Lake (m/d)	1	0.05	4	0.48	1.00	0.47	NO
Lake Bed HC Lake Warden (m/d)	1	0.05	4	0.48	0.88	0.45	NO
Lake Bed HC Windabout and Woody Lakes (m/d)	1	0.05	4	0.48	1.00	0.47	NO
HC Marine Sands (m/d)	100	20	150	0.22	49.49	0.14	30
HC Quaternary (m/d)	10	5	30	0.19	30 [5]	0.16	12
HC Pallinup (m/d)	3	0.1	12	0.52	4.42	0.37	NO
HC Werillup (m/d)	10	2	24	0.27	24 [5]	0.21	8
HC Weathered (m/d)	7	2	12	0.19	12 [5]	0.18	5
Groundwater Inflow (m^3/d)	10	2	100	0.42	11.93	0.40	NO
Vertical HC Pallinup (Silt) (m/d)	0.05	0.01	6	0.69	0.041	0.61	NO
GW Recharge Dense Vegetation (-)	0.5	0.05	1	0.33	0.49	0.11	0.52
GW Recharge Sparse Vegetation (-)	0.5	0.05	1	0.33	0.09	0.086	0.16

5 Upperbound reached

GW Recharge Urbanised (-)	0.5	0.05	1	0.33	0.5 [6]	0.33	0.5
Evapotranspiration Dense Vegetation (-)	1.1	0.3	1.2	0.15	0.85	0.10	NO
Evapotranspiration Sparse Vegetation (-)	1.1	0.3	1.2	0.15	0.71	0.13	NO
Specific Yield Quaternary (-)	0.15	0.1	0.4	0.15	0.23	0.15	NO
Specific Yield Pallinup (-)	0.15	0.1	0.4	0.15	0.28	0.15	NO
Specific Yield Werillup (-)	0.15	0.1	0.4	0.15	0.14	0.15	NO
Specific Yield Weathered (-)	0.15	0.1	0.4	0.15	0.16	0.15	NO
Precipitation Multiplier (Overland Inflow) Pink Lake (-)	1.7	1	4	0.15	1.23	0.05	1.60
Precipitation Multiplier (Overland Inflow) Lake Warden (-)	1.7	1	4	0.15	2.24	0.031	2.0
Precipitation Multiplier (Overland Inflow) Windabout and Woody Lakes (-)	1.7	1	3	0.15	3.0 [5]	0.05	NO
Assumed Evapotranspiration Urbanised (-)	NA	NA	NA	NA	NA	NA	0.5
Assumed Vertical HC Quaternary or Werillup or Weathered (-)	NA	NA	NA	NA	NA	NA	0.16667 x HC of Quaternary HC or Werillup HC or Weathered HC
Assumed Specific Yield Marine Sands (-)	NA	NA	NA	NA	NA	NA	0.325

4.5.3 Parameter Uncertainty Statistics

Table 9 below shows the result of the linear parameter uncertainty analysis from GENLINPRED and IDENTPAR with 7 singular values. Some parameters such as the

6 Insensitive parameter, PEST++ did not adjust this parameter

runoff/quickflow parameter, the hydraulic conductivity of the upper soils and the recharge have a relatively high reduction in the error and uncertainty and have high identifiability. The parameters with low identifiability are either insensitive to the calibration dataset and/or are highly correlated with other parameters.

In general, large identifiability suggests high error and uncertainty reduction. For the sake of this discussion, the error and uncertainty reduction and identifiability will be collectively referred to as identifiability.

The runoff/quickflow parameters have the highest identifiability followed by the recharge of the sparse and dense vegetation. Other highly identifiable parameters are the evapotranspiration of the dense vegetation followed by the hydraulic conductivities of the Marine Sands, Werrilup and the Quaternary soils. The identifiability of the evapotranspiration of the sparse vegetation area is low (0.13) which may be because the water table is below the evapotranspiration extinction depth for a large part of the area with sparse vegetation.

Specific yields are not identifiable contrary to what is normally observed in most models. Its value (effective porosity of the soil) usually has a large effect on the seasonal fluctuations of the water table and it should be well identifiable. In this model however, the seasonality is governed mainly by the recharge and evapotranspiration factors.

The parameters for the lakebed resistance is not identifiable which is somewhat surprising. Apparently, the lakebed resistance hardly contributes to the change in water levels in the lakes. The lake stage is dominated by the recharge factor of 1 (no need to calibrate), the calibrated runoff/quickflow factor and evapotranspiration factor of 1 (no need to calibrate). It is likely that the lake is well connected to the groundwater and is relatively independent of the specific resistance of the lakebed at least on the monthly time steps in the model. Another explanation is that the vertical hydraulic conductivity of the quaternary layer may be governing the groundwater in and outflow of the lakes.

It must be realised that a non-linear uncertainty analysis has not been carried out. Some parameters that are found unidentifiable may become sensitive when the parameter is value increased or decreased below a threshold. Although non-linear uncertainty analysis is more thorough, it was beyond the scope of this study.

Table 9 – Parameter Identifiability, Relative Error Reduction and Relative Uncertainty Reduction.

Parameter	Par	Identifiability GENLINPRED	Identifiability (IDENTPAR, 7 Singular Values)	Relative Error Variance Reduction	Relative Uncertainty Variance Reduction
Lake Bed HC Pink Lake (m/d)	plr	1.08E-03	1.42E-04	1.06E-03	3.53E-03
Lake Bed HC Lake Warden (m/d)	lwr	5.24E-04	4.84E-05	4.67E-04	9.26E-02
Lake Bed HC Windabout and Woody Lakes (m/d)	olr	4.12E-03	4.59E-04	4.01E-03	2.03E-02
HC Marine Sands (m/d)	hc52	0.57	0.55	0.43	0.61
HC Quaternary (m/d)	Hc_5	0.15	0.27	0.14	0.34
HC Pallinup (m/d)	Hc_4	0.52	0.18	0.43	0.50
HC Werillup (m/d)	hc_3	0.34	0.43	0.28	0.38
HC Weathered (m/d)	hc_2	7.75E-02	0.17	6.55E-02	9.64E-02
Groundwater Inflow (m^3/d)	Flw	1.77E-02	7.12E-03	1.32E-02	0.10
Vertical HC Pallinup (Silt, Confining Layer) (m/d)	vka4	1.84E-02	2.08E-03	1.50E-02	0.22
GW Recharge Dense Vegetation (-)	pc_1	0.85	0.66	0.84	0.89
GW Recharge Sparse Vegetation (-)	pc_2	0.98	0.96	0.91	0.93
GW Recharge Urbanised (-)	pc_3	0	0	0	0
Evapotranspiration Dense Vegetation (-)	ev_1	0.54	0.78	0.45	0.59
Evapotranspiration Sparse Vegetation (-)	ev_2	0.13	0.13	0.12	0.24
Specific Yield Quaternary (-)	sy_5	2.26E-04	6.05E-04	1.61E-04	7.11E-02
Specific Yield Pallinup (-)	sy_4	1.67E-04	5.62E-04	1.18E-04	2.97E-03
Specific Yield Werillup (-)	sy_3	9.64E-07	1.62E-06	7.00E-07	2.40E-04
Specific Yield Weathered (-)	sy_2	1.03E-08	2.50E-08	0	1.80E-06

Precipitation Multiplier (Overland Inflow) Pink Lake (-)	ol_1	0.94	0.96	0.87	0.89
Precipitation Multiplier (Overland Inflow) Lake Warden (-)	ol_2	0.97	0.98	0.95	0.96
Precipitation Multiplier (Overland Inflow) Windabout and Woody Lakes (-)	ol_3	0.90	0.91	0.88	0.90
Assumed Evapotranspiration Urbanised (-)	ev_3	NA	NA	NA	NA
Assumed Vertical HC Quaternary or Werillup or Weathered (-)	vka5	NA	NA	NA	NA
Assumed Specific Yield Marine Sands (-)	sy52	NA	NA	NA	NA

Figure 45 below visualises the output of the analysis from running the IDENTPAR utility. The identifiability bars are colour coded according to the magnitude of their individual singular values. Warmer colours represent parameters that are more supported by observation targets whereas the cooler colours are parameters less supported by observation targets. Figure 45 also indicates that the collection of field data should be targeted around parameters with cooler singular values to improve the effectiveness of the calibration data set.

It is shown the identifiability of most parameters is composed of several singular values. Parameters are correlated if they share a large contribution from the same singular value. For example, the hydraulic conductivity of a variety of layers (hc_3, hc_3, hc_4 and hc_2) are correlated to the dominant singular (sv_5: green) value of the recharge parameter in sparsely vegetated areas (pc_2).

Finally, as mentioned before, the calibration of this model is not completed and improvements can be made by running more calibration iterations, longer spin-up times and the use of more detailed spatially hydraulic variability. The parameter set can also be extended by identifying and including more identifiable parameters.

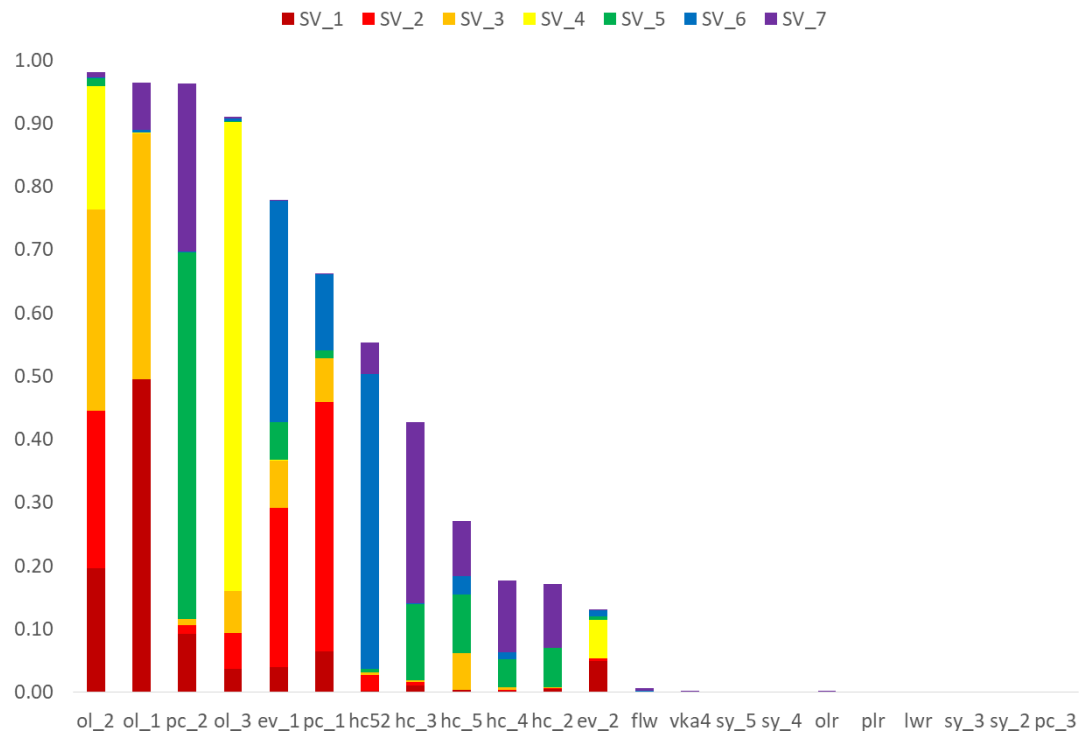

Figure 45: Linear Uncertainty Analysis. A value of 1 indicates a Completely Identifiable Parameter. Warmer Colours Represent Parameters that are Better Supported by Observation Targets

4.5.4 Head Observations vs Modelled Heads

Figure 46 below compares the simulated heads with the observed heads. The water level in the lakes is generally well reproduced. An exception is Lake Warden where the observed heads are systematically low between 2011 and 2017. This trend is poorly reproduced by the model and not well understood conceptually, refer to Section 2.4.2. It is not clear what caused the temporarily reduced water level.

Less well-reproduced are the groundwater heads at the observation bores. As mentioned earlier the declining trend of hydrographs in a couple of bores (Section 4.5.7) are not well reproduced. The parameter set that best reproduces this trend overestimates the hydraulic conductivity resulting in unrealistically low groundwater heads if the simulation is extended, and manual parameter adjustments were required.

Figure 46 below shows the hypothetical ideal line where the observed data exactly matches the simulated data. This line (after manual adjustment) equally divides the scattered points indicating that the model on average produces a reasonable water table.

The reliability of some observations is doubtful. It is advised that for calibrations of future model updates the observed groundwater levels are confirmed by a quality control department from the Department of Water or Water Corporation.

a) Lakes **b) Observation Wells**

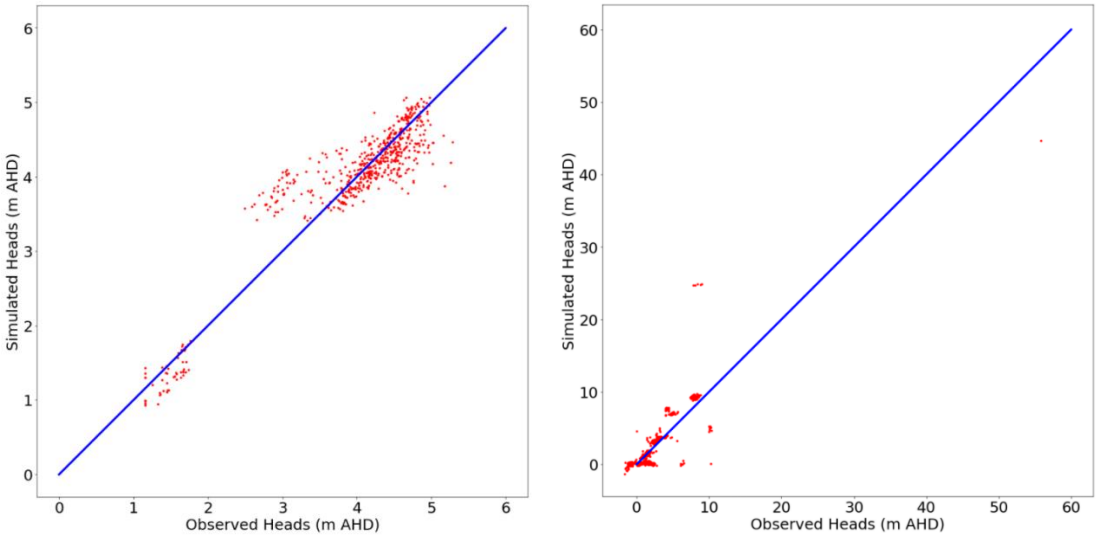

Figure 46: Scatter Plots of Groundwater Model Results

4.5.5 Simulated vs Observed Water Tables

Figure 47 below shows the simulated heads in summer which are in reasonable agreement with the observed heads. At one location in the north, the simulated heads are too high (marked red). Only one data point exists at this location and its reliability should be checked. In one location in the southeast of the town, the simulated head is too low (marked purple).

Figure 48 below show the simulated heads in winter. The observation in the north (red) indicates a mismatch as described before. There are slightly more simulated groundwater heads that are lower than the observed head, however, no single zone with exclusively high or low heads can be identified. The manual parameter post-calibration adjustments are sufficient in this stage of model development before density-dependent-flow is included and recalibration is performed.

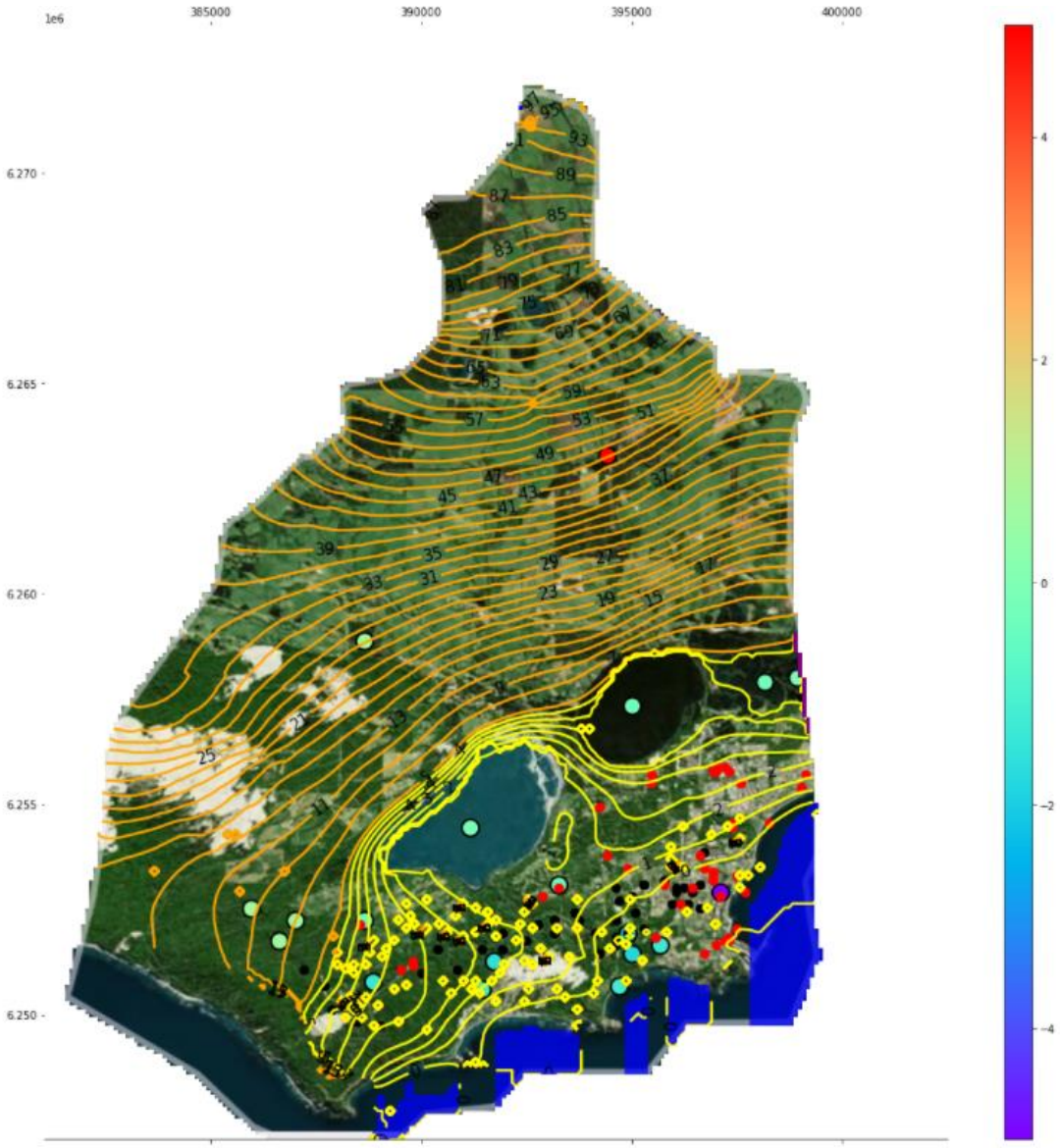

Figure 47: Water Table Contour Map Summer Conditions (Mar 2018). Orange Contours Indicate Levels > 5 m AHD, 2m Interval. Yellow Contours Indicate Levels < 5 m AHD, 0.5m interval. Purple Observation Points Indicate Low Simulated Value. Red Observation Points Indicate High Simulated Value. Red small points indicate Privately Owned Bores. Black small points indicate Water Corporation Bores

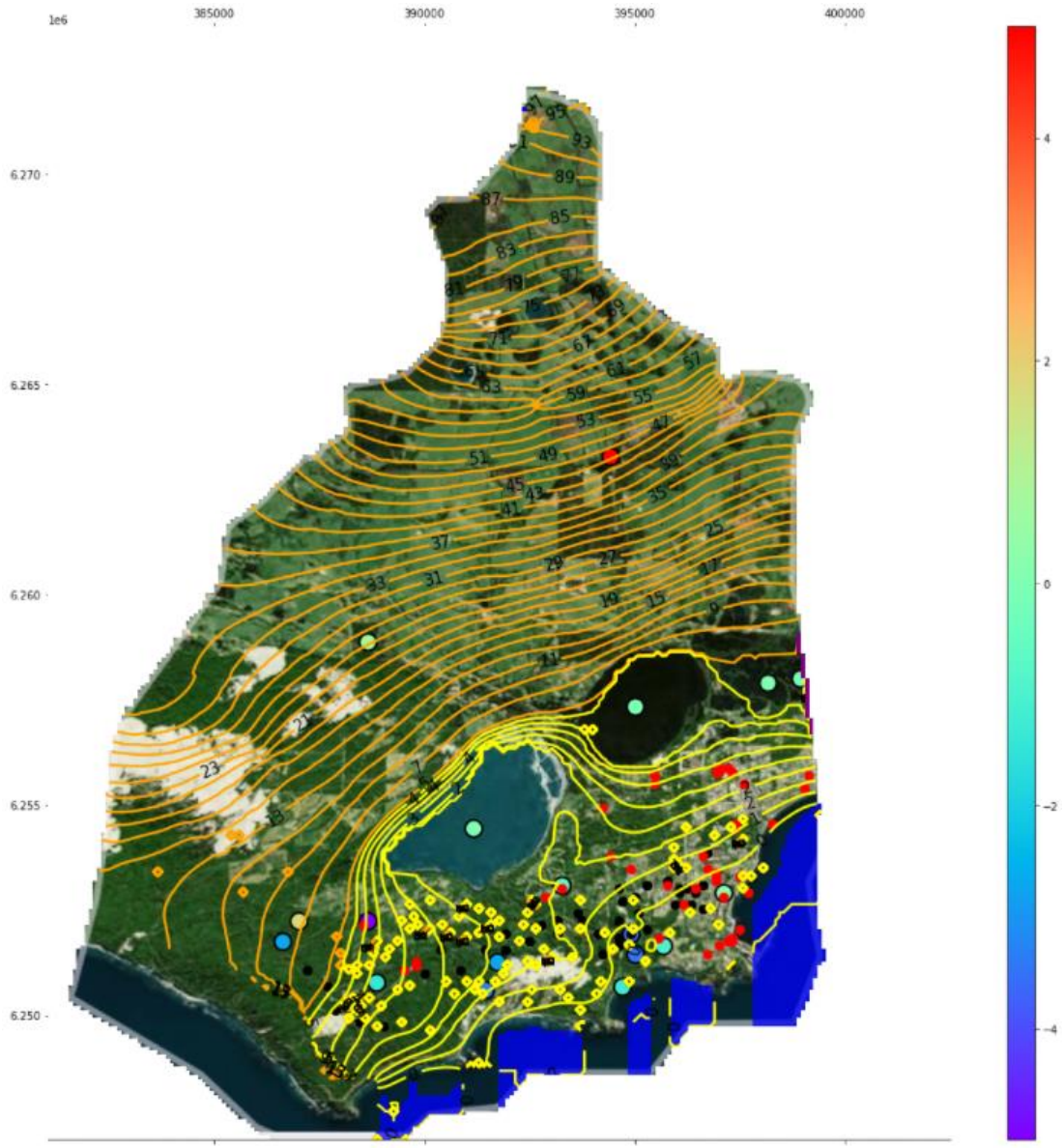

Figure 48: Water Table Contour Map Winter Conditions (Sept 2017). Orange Contours Indicate Levels > 5 m AHD, 2m Interval. Yellow Contours Indicate Levels < 5 m AHD, 0.5m interval. Purple Observation Points Indicate Low Simulated Value. Red Observation Points Indicate High Simulated Value. Red small points indicate Privately Owned Bores. Black small points indicate Water Corporation Bores

4.5.6 Lakes Time Series

Figure 49 below shows the time series of the observed heads and the simulated heads for the lakes. The lakes, occupying a large area in the lower part of the subcatchment have been of particular focus for the calibration. Firstly, the lake levels provide information on the groundwater heads below and in the vicinity of the lakes. Secondly, lake level observations are generally accurate and many data points are available. Finally, evaporation is a dominant flux influencing the lake levels and is known in reasonable accuracy. The lakes are thus an ideal tool for the calibration of the model.

An important observation is that the amplitude of the seasonal water level fluctuations in the lakes are larger (~ 0.8 m in Pink Lake) than the groundwater level fluctuations in bores near the lakes (~ 0.4 m in OBS SWIM Bore 24-97 Twilight Pink Lake). Therefore, aside of direct precipitation in the lakes, an additional flow in the form of surface water (runoff/quickflow) not part of the groundwater system must exist. The DEM of the subcatchment shows clear signs of drainage patterns and local catchment areas surrounding the lakes, refer to Figure 39.

a) Pink Lake

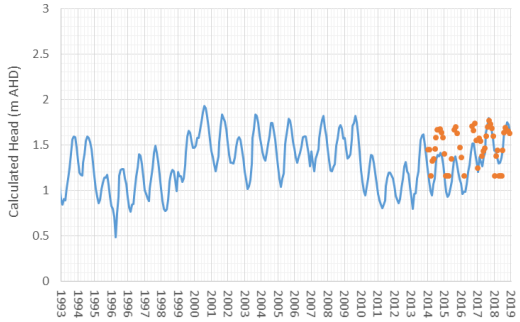

b) Lake Warden

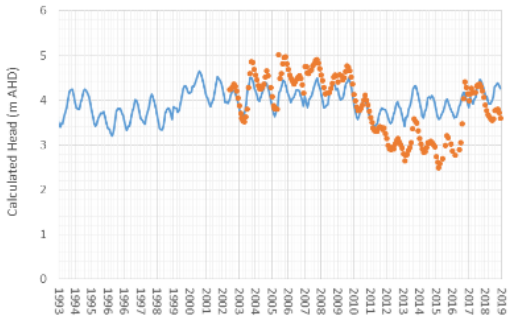

c) Lake Windabout

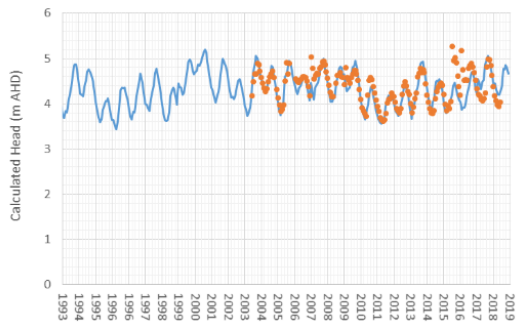

d) Woody Lakes

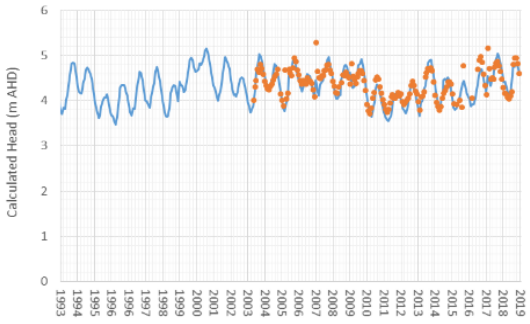

Figure 49: Lake Levels Calculated (blue) and Observed (Orange) (1993 – 2019)

4.5.7 Observation Bores Timeseries

Figure 51 below shows the time series of the observed heads and the simulated heads for the observation wells. Some of the observation's bores (especially OBS Bore 04-93 Twilight Esperance, OBS Bore 02-93 Twilight Esperance and OBS Bore 03-93 Twilight Esperance) follow a declining trend in groundwater level as can be seen in (i, k and l) below. The location of the 3 bores is marked with a blue dashed line on the map of Figure 50.

The reason for this drop in groundwater level is unknown. Note that the precipitation rates have not significantly decreased in the 117 years before 2019 and the annual average open water evaporation rate is not trending up or down as explained in Section 2.3.3. Groundwater abstraction may have affected the groundwater levels in some locations more than elsewhere, although this location modelling suggests that the effect of abstraction is less pronounced, refer to Figure 62 j, k and I in Section 4.7.1. Another hypothesis is that vegetation has recovered or replanted after land degradation and that deeper root systems are developing and absorbing more groundwater.

Figure 50: Map of the Observation Bores Used for Calibration (Yellow: Water Corporation Naming. Orange: DWER Naming. Decreasing groundwater levels within the blue dashed circle)

a) OBS Bore 07-93 Butty Canning Drive

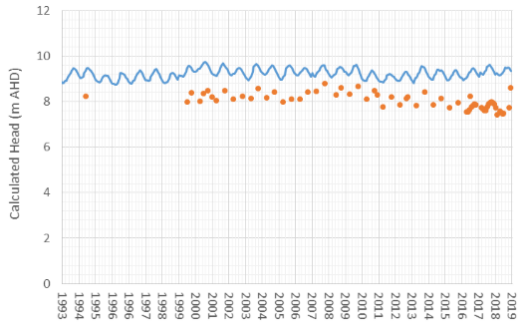

b) OBS Bore 02-13 Butty

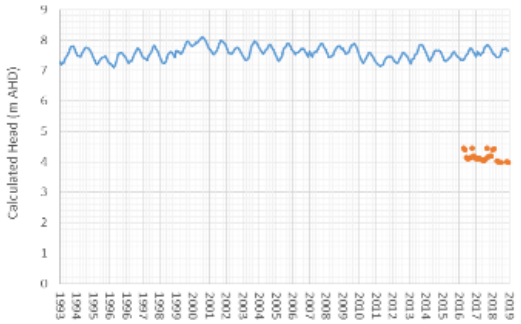

c) **OBS Bore 03-13 Butty**

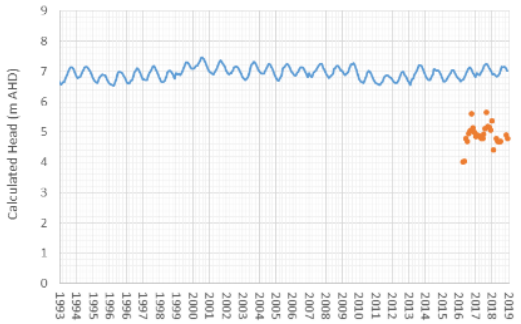

d) 60119503

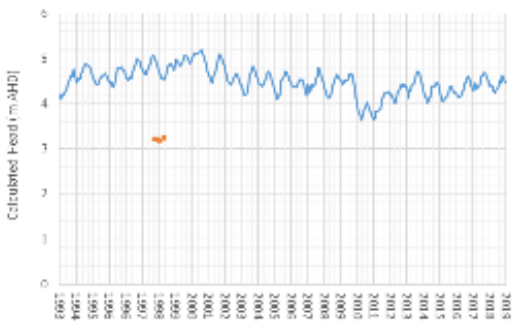

e) 60119502

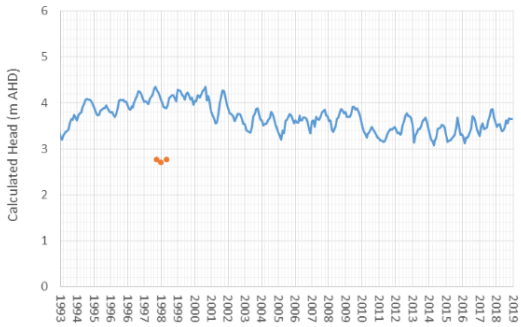

f) 60119506

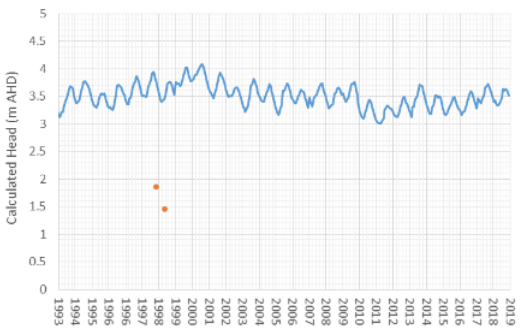

g) OBS Bore 06-93 Twilight Esperance

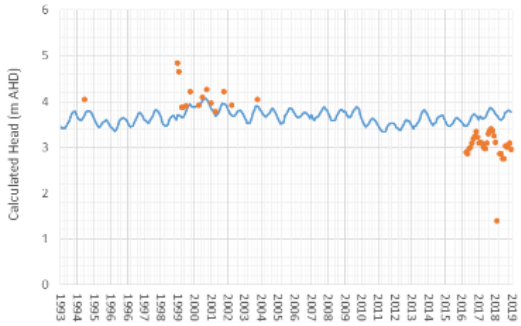

h) 6011079

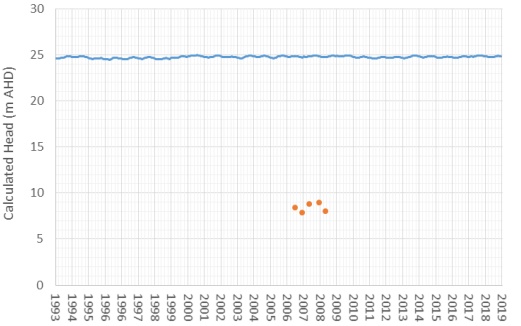

i) OBS Bore 04-93 Twilight Esperance

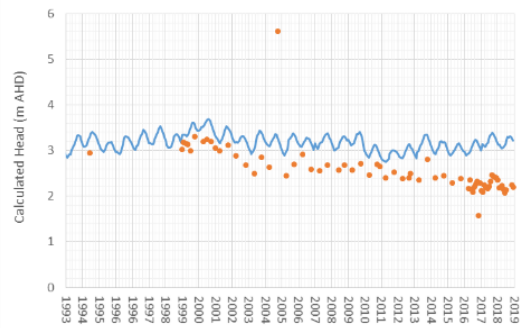

j) 60119500

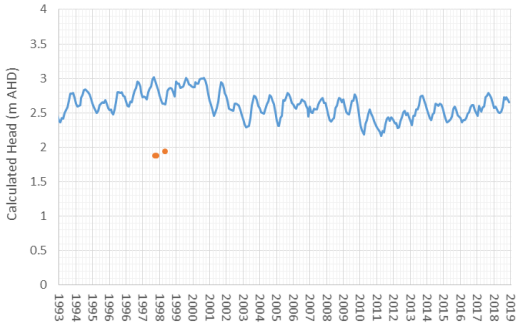

k) OBS Bore 02-93 Twilight Esperance

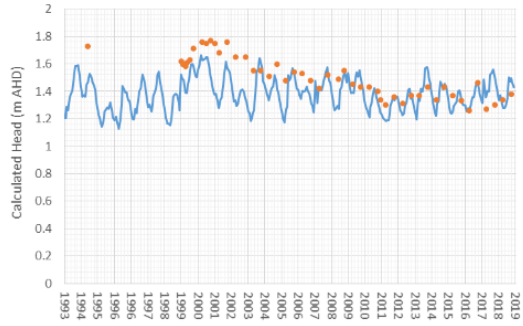

l) OBS Bore 03-93 Twilight Esperance

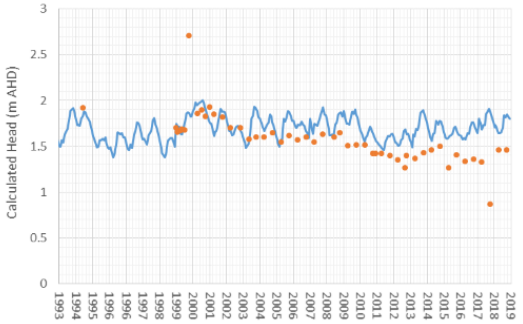

m) Esperance Tws - 7-83 / 60118029

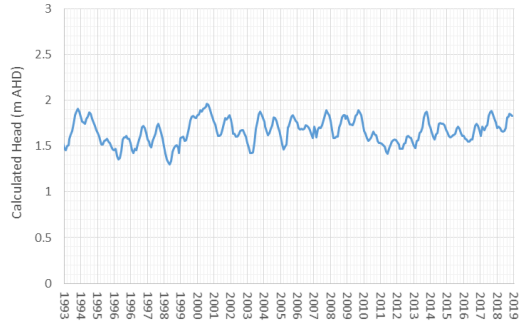

n) Esperance Tws - 4-83 / 60118026

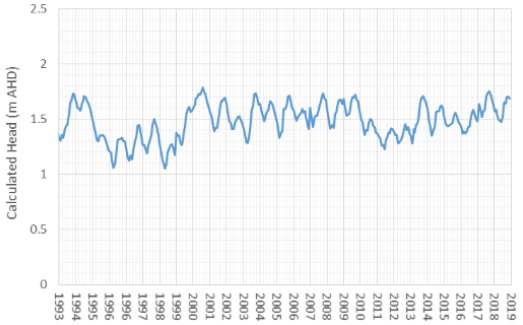

o) OBS SWIM Bore 24-97 Twilight Pink Lake

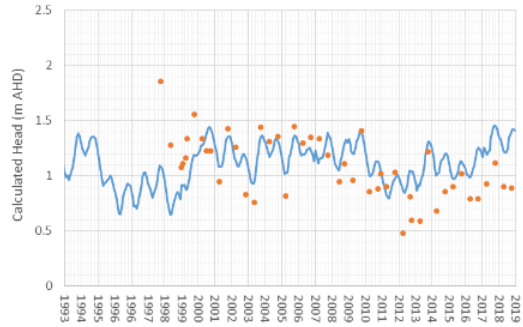

p) 60119302

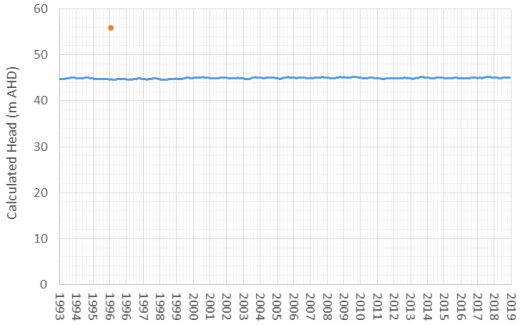

q) 6011185

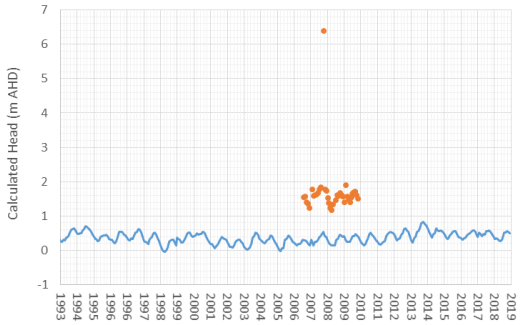

r) OBS SWIM Bore 26-97 Town

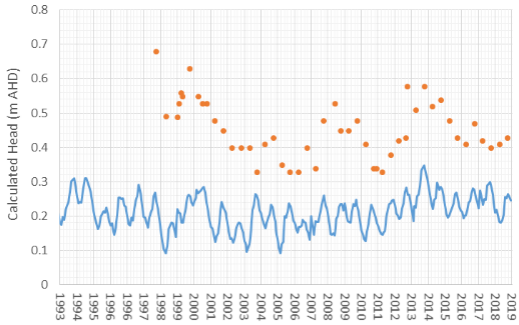

s) OBS SWIM Bore 21-97 Town btwn 22-23

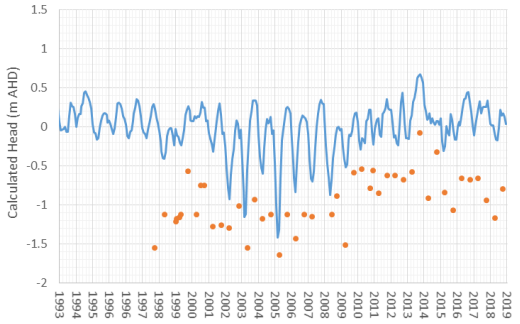

t) OBS SWIM Bore 04-15 Town Esperance

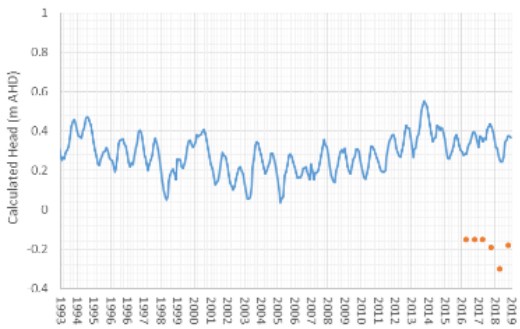

u) 6011186

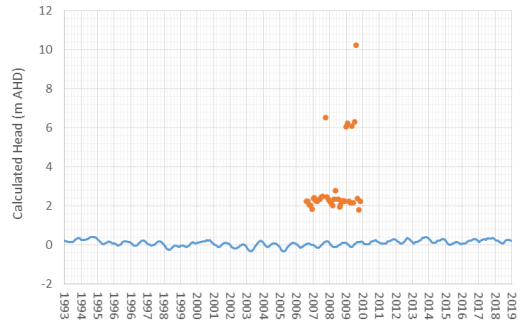

v) Esperance Monitoring Bore 8 D'Comm

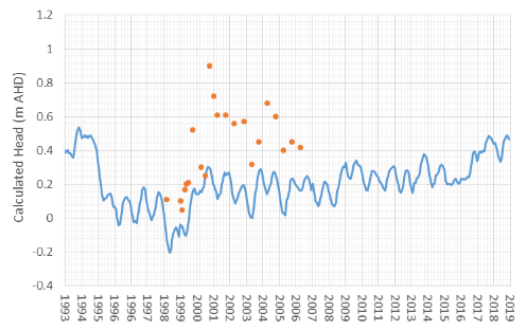

w) 601011

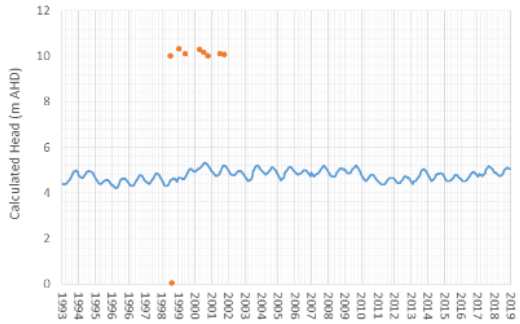

x) OBS SWIM Bore 22-97 Town Esperance

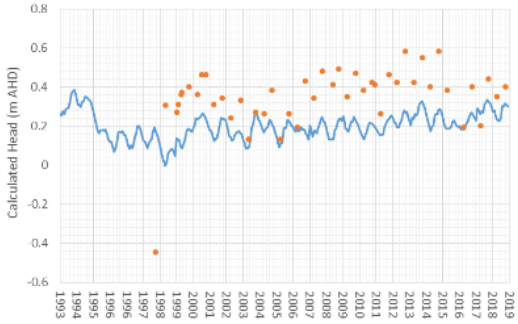

y) Esperance Monitoring Bore 7 (D'Comm)"

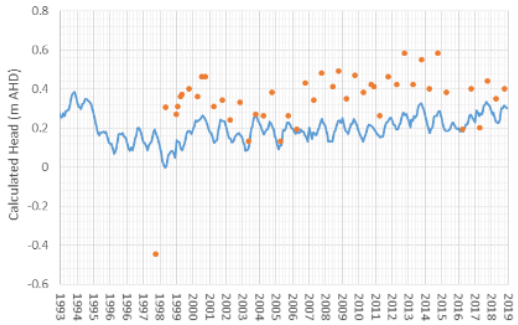

z) OBS SWIM Bore 25-97 Town Jane St

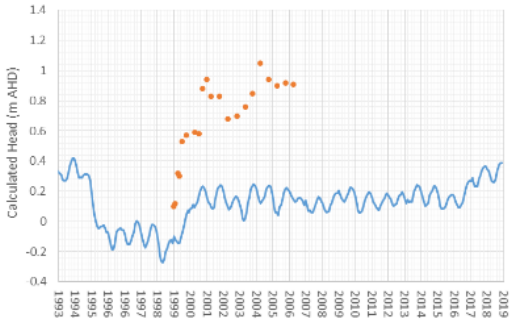

Figure 51: Groundwater Levels Calculated (blue) and Observed (Orange) (1993 – 2019)

4.5.8 Improving Modelling Accuracy

Frequently monitoring groundwater heads at densely spaced locations is important for the development of an accurately calibrated groundwater model. Inaccuracies can be further limited by sampling geological data with sufficient spatial density or by AEM. Pump tests and measuring the hydraulic conductivity at various locations can further enhance the model's accuracy by constraining hydrologic conductivities for parameter calibration.

Several key uncertainties for the construction and calibration of this model are the following:

- Geological data was very well defined within the boundaries of the AEM survey. Outside these boundaries the borehole spacing was sparse and the lithographical date was not always of good quality. For example,
    - In the area between the Pink Lake and 5 km north of the Pink Lake no bore logs exist.
    - Approximately half the bores are not drilled into the basement material
    - No bore logs exist that indicate the elevation of the basement material between the 11-mile beach and Observatory Point. An impermeable basement with an elevation greater than saltwater level can have far-reaching implications for aquifer management, borefield design and saltwater intrusion as explained in Section 3.5.2.
    - Elevation mapping of the basement material is important for selecting the model boundaries such as no-flow boundaries and selecting locations where flow can from outside the domain

- With 26 usable groundwater observation locations, a reasonable coverage is established in the area around the borefield. Greater accuracy of the model can be achieved by the following:
    - The downloadable database of groundwater observations does not always show the observations relative to AHD. As such, some groundwater elevations were estimated using the local surface elevation.
    - Groundwater monitoring bores north of the lakes in the subcatchment is sparse.
    - Most observation bores contain infrequent head data of less than once a month or less.
    - The depths of the screens of the bores are absent and it is assumed that screens are dissecting the highest aquifer only. Note that artesian water may be present in the deeper aquifers (below Pallinup).
    - Observation bores at various locations with screens only dissecting the lower aquifer (i.e., below Pallinup layer) should indicate the extent of the area with artesian water.

As mentioned before, Figure 45 in Section 4.5.3 indicates that the collection of field data should be targeted around parameters with cooler singular values to improve the effectiveness of the calibration data set. These are in particular around values related to hydraulic conductivity.

Although the model calibration can be improved, general groundwater simulations are consistent with the conceptual models and existing literature. The model can be used for an approximate quantitative analysis with the note that the accuracy and precision can be improved. The model should perform well enough for qualitative analysis of the hydrology in the subcatchment.

4.6 QUANTIFICATION OF FLOWS AND WATER BUDGETS

4.6.1 Introduction

This section is included to provide more insight into the magnitude of flows (or fluxes) in the subcatchment and to investigate their relative importance. Figure 52 below shows a schematic of the flows at the subcatchment level illustrating the water balance.

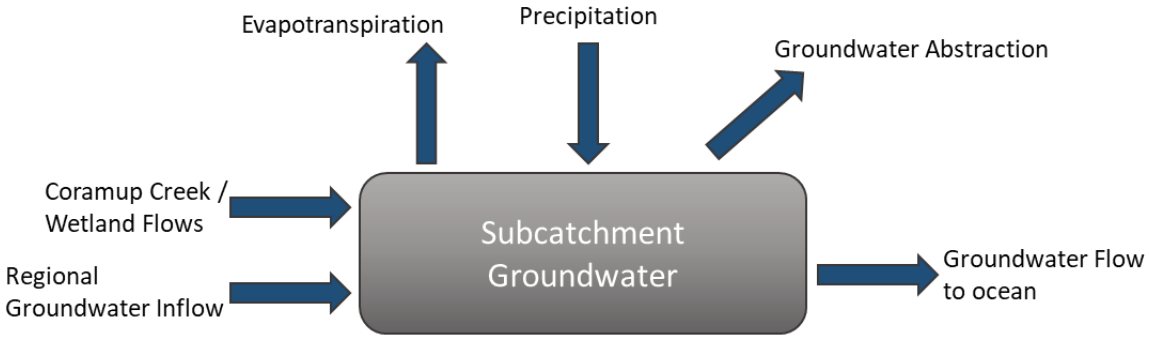

Figure 52: Water Balance and Flows within the Subcatchment as Applied in the Groundwater Model. Only the Most Dominant Direction of the Flows Is Shown

Four flows determine the lake levels (the water balance). These flows are groundwater entering the lake, groundwater leaving the lake, recharge (direct precipitation and runoff/quickflow) and evaporation. The schematic of the flows applicable to the lakes are shown in Figure 54 below. The existence of the hypersaline lakes becomes apparent when the magnitude of saline and freshwater inflow is compared to the outflow. Accumulation of salts will occur when the average groundwater inflow is larger than the groundwater outflow.

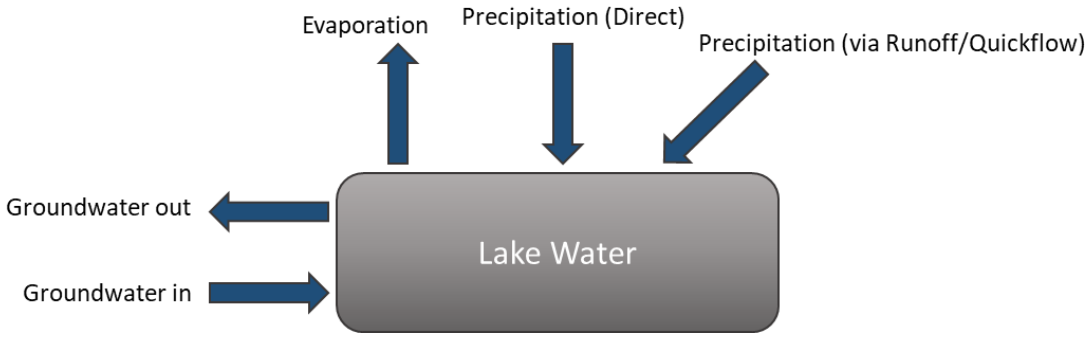

Figure 53: Water Balance and Flows within the Lakes as Applied in the Groundwater Model.

4.6.2 Groundwater Inflow Estimation and Model Selection

Analysis with GENLINPRED showed that the heads in the domain were not sensitive to the steady groundwater inflow ('regional inflow') included in the model. It may be that the upper and lower bounds of this parameter were not selected realistically or that the regional inflow is only an insignificant part compared to the volume of recharge.

Regional inflow is especially important when the density-dependent flow is added to the model and saline water enters the model domain as groundwater. Figure 54 below shows the annual rate of groundwater net inflow entering the model domain which is constant (at 3,770 m^3/d) as expected.

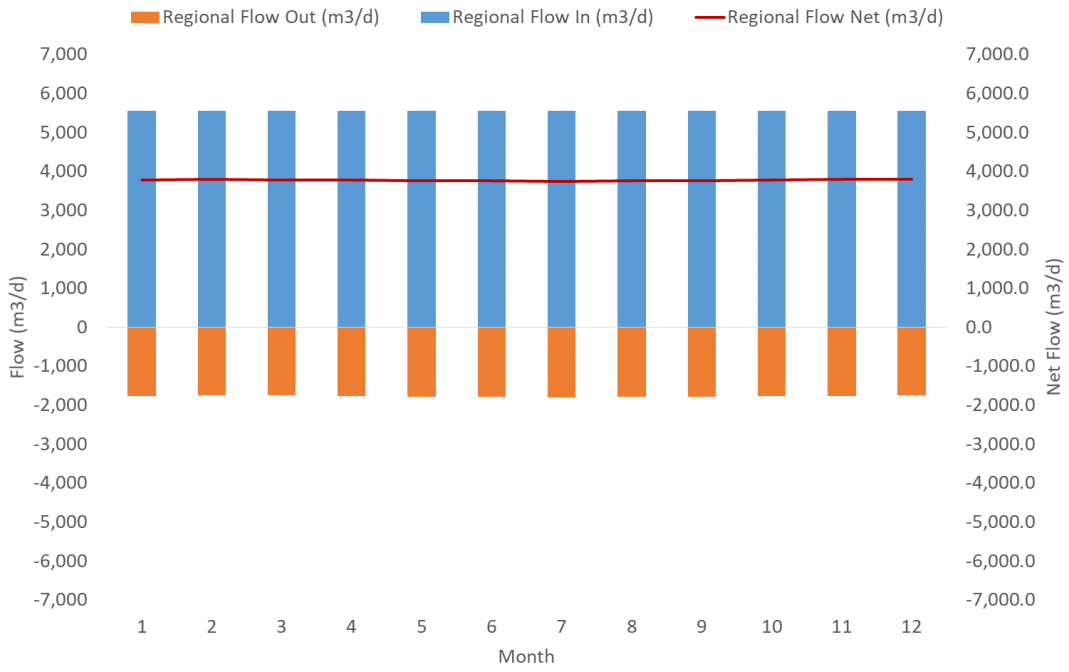

Figure 54: Regional Flow Entering the Model Domain (Averaged 1993 – 2019)

4.6.3 Net Recharge and Evapotranspiration

The recharge and evapotranspiration fluxes are the largest in the model and are comparable in magnitude, refer to Figure 55 below. The annual average of the net recharge (recharge minus evapotranspiration) between 1993 and 2019 is ~400 m^3/d, equivalent to 0.0019 mm/d when divided by the surface area of the entire domain.

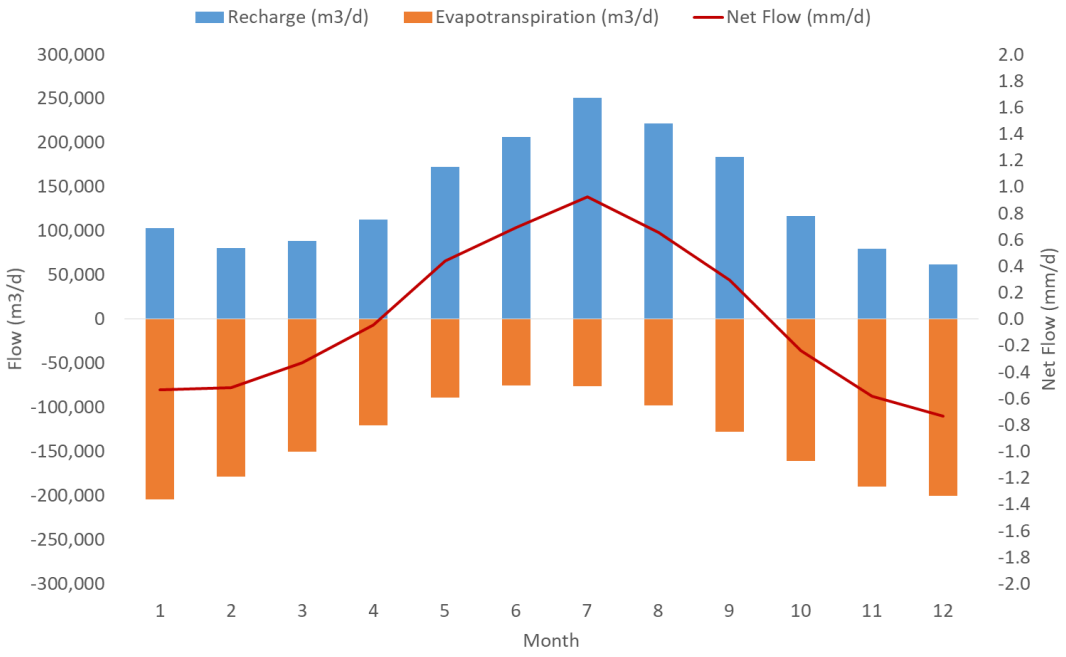

Figure 55: Recharge and Evapotranspiration Fluxes (Averaged 1993 – 2019)

4.6.4 Wetlands / Coramup Creek Inflow

The Coramup Creek discharges the wetlands of the central hydrological suite on the east of the model domain. The effect of the discharge from Coramup Creek and other flows into the wetlands was simulated by applying a (seasonally) fluctuating head boundary. The average flow entering the domain between 1993 and 2019 is shown in Figure 56 below. On average, in both summer and winter, water is delivered to the model domain. In very wet winters, water is removed from the model domain. Compared to the largest flux, recharge, the flow entering the domain via the wetlands is small, 0.17 %.

The Coramup Creek and the wetlands deliver groundwater flow from east to west which is consistent with existing literature from Marimuthu [4], [26], [27], Abbot [28] and DEC [23]. According to the model, an annual average net inflow of 240 m^3/d enters the domain between the years 1993 and 2019.

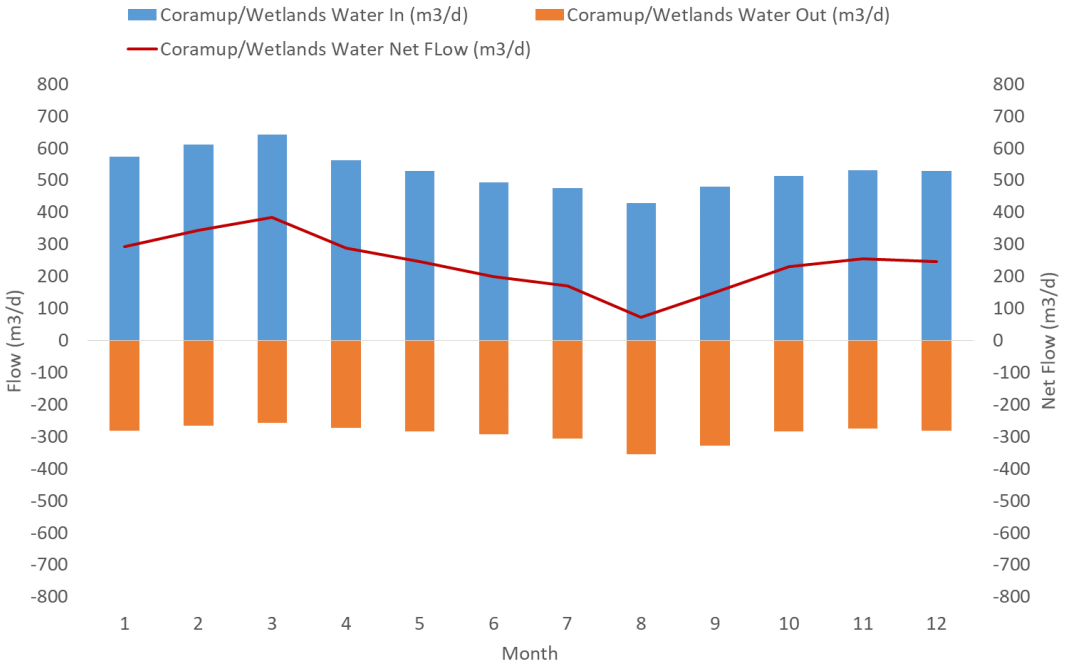

Figure 56: Coramup Creek Wetland Flows (Averaged 1993 – 2019)

4.6.5 Pink Lake, Lake Warden and Windabout/Woody Lakes

The average magnitude of the flows between 1993 and 2019 for each lake are shown in Figure 57, Figure 58 and Figure 59 below.

The following observations are made:

- The Groundwater flows into the Pink Lake is always greater than groundwater flows out of the lake Pink Lake. This behaviour is expected for terminal hypersaline lakes. The contribution of runoff/quickflow to the lake is 1.6 times the precipitation, refer to Table 8.
- In most months, except some winter months, the groundwater flow into Lake Warden is greater than flow entering groundwater from Lake Warden in line with findings from Marimuthu [4], [26], [27]. Furthermore, observed hypersalinity in Lake Warden, DEC [23] and Lizamore [29], suggest a net groundwater inflow. The contribution of runoff/quickflow is 2.0 times the precipitation, refer Table 8.

- Woody Lakes and Windabout Lake only receive net groundwater inflow in the winter months. The runoff/quickflow factor of 3.0 increases the stage of the lakes resulting in a net groundwater outflow for most of the year. These lakes are acting as flow-through lakes in line with the findings of Marimuthu [4], [26], and [27].

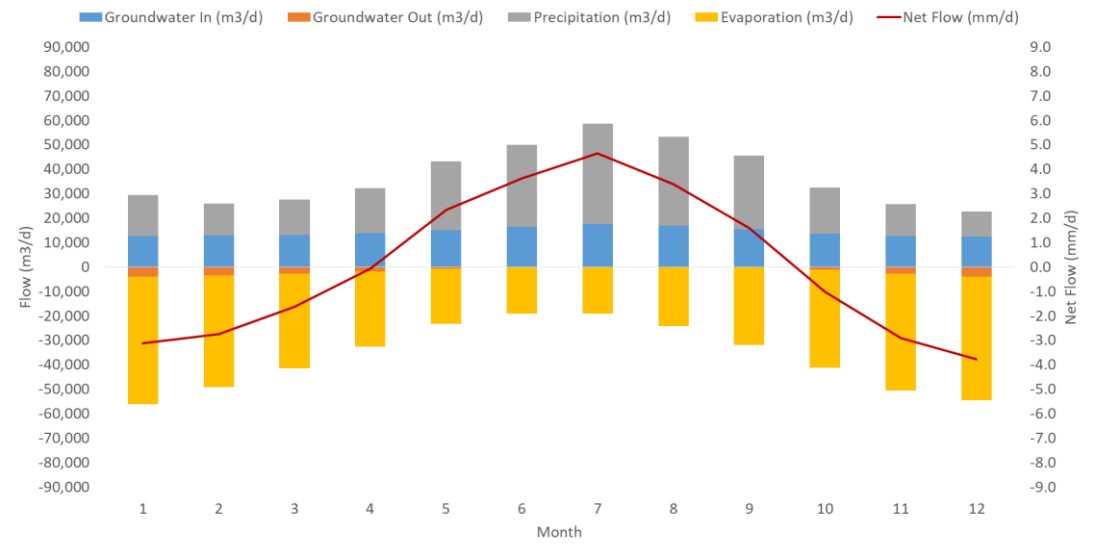

Figure 57: Pink Lake Flows (Averaged 1993 – 2019)

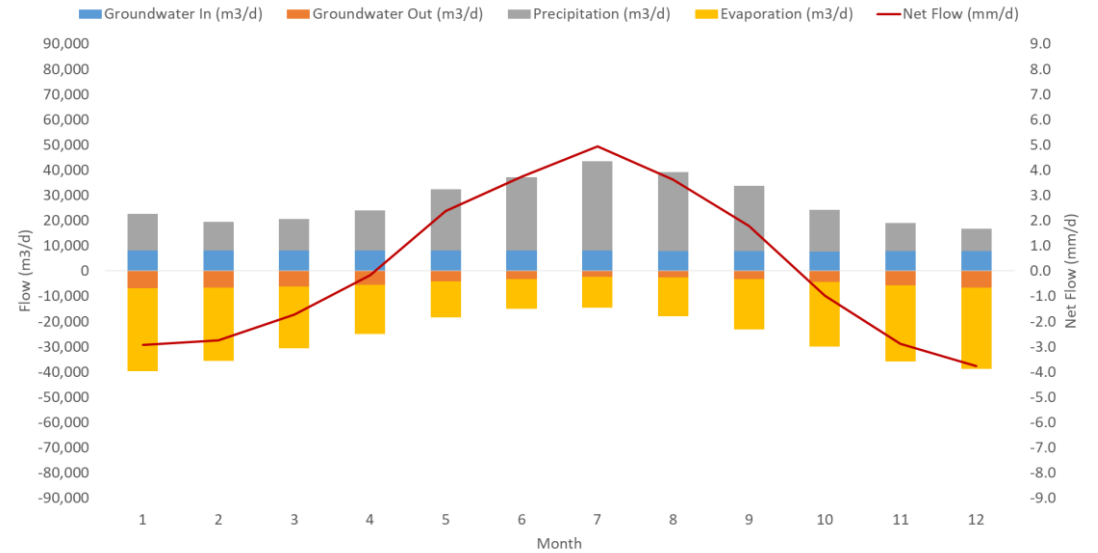

Figure 58: Lake Warden Flows (Averaged 1993 – 2019)

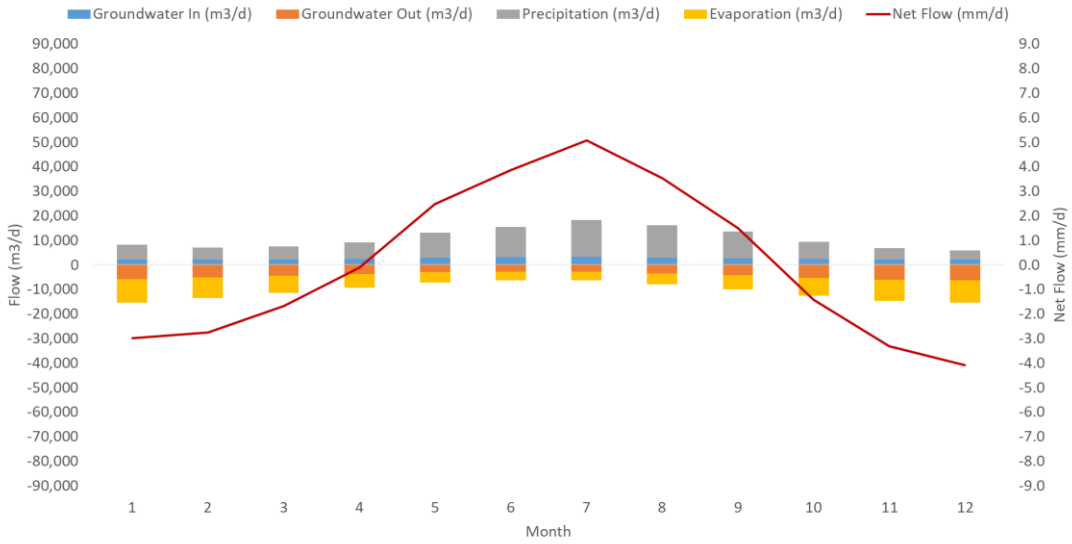

Figure 59: Lake Windabout/Woody Lakes Fluxes (Averaged 1993 – 2019)

4.6.6 Interaction Ocean and Groundwater

The model calculates an average net saltwater flow between 1993 and 2019 of 8,200 m^3/d which is second-largest flow leaving the domain after evapotranspiration. The volume of groundwater entering the ocean exceeds flow from the ocean into the groundwater as shown in Figure 60. With pumps online, the groundwater flow entering the ocean exceeds the ocean water entering the ground by a factor of 14. Although this is a large difference, ocean water is indeed entering the subcatchment and a more detailed analysis should indicate the extent of saltwater intrusion into the drinking aquifer. For example, it is expected that if variable-density flow is included, more saltwater will enter the subcatchment due to the relatively larger increase of heads above the freshwater/saltwater interface compared to heads further inland.

Saltwater intrusion is a seasonal and a local phenomenon depending on groundwater head and local geological features. Section 4.7 provides an overview of the effect of pumping and the areas that are believed to be at risk of saltwater intrusion.

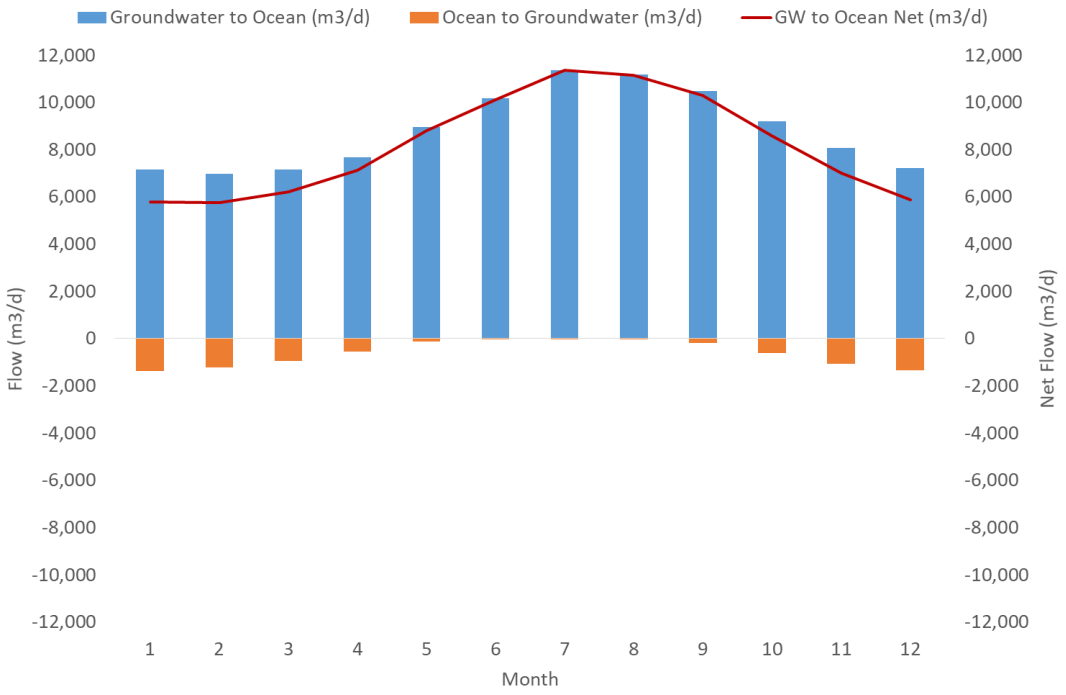

Figure 60: Ocean Groundwater Flows (Averaged 1993 – 2019)

4.6.7 Discussion Water Budgets

The water budget over the entire domain was analysed for the period between 1993 and 2019. A net decrease in groundwater storage was simulated which is most probably the result of a slightly high value of the starting heads at the beginning of the simulation and a not entirely complete spin-up period. Various factors of environmental nature or abstraction rates may otherwise be the reason for the net decrease in storage however, analysis of observed precipitation and evaporation does not point to climatological changes. The increase of groundwater abstraction in this period can only explain a small part of the increase in the net outflow.

A different outcome is expected if the density-dependent flow is included and other model updates are implemented in combination with subsequent recalibration.

As mentioned before, DWER estimates that groundwater abstraction of 70 per cent of the total recharge is sustainable in the Esperance groundwater area of 360 km^2 [3]. The Esperance Groundwater area is not based on any hydrological boundary and it is unlikely that all recharge can replenish abstracted water in the catchment area of the public water borefield.

In the 26 years that are reported here, the actual abstraction is calculated 15.7 times greater than the net recharge (recharge minus evaporation). However, in some years,

the net recharge is much larger (or negative) than the average abstraction as shown in Figure 61 below. Therefore, relative small change in climate can have a large effect on the sustainable abstraction rate.

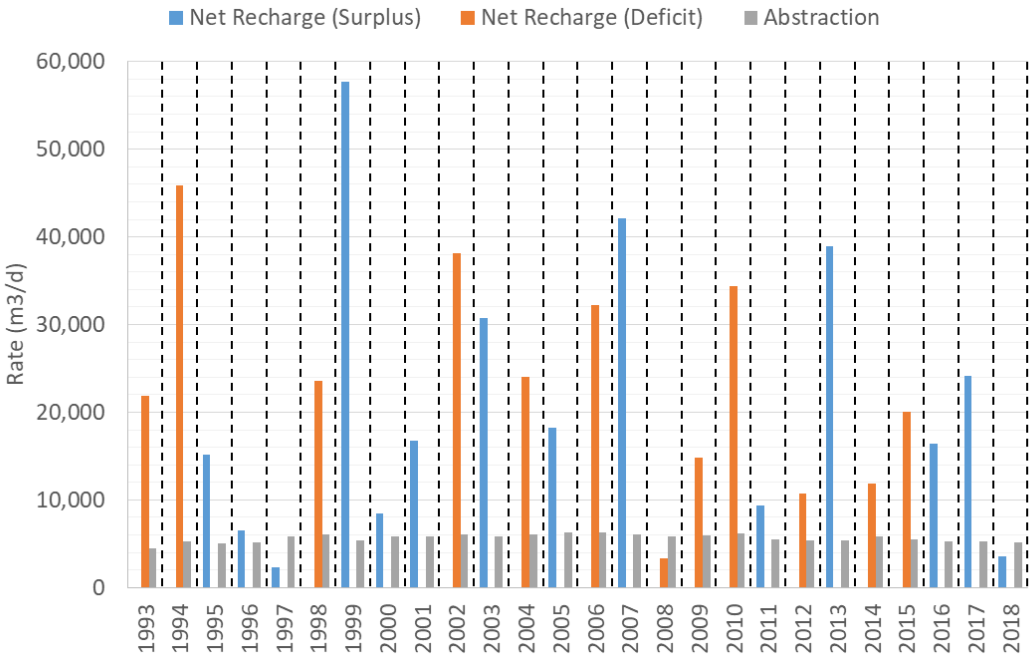

Figure 61: Annual Net Recharge in the Subcatchment Compared to Abstraction Rates. Blue: Years with Recharge Surplus, Orange: Years with Recharge Deficit, Grey: Abstraction

Lake stages are in a dynamic equilibrium between four flows i.e., groundwater in and outflow, evaporation and recharge. The runoff/quickflow factor as part of recharge is a crucial parameter to simulate the seasonal fluctuation in lake levels. In theory, the lakebed conductivity alters the seasonally fluctuating amplitude of the lake stage however IDENTPAR showed that this parameter is not identifiable.

The runoff/quickflow factor flow factor was manually calibrated (increased) after the PEST++ calibration to avoid lakes from draining completely when the simulation time is extended. The Pink Lake and Lake Warden both receive net groundwater inflow which is consistent with the observed hypersalinity of the lakes.

It is interesting to note that Marimuthu investigated the water balance of the Pink Lake by constructing a daily water budget that included inflow, outflow and a storage change term [77]. The water budgets of this study (finite difference method) and Marimuthu's study (daily water balance) were generated completely independently and in different approaches. The groundwater inflow, evaporation and direct

precipitation in both models are of comparable magnitude (around 10% difference) as shown in Table 10. The largest difference is the runoff/quickflow component in the daily water balance method which is 6% versus 38% in the finite difference method. The value of the runoff/quickflow for the finite difference method is larger to compensate for the relatively larger outflow (~10 % more evaporation) and smaller inflow (~10 % less precipitation and groundwater inflow).

The observation that a 10% discrepancy on main fluxes has a large effect on the calculated magnitude of the runoff/quickflow flow, highlights the importance of accurately determining fluxes for hydrological interpretation and quantification of a lake system. Accuracy and confidence can be improved by calibrating the observations of constituents in groundwater and lake water and by field measurements of the evaporation rate and precipitation. In absence of accurate evaporation rates, the effect of lake salinity on the evaporation rate (evaporation energy as a function of salinity) can be incorporated in the Penman-Monteith equation.

Table 10 – Water Balance Pink Lake Comparison Finite Difference Method vs. Daily Water Balance Modelling

Component	**Value Daily Water Balance (Marimuthu [77]) (m^3/d)**	**Value Finite Difference Method (This Study) (m^3/d)**
Precipitation (Direct)	17,042	14,289
Evaporation	31,721	35,214
Groundwater net inflow	13,754	12,564
Runoff/Quickflow	1,166	8,574
Net Inflow	241	213

The infiltration of lake water into the ground in Woody Lakes and Lake Windabout is caused by the relatively large runoff/quickflow factor. As a result, the salinity levels in these lakes are much lower compared to Lake Warden and the Pink Lake which is in line with field observations. It is expected that salinity in lakes will be an important calibration parameter resulting in a more precise estimate of the contribution of the 4 main flows.

4.6.8 Overview of Flows

Groundwater abstraction is the second-largest flow leaving the subcatchment. On average, in the period that was analysed, the abstraction exceeds the 70% recharge that was regarded as sustainable by DWER [3]. One extreme year can make a big difference in the relative abstraction rate due to large annual variation in recharge compared to the abstraction rate.

Table 11 below shows an overview of the flows in absolute values and percentages of the largest (Recharge). Over the period 1993 to 2019, a net outflow occurred with a rate 9,448 m^3/d equivalent of a rate of 0.050 mm/d.

Recharge and evapotranspiration dominate the flows in the subcatchment however, they almost cancel during the period 1993 to 2019. Seasonal fluctuations in groundwater levels in the model are a direct result of this.

Groundwater flows into the ocean is the largest net flow leaving the domain followed by groundwater abstraction.

The regional inflow entering the domain in the north is the largest net flow entering the domain. This flow is however unidentifiable according to the GENLINPRED procedure meaning that the true magnitude may be very different.

The lake stage of all lakes has increased slightly which may relate to the not entirely complete spin-up period. In general, the ratio of the groundwater inflow and outflow are in line with the (hyper) salinity that is observed in the lakes. Evaporation is the largest flux in all lakes.

Groundwater abstraction is the second-largest flow leaving the subcatchment. On average, in the period that was analysed, the abstraction exceeds the 70% recharge that was regarded as sustainable by DWER [3]. One extreme year can make a big difference in the relative abstraction rate due to large annual variation in recharge compared to the abstraction rate.

Table 11 – Overview of Average Annual Flows (1993 – 2019). Positive values indicate that flows enter and negative values indicate flows leaving the domain.

Domain Flow	Flow (m3/d)	Percentage of Largest Flow
Evapotranspiration	-139446	99.74
Recharge	139807	100.00
Net Flow	**361**	0.26
Ocean Flow In	629	0.45
Ocean Flow Out	-8797	6.29
Ocean Flow Net	**-8169**	5.84
Interflow In	5547	3.97
Interflow Out	-1776	1.27
Interflow Net	**3770**	2.70
Production Bores Abstraction	-4720	3.38
Private Bores Abstraction	-930	0.67
Total Abstraction	**-5651**	4.04
Coramup/Wetlands Water In	530	0.38
Coramup/Wetlands Water Out	-290	0.21
Coramup/Wetlands Water Net Flow	**240**	0.17
Inflow Total (m3/d)	**-9448**	6.76
Pink Lake, Lake Warden, Windabout/Woody Lakes	**Flow (m3/d)**	**Percentage of Largest Flow**
Pink Lake Groundwater In	14330	10.25
Pink Lake Groundwater Out	-1766	1.26
Pink Lake (Direct) Precipitation	14289	10.22
Pink Lake Runoff / Quickflow In	8574	6.13
Pink Lake Evaporation	-35214	25.19
Pink Lake Net Flow	**213**	0.15
Lake Warden Groundwater In	8002	5.72
Lake Warden Groundwater Out	-4774	3.42
Lake Warden (Direct) Precipitation	9836	7.04
Lake Warden Runoff / Quickflow In	9836	7.04
Lake Warden Evaporation	-22286	15.94
Lake Warden Net Flow	**615**	0.44
Windabout/Woody Groundwater In	2431	1.74
Windabout/Woody Groundwater Out	-4498	3.22
Windabout/Woody (Direct) Precipitation	2808	2.01
Windabout/Woody Runoff / Quickflow In	5616	4.02
Windabout/Woody Evaporation	-6352	4.54
Windabout/Woody Net Flow	**6**	0.00

4.7 GROUNDWATER ABSTRACTION AND BOREFIELD OPERATION

4.7.1 Modelled Impact on Water Levels due to Abstraction

The volume that is abstracted from groundwater by the drinking water borefield and the private bores are already shown in Section 2.3.6 in Figure 24 and Figure 27 respectively. The average abstraction rate over the past 26 years is approximately 60% of the average flow entering the ocean underlining the relative magnitude of the disruption of natural groundwater flow in the coastal region.

The groundwater level time series of the 26 observation bores are shown in Figure 62 below. The calculations cover a period between 1993 and 2019. A map of the location of the monitoring bores is shown in section 4.5.7. The effect of groundwater abstraction on groundwater levels has been tested by running the model with and without abstraction. Note that the various subareas are shown in Figure 15. 'Butty' and the 'Eleven Mile' subarea are referred to as the 'Butty' subarea.

Modelling shows that groundwater abstraction (within the limits set by DWER) is significantly decreasing groundwater heads and thereby increasing the risk of saltwater intrusion in the town area, refer to Figure 63.

The twilight subarea directly south of the Pink Lake is less affected which may be attributed to the lower abstraction rates. The groundwater levels around the 4 production bores in the Butty area have declined slightly more than the area south of the Pink Lake, with the notion that the abstraction rates are high in these bores.

Furthermore, groundwater abstraction has the following effect:

- The water level in Pink Lake decreases by 0.20 m, Lake Warden decreases by 0.09 m and the Lake Windabout 0.04 m.
- A negligible effect is calculated north of the lakes.
- The decrease in groundwater levels in the 3 monitoring bores furthest to the west is between 0.10 m and 0.16 m.
- Saltwater intrusion in the Butty area is less likely due to the naturally high groundwater levels.

Future modelling including density-dependent flow and recalibration of the model should result in a larger confidence and accuracy, and provide more details on the locations that are at risk.

a) OBS Bore 07-93 Butty Canning Drive

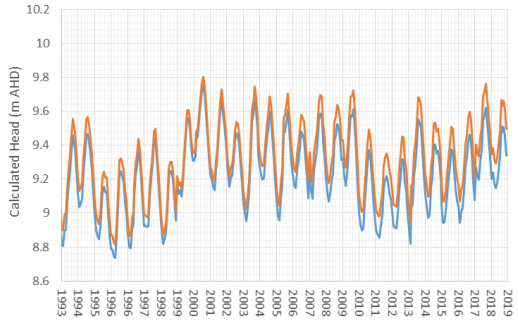

b) OBS Bore 02-13 Butty

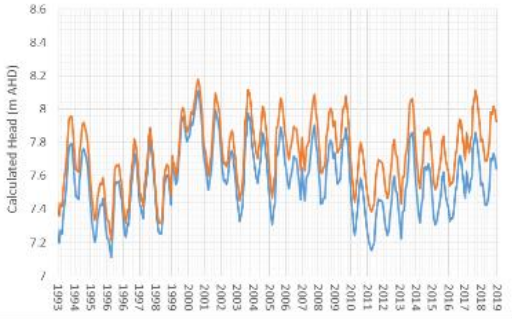

c) **OBS Bore 03-13 Butty**

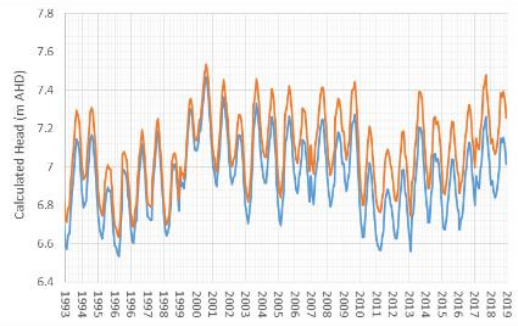

d) 60119503

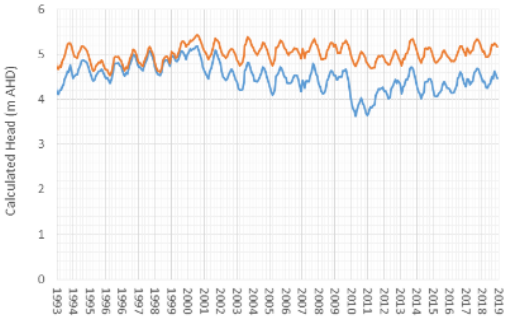

e) 60119502

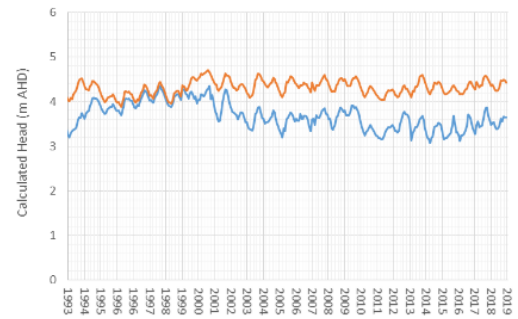

f) 60119506

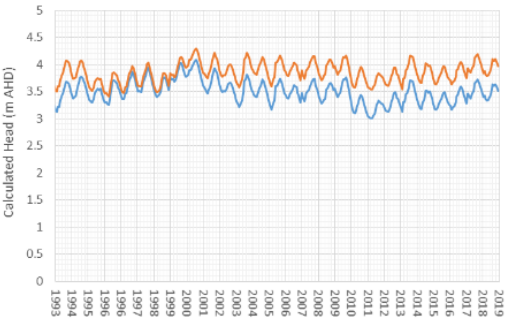

g) OBS Bore 06-93 Twilight Esperance

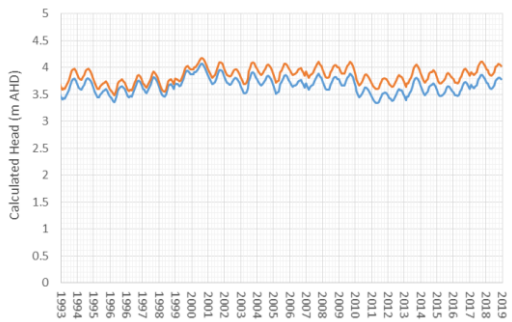

h) 6011079

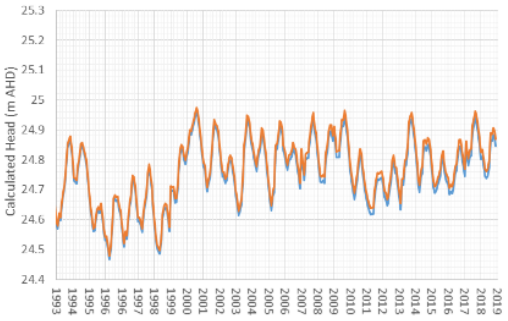

i) OBS Bore 04-93 Twilight Esperance

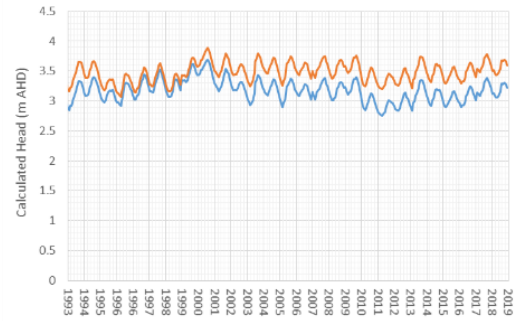

j) 60119500

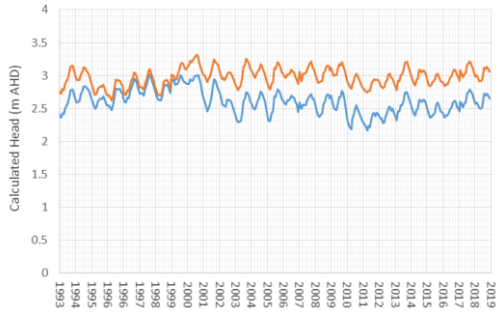

k) OBS Bore 02-93 Twilight Esperance

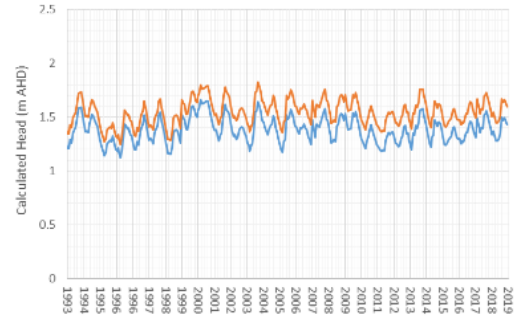

l) OBS Bore 03-93 Twilight Esperance

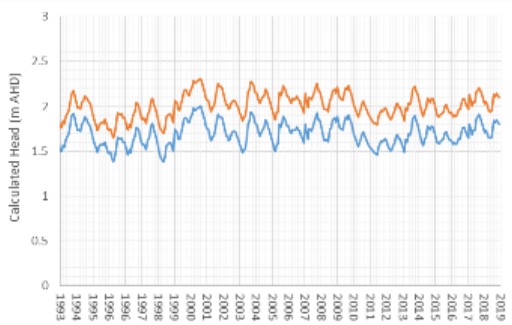

m) Esperance Tws - 7-83 / 60118029

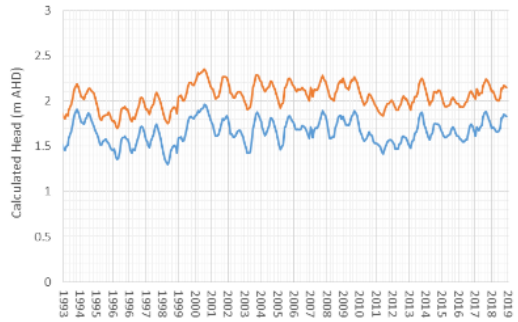

n) Esperance Tws - 4-83 / 60118026

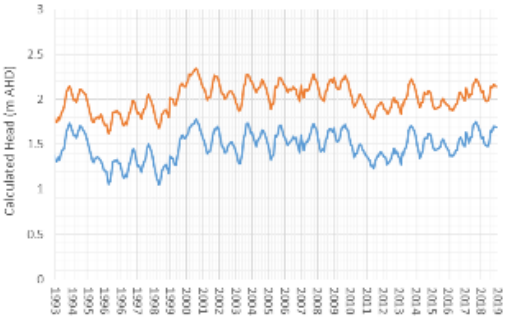

o) OBS SWIM Bore 24-97 Twilight Pink Lake

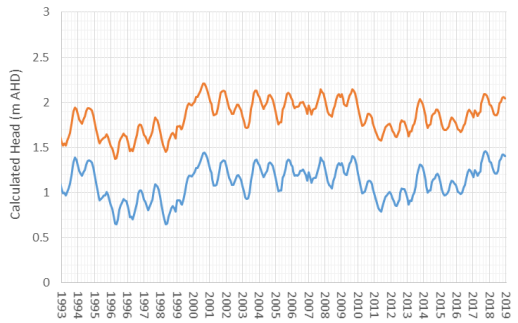

p) 60119302

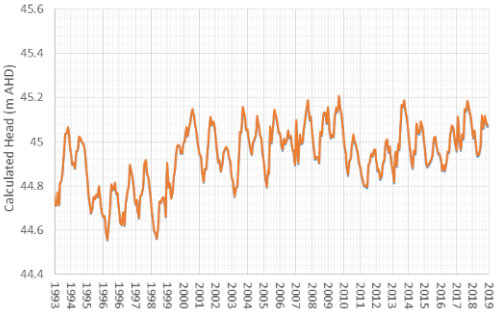

q) 6011185

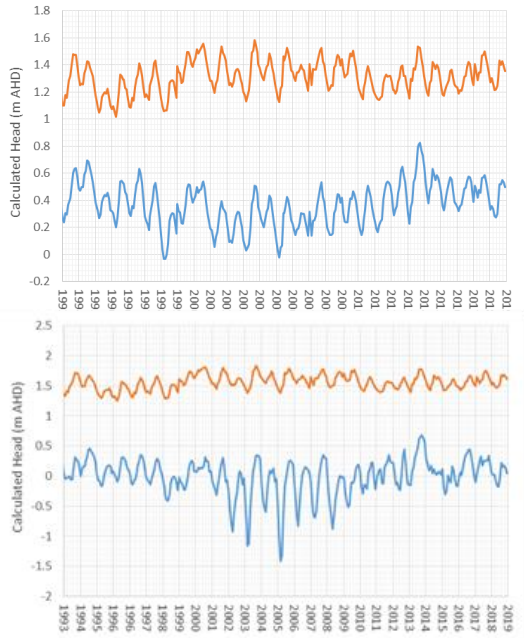

r) OBS SWIM Bore 26-97 Town

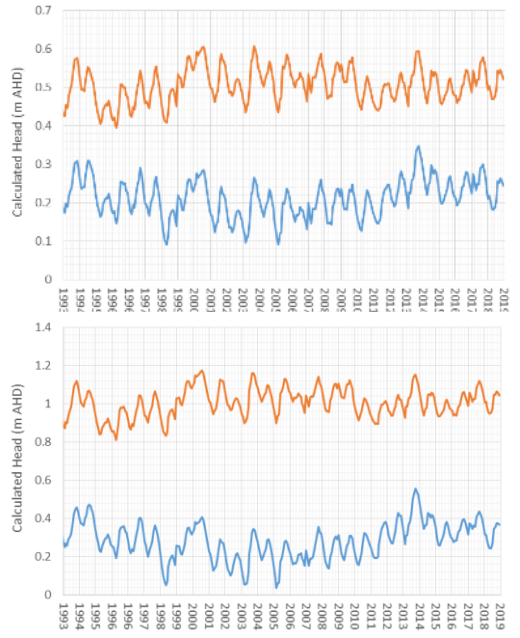

u) 6011186

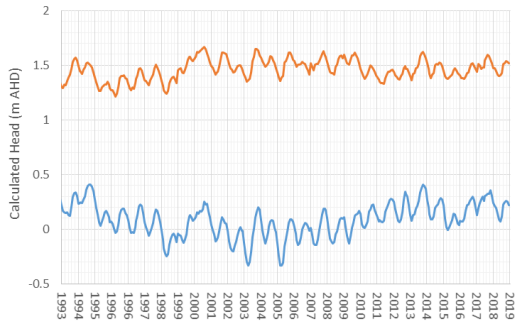

v) Esperance Monitoring Bore 8 D'Comm

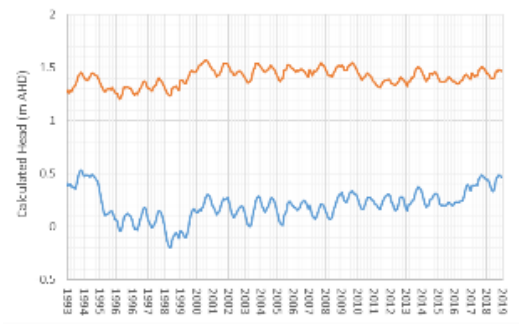

w) 601011

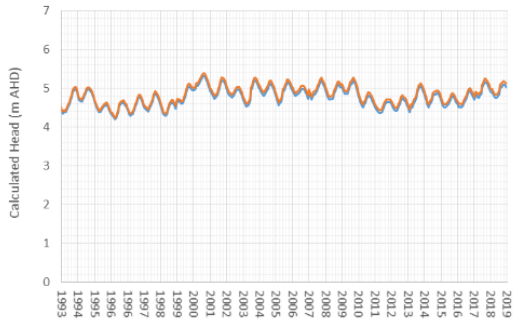

x) OBS SWIM Bore 22-97 Town Esperance

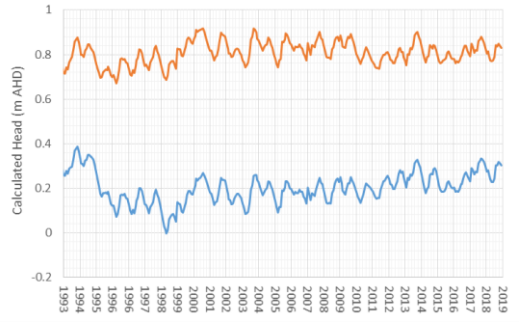

y) Esperance Monitoring Bore 7 (D'Comm)"

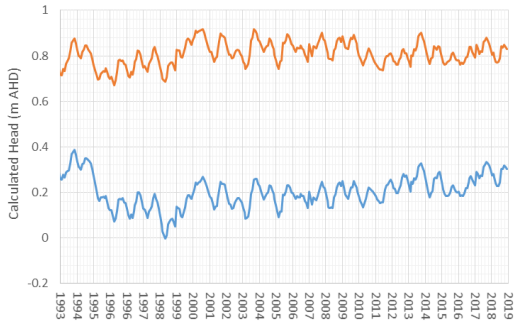

z) OBS SWIM Bore 25-97 Town Jane St

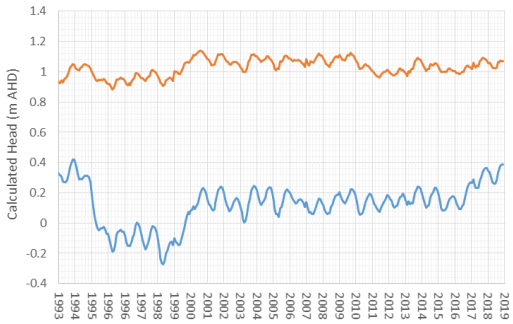

Figure 62: Time Series of Groundwater Levels between 1993 and 2019 with Pumping (Blue) and without Pumping (Orange) Arranged from West (a) to East (z)

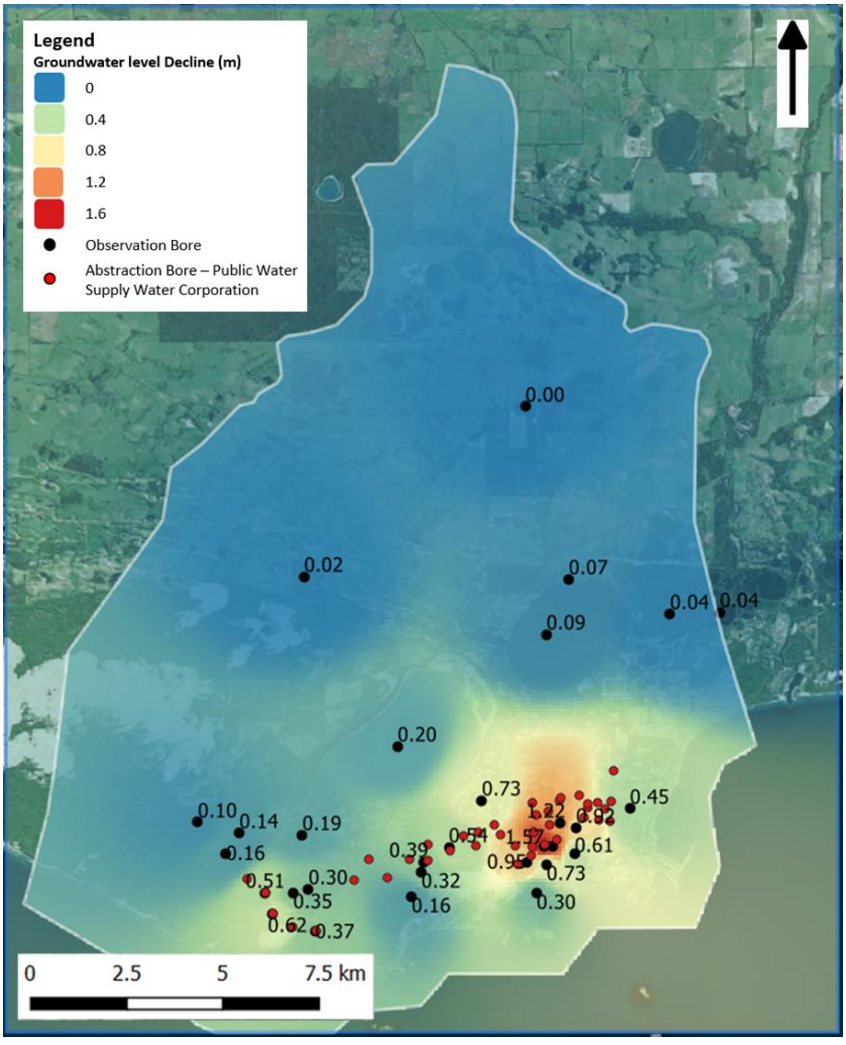

Figure 63: Modelled Absolute Effect on (Ground) Water Levels in Monitoring Bores as a Result of Historical Abstraction Rates. Interpolation with IDW with an Inverse Distance Power of 5

4.7.2 Vector Flow Fields

Figure 66 below shows the vector flow fields of groundwater in various locations and at various depths. In the left column are parts of the domain with all the bores abstracting according to the SCADA data issued by Water Corporation and estimated rates for the privately-owned bores. The right column shows the same location and layer as on the left with all the bores turned off.

Three different locations have been selected as an example: 1) around Observatory Point in the west at the most southern tip of the domain, 2) in the east slightly north of the harbour, and 3) south of the Pink Lake as shown in Figure 65.

The flows at the first location at Observatory Point are always large whether pumps are on or off, refer to Figure 66 a - j. The risk of saltwater intrusion at this location is considered low due to the relatively large head gradient towards the ocean. The Ghyben-Herzberg interface model [78] of a coastal unconfined aquifer provides more insight. This model is an idealised case where the interface between salt and freshwater is thin, the freshwater flows seawards and the saltwater is at rest. Figure 64 below shows a schematic drawing of the Ghyben-Herzberg interface model.

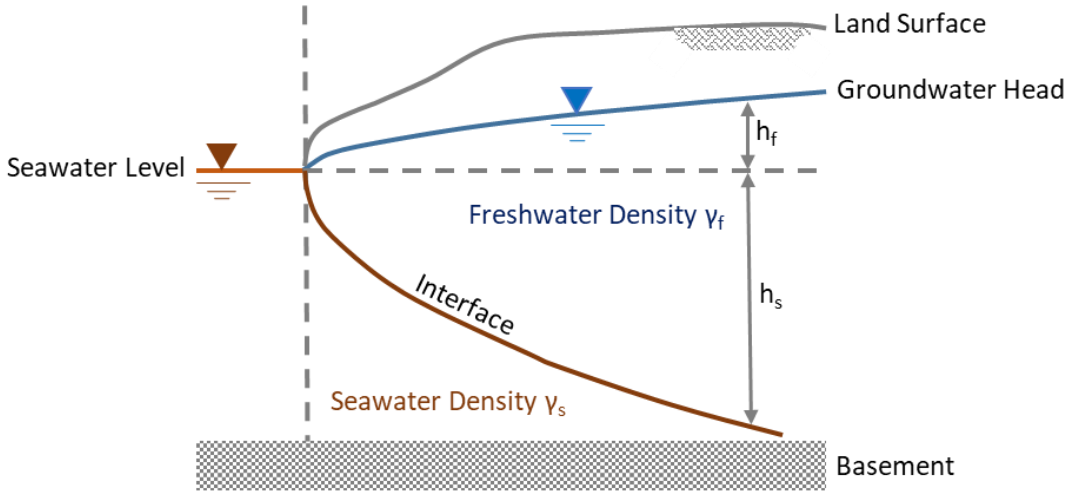

Figure 64: Ghyben-Herzberg's Interface Model

The Ghyben-Herzberg Equation can be derived by assuming the Dupuit-Forchheimer approximation of, in this case, horizontal flow in the freshwater region. The head is approximated as constant in the vertical direction. Equation 4 shows that by measuring the groundwater level relative to the seawater level the depth to the saltwater interface can be calculated. It follows that for steep groundwater head gradients, the extent of the saltwater interface is smaller.

$$h_s = \frac{\gamma_f}{\gamma_s - \gamma_f} \times h_f$$ Equation 4

Where,

- h_f is the groundwater head above sea level
- h_s is the depth of the interface below sea level
- γ_f is the density of freshwater
- γ_f is the density of seawater

Furthermore, basement outcrops accelerate the flow towards the ocean by increasing the head gradient. Note that it is assumed that the basement along the coast between Observatory Beach and 11 Mile beach further west is higher than the seawater level. This results in a higher groundwater head difference (and flow velocities) between groundwater and the ocean compared to the setup where ocean access is completely clear. The assumed basement outcrops at this location decrease the risk of seawater intrusion.

Figure 66 k – t shows that the location south of the town is at great risk of saltwater intrusion. Flows without groundwater abstraction are small and are virtually non-existent in some cells when pumping is switched on. The small head difference between land and ocean in the town subarea makes this location very susceptible to saltwater intrusion. The head difference will become more unfavourable when heads are corrected from freshwater to point water head.

Finally, Figure 66 u – ad shows that production bores affect the groundwater flow and are capturing groundwater originating from the domain below the Pink Lake. The salinity distribution is shown in Figure 42 in Section 4.2 and analysis of the raw data indicates that the TDS concentration of groundwater directly south of the Pink Lake is generally saline to hypersaline. The salinity decreases from north to south and from deep to shallow and reaches TDS concentrations that are borderline suitable for potable use (< 600 mg/L) around the screens in the twilight borefield.

The vector flow field suggests that production bores abstract saline water originating from the domain underneath the Pink Lake so that extensive recovery periods may be required. Analysis of the operation of the borefield is consistent with this observation.

Figure 66 also shows that groundwater from Lake Warden flows to the Pink Lake consistent with findings of Marimuthu [4], [26], [27], Abbot [28] and DEC [23].

Further modelling including density-dependent flow is required to obtain more details.

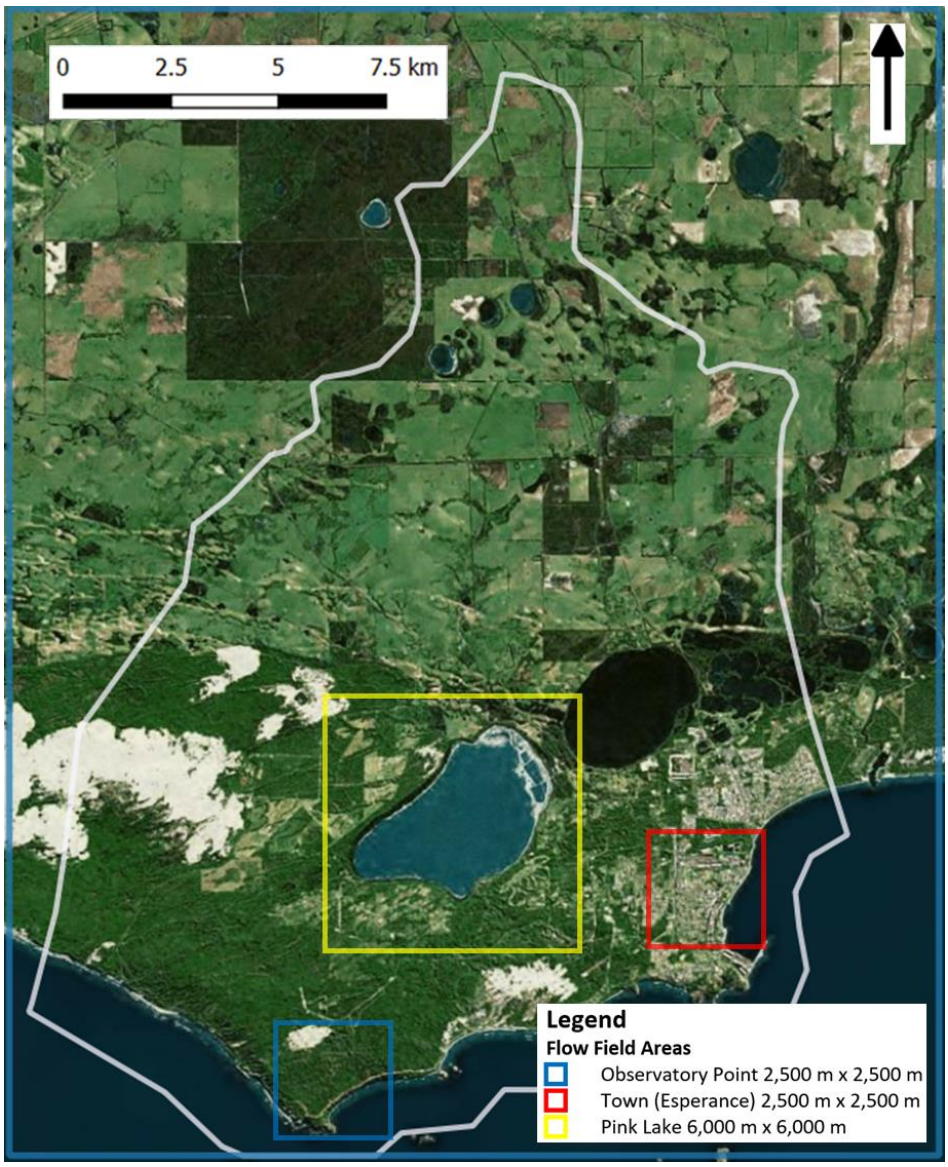

Figure 65: Locations of Flow Fields as Presented in Figure 66

a) Observatory Point: 9.1 m AHD to -0.7 m AHD

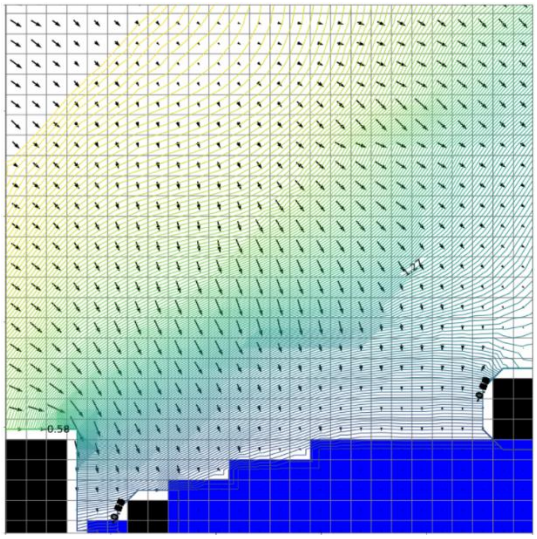

b) Observatory Point: 9.1 m AHD to -0.7 m AHD

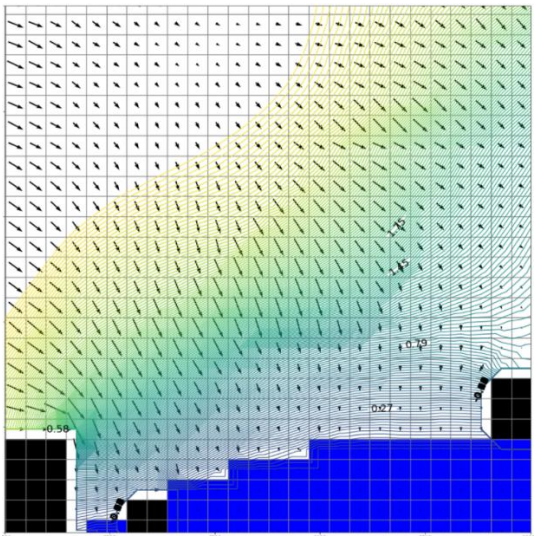

c) **Observatory Point: -0.7 m AHD to -10.0 m AHD**

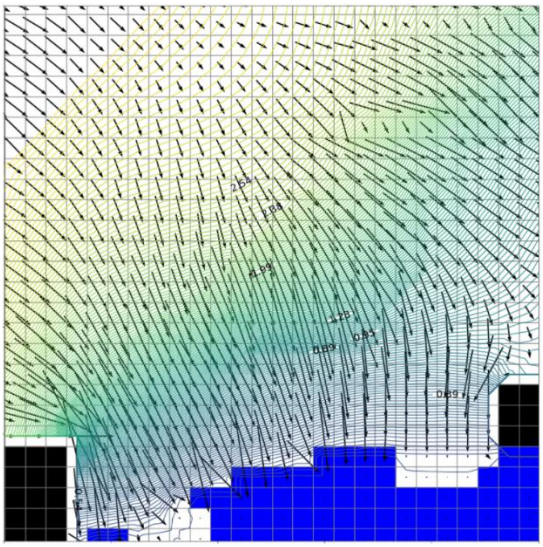

d) Observatory Point: -0.7 m AHD to -10.0 m AHD

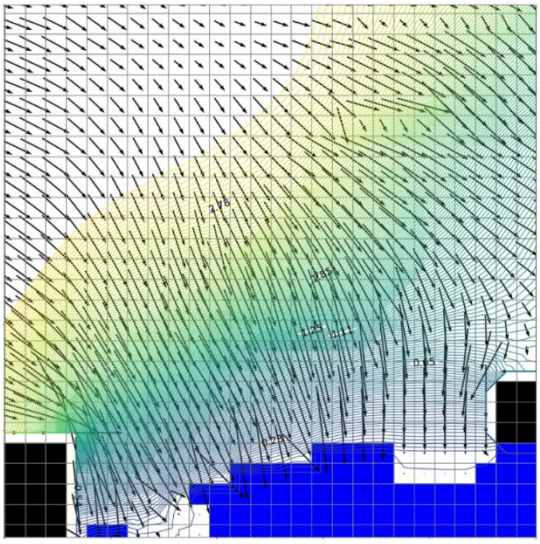

e) Observatory Point: -10.0 m AHD to -20.0 m AHD

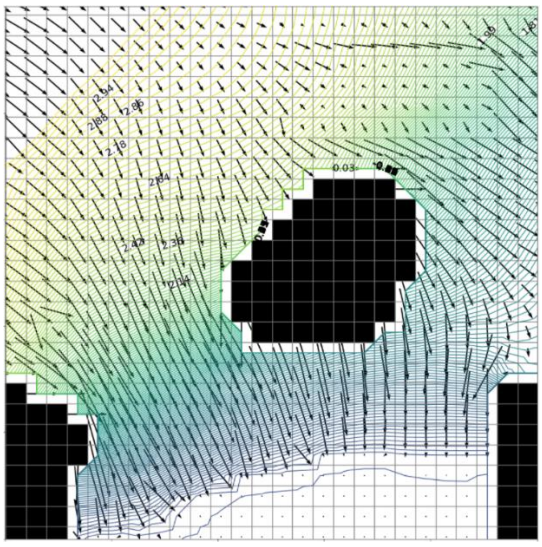

f) Observatory Point: -10.0 m AHD to -20.0 m AHD

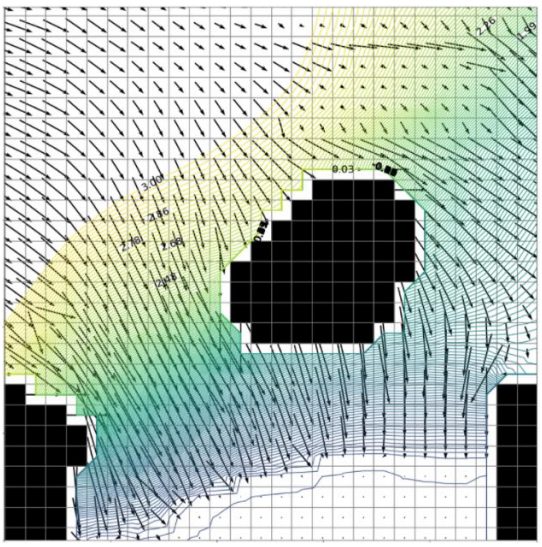

g) Observatory Point: -20.0 m AHD to -30.0 m AHD

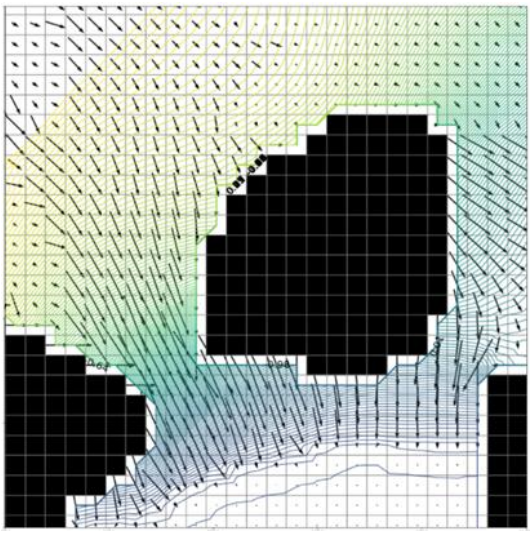

h) Observatory Point: -20.0 m AHD to -30.0 m AHD

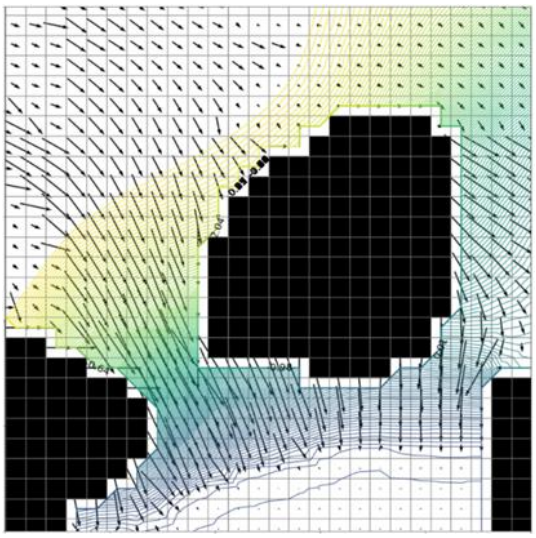

i) Observatory Point: -30.0 m AHD to -40.0 m AHD

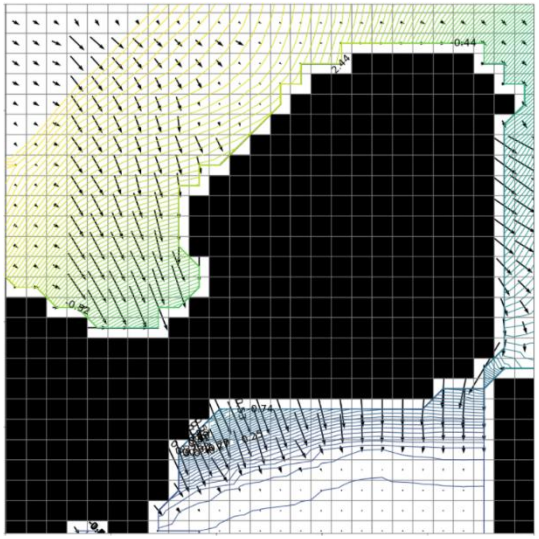

j) Observatory Point: -30.0 m AHD to -40.0 m AHD

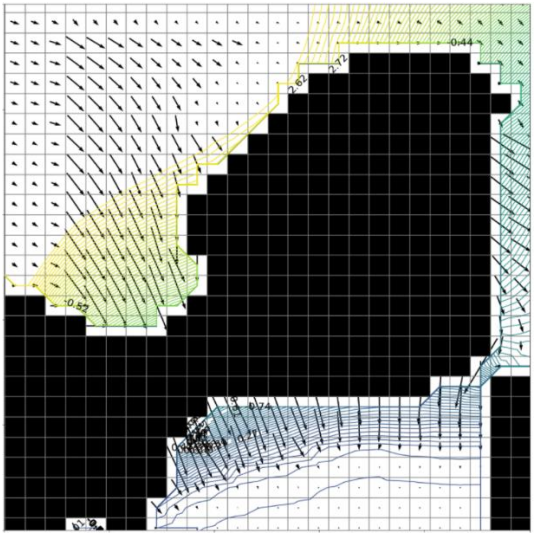

k) Town: 9.1 m AHD to -0.7 m AHD

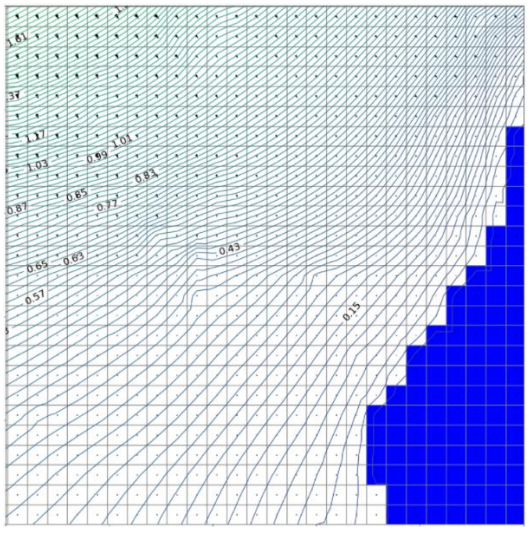

l) Town: 9.1 m AHD to -0.7 m AHD

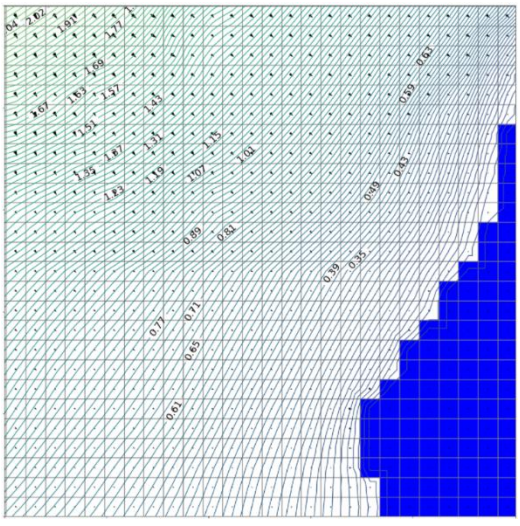

m) Town: -0.7 m AHD to -10.0 m AHD

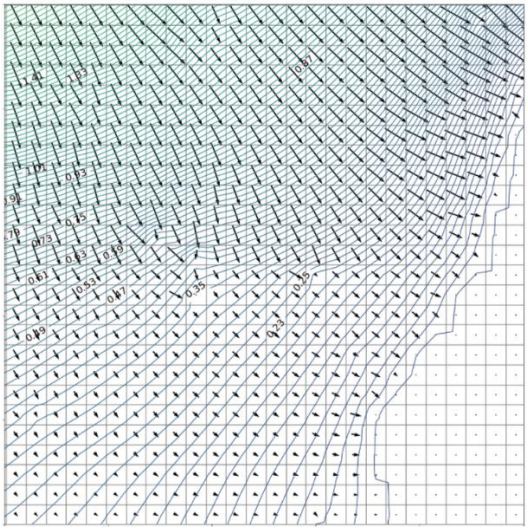

n) Town: -0.7 m AHD to -10.0 m AHD

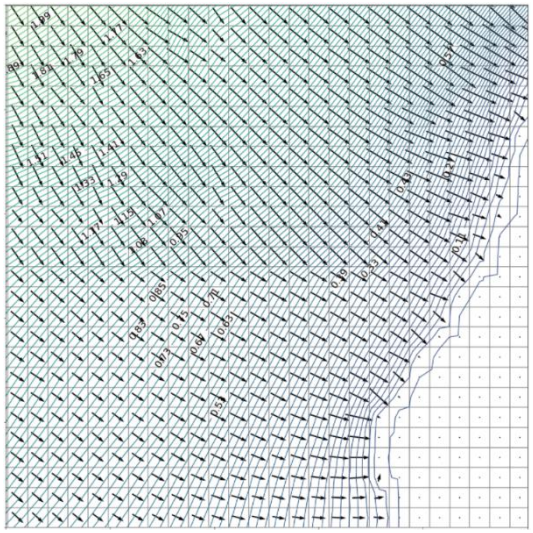

o) Town: -10.0 m AHD to -20.0 m AHD

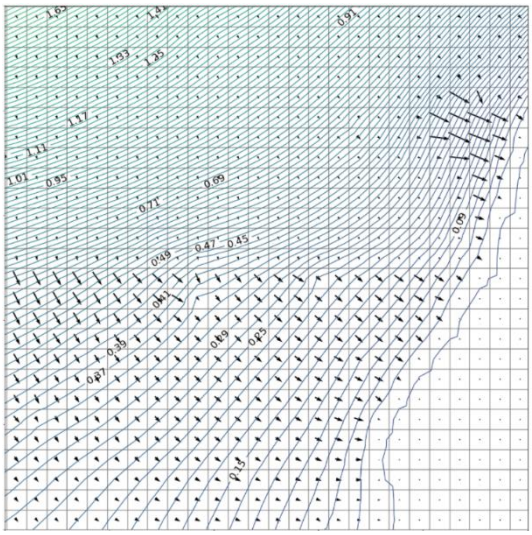

p) Town: -10.0 m AHD to -20.0 m AHD

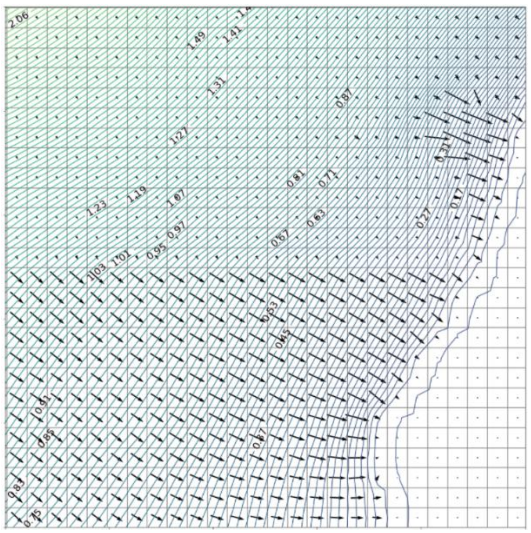

q) Town: -20.0 m AHD to -30.0 m AHD

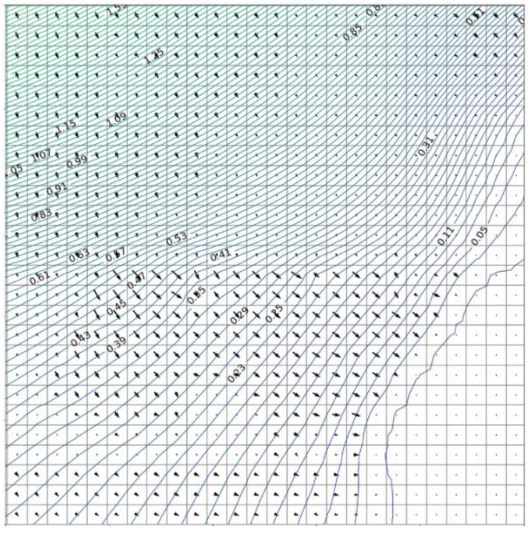

r) Town: -20.0 m AHD to -30.0 m AHD

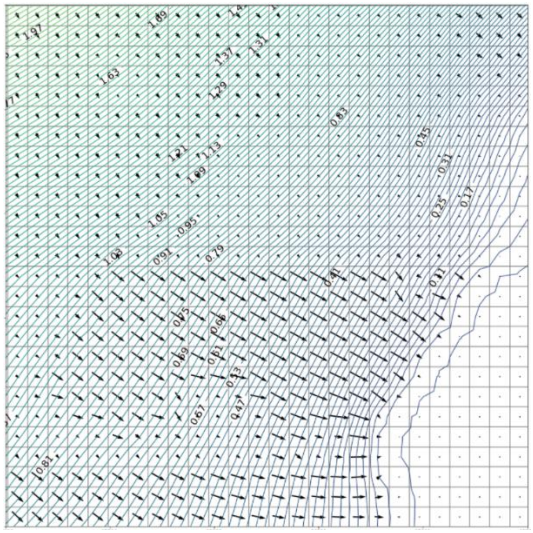

s) Town: -30.0 m AHD to -40.0 m AHD

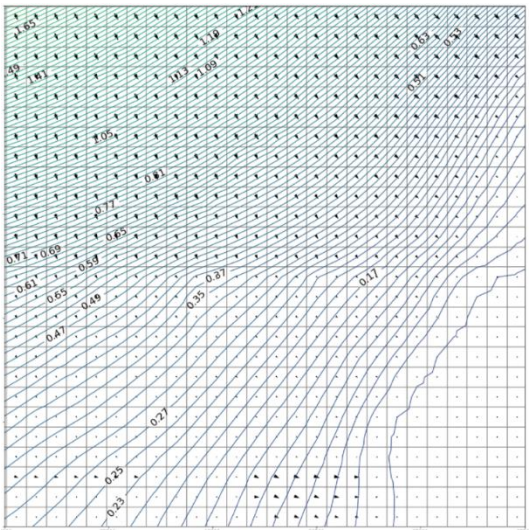

t) Town: -30.0 m AHD to -40.0 m AHD

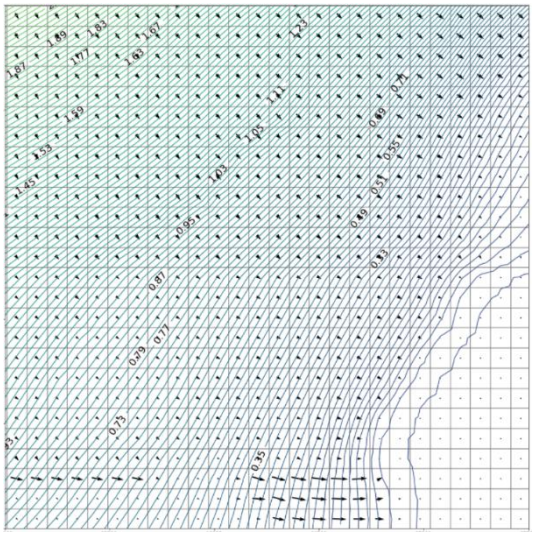

u) Pink Lake: 9.1 m AHD to -0.7 m AHD

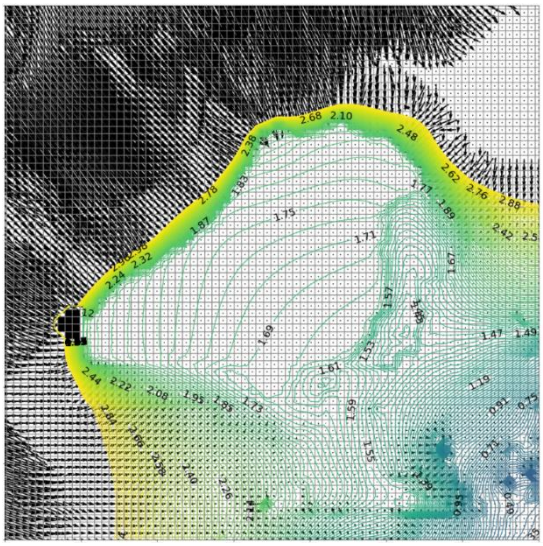

v) Pink Lake: 9.1 m AHD to -0.7 m AHD

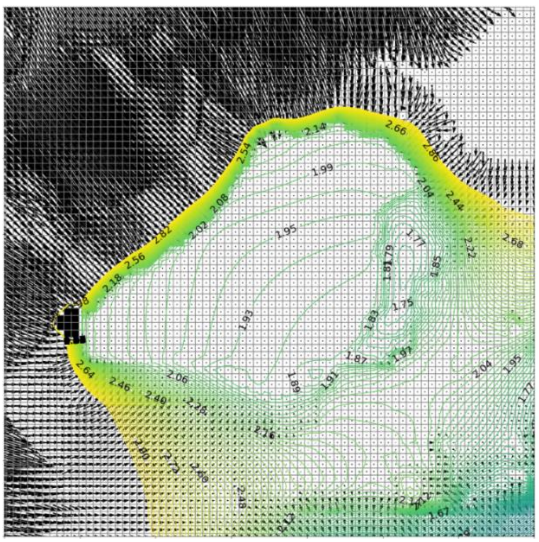

w) Pink Lake: -0.7 m AHD to -10.0 m AHD

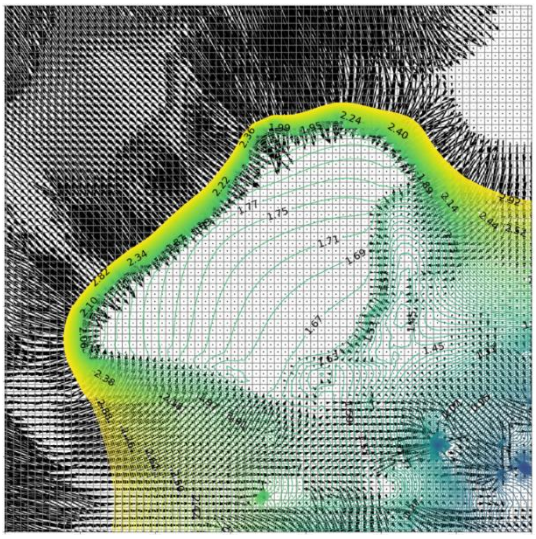

x) Pink Lake: -0.7 m AHD to -10.0 m AHD

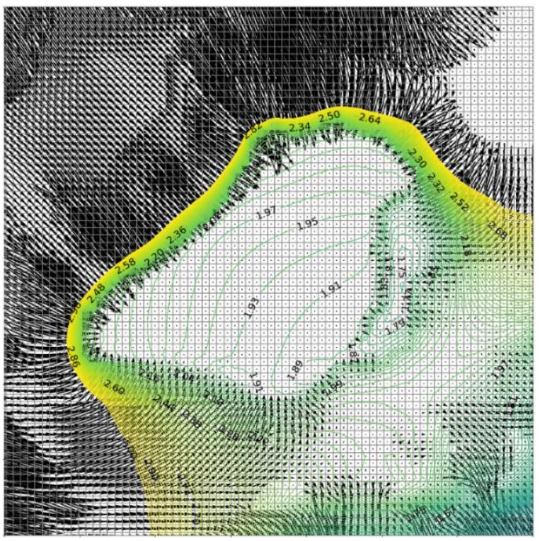

y) Pink Lake: -10.0 m AHD to -20.0 m AHD

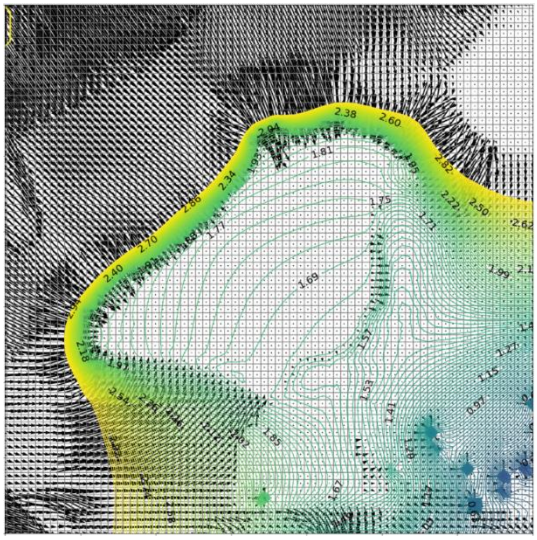

z) Pink Lake: -10.0 m AHD to -20.0 m AHD

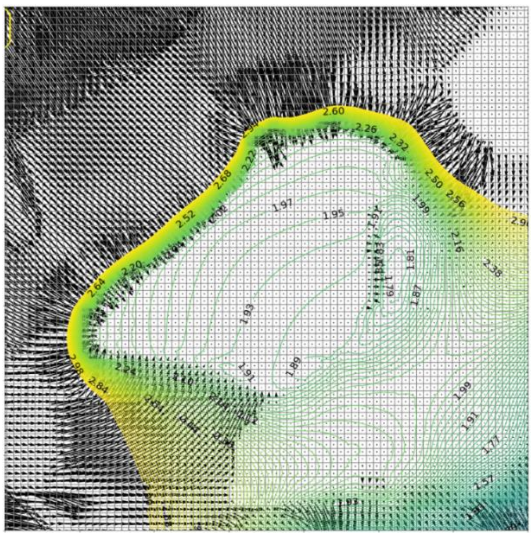

aa) Pink Lake: -20.0 m AHD to -30.0 m AHD

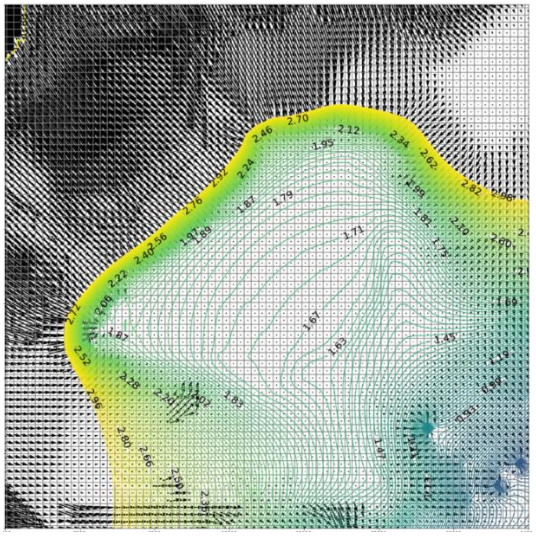

ab) Pink Lake: -20.0 m AHD to -30.0 m AHD

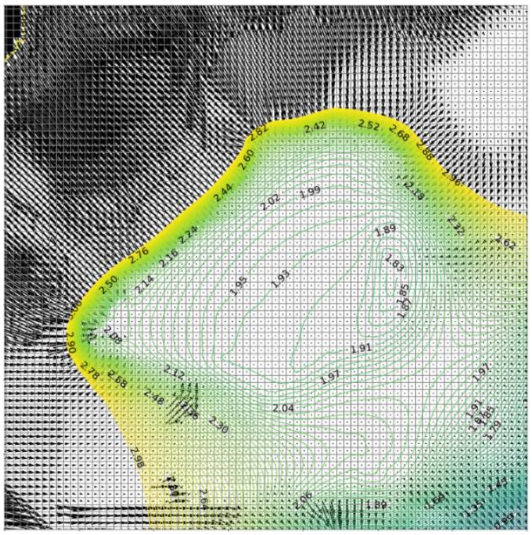

ac) Pink Lake: -30.0 m AHD to -40.0 m AHD

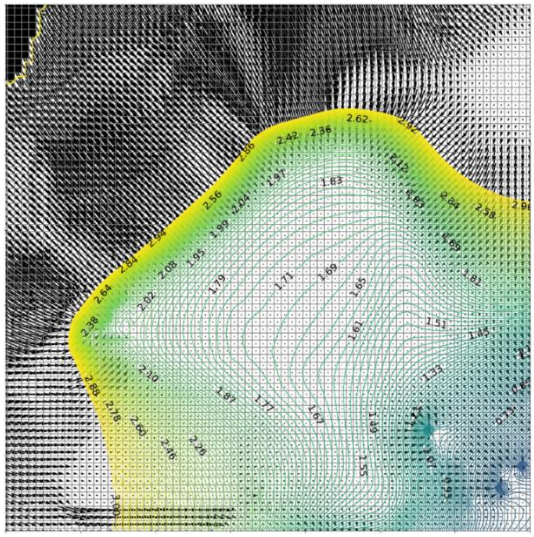

ad) Pink Lake: -30.0 m AHD to -40.0 m AHD

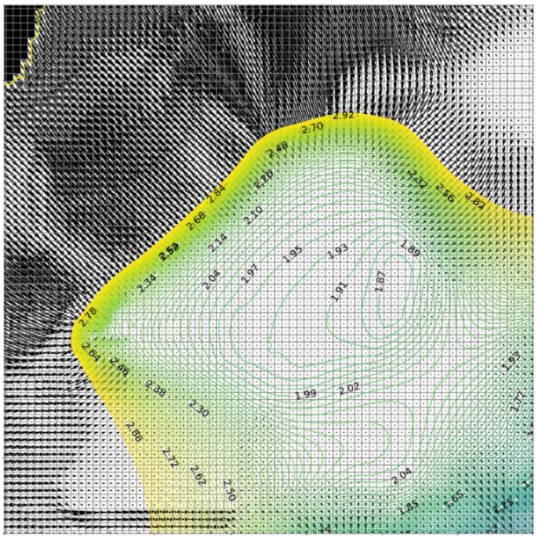

Figure 66: Simulated Flow Vector Fields of Various Layers in November 2018. Left Column: Pumping. Right Column: No Pumping. Contour Plots from -1 m AHD (Purple) to +3 m AHD (yellow). Same Scaling of Vectors in all figures. Blue represents Constant Head (Ocean). Black Represents No Inactive Grid (Basement). Lines with Numbers Represent Piezometric Isolines in m AHD.

4.7.3 Production Borefield Design and Past Operation

Groundwater abstraction by bores with screens near or in the saltwater interface (if present at the location) may result in upconing, saline water uptake and disturbance of the otherwise stationary saline water layer. The salinity analysis for this study has confirmed that the TDS concentrations increase with depth as expected. Saline water is expected to accumulate in the Pallinup layer due to lower flow velocity and a larger surface area for binding ions per unit volume. Potable water abstraction is targeted from the Quaternary layer.

The screen depth and the local depth of the quaternary aquifer is important design features to prevent saline water abstraction and disturbance of the interphase.

Table 12 presents the screen depths and the depth from the bottom of the screen to the Pallinup layer. Most of the screens entirely or almost entirely span across the Quaternary layer.

It is hypothesised that part of the saline water abstraction and interface disturbance in the Esperance aquifer may have been avoided if screens were installed more shallow.

Other measures are reducing abstraction rates and more evenly distributing the production volumes over the bores (if possible for mechanical reasons). In case the water demand allows, the use of less productive (saline water producing) bores may be omitted altogether to avoid disturbance of the saline water interface. Bore production rates are discussed below.

Table 12 - Production Bores Screen Depths and Distance to Pallinup Layer. Bores Arranged from West to East (Green Bores: East; Pink Bores: South of Pink Lake; Blue Bores: Between Pink Lake and Lake Warden; Yellow Bores: Town Area/South Lake Warden)

West

East

Bore (WC Naming)	Coordinates (Easting)	Coordinates (Northing)	TOC (AHD)	Screen Length (m)	Max Depth (Rel. AHD)	Distance Screen to Pallinup (m)	
Bore 01-13 (44)**	387277	6251002	37.82	9	-27.18	-3.52	West of Pink Lake
Bore 29-97 (43)	387753.4	6250661	37.4	9	-27.3	0.55	
Bore 32-97 (42)	387947.2	6250114.2	30.8	8.7	-26.4	0.6	
Bore 28-97 (41)	388463.4	6249774.4	17.9	5.7	-26.8	-5.34	
Bore 27-97 (40)	389061.8	6249672.8	9.8	5.7	-24.9	-7.84	South of Pink Lake
Bore 03-85 (34)	390034.6	6250968.8	8.59	22.32	-16.51	6.75	
Bore 02-85 (33)	390412.9	6251523.8	9.12	11.8	-8.68	14.9	
Bore 01-85 (32)	390888.9	6251045.3	22.87	24.3	-17.13	9.87	
Bore 10-83 (31)	391475.7	6251508.4	6.45	12	-11.37	16.34	
Bore 08-83 (30)	391935.1	6251907.1	14.2	14.7	-10.4	1.74	
Bore 01-88 (36)	391946.5	6251493.8	17	10.7	-9.1	6.35	
Bore 02-88 (35)	392515.2	6251743	20.02	21.3	-9.78	9.25	
Bore 09-83 (28)	392880	6252121.3	8.33	14.53	-12.2	6.96	
Bore 11-83 (29)	393183.3	6251866.1	10.4	15	-12.9	10.58	
Bore 03-83 (27)	393242.7	6252230.2	13.89	3.8	-17.91	4.42	
Bore 02-83 (26)	393653	6252396.9	7.27	12.1	-23.03	-6.08	Between
Bore 01-83 (25)	393827.9	6252164.4	7.07	12.4	-23.73	-7.25	
Bore 04-91 (38)	394212	6251868.7	7.89	5.4	-16.01	0.63	South of Lake Warden
Bore 05-91 (39)	394254.2	6251381.3	14.59	5.8	-16.51	3.96	
Bore 10-00 (24)	394628	6251609.5	15.53	42	-54.77	-38.65	
Bore 71-80 (23)	394651	6251843	6.9	6.2	-15.2	-0.09	
Bore 13	394661.2	6252972.1	7.34	5	-10.16	0.9	
Bore 01-08 (37)	394676	6252234	8.26	6	-10.14	4.51	
Bore 10-01 (12)	394732.3	6252679	7.29	11.7	-15.71	-4.71	
Bore 09-01 (22)	394967.3	6251908.2	12.47	12	-17.73	-0.23	
Bore 31-97 (10)	395055	6252766	8.63	15.06	-18.57	-3.87	
Bore 01-91 (9)	395106	6252423	7.5	5.9	-10.8	3.82	
Bore 11-00 (21)	395291.2	6252023.8	17.759	12	-20.541	-10.281	
Paine Rd Bore 17*	395339	6253042.5	7.9	3.378	-10.794	-3.374	
Paine Rd Bore 18*	395377	6253100.5	7.83	4.877	-13.76	-6.49	
Bore 01-00 (15)	395856.7	6253162.6	7.41	11.8	-12.79	-1.44	
Bore 11-01 (5)	395990	6252608	10.62	11.7	-14.38	-0.59	
Paine Rd Bore 19*	396066	6252866.5	7.06	4.876	-14.428	-0.248	
Bore 6A-80 (6)	396075.8	6252948.9	8.3	6.1	-13	1.07	
Bore 09-00 (3)	396330	6252986	7.82	12	-17.68	-2.01	
Bore 4A-80 (4)	396361	6252524	6.63	6.1	-11.67	-1.53	
Paine Rd Bore 14*	396511	6252817.5	7.11	5.03	-9.883	5.677	
Paine Rd Bore 1*	396636	6252492.5	6.9	5.029	-9.407	7.233	
Bore 2A-80 (2)	396666	6253023	6.02	6.1	-15.28	2.92	
Paine Rd Bore 16*	396741	6253795.5	9.425	6	-14.575	2.425	

* Decommisioned (Original Screen Depth Unknown)

** Screendepth assumed

Table 13 shows the monthly production of bores on 16 different snapshots in time between 2004 and 2019 in winter (month 6) and in summer (month 12). The bores are organised from the west (at the top) to east (at the bottom).

Bores that are consistently producing relatively large volumes are located in the west of the borefield (marked green) while bores directly south of the Pink Lake (marked pink) are less productive. Note that Bore 44 (far west) was installed in January 2013 and has been producing large volumes since. Productive bores are also located in the town area (marked yellow) although, for unknown reasons, other bores in the town subarea are not productive.

4.7.4 Preferred Abstraction Location

Operationally, the four bores installed furthest to the west are consistently producing large volumes. This location is preferred over the other locations in the domain for the following reasons:

- The presence of an inland saltwater wedge is unlikely due to the higher head gradient from the aquifer towards the ocean
- It is proposed (and modelled in this study) that the basement directly south of these bores, between Observatory Point and the west of the subcatchment, is higher than sea level. As such the presence of a saltwater wedge within the aquifer is unlikely. Geological investigations should determine the existence of the elevated basement. Saline groundwater distribution analysis supports this proposal.
- Saltwater intrusion is unlikely even in case for relatively large abstraction rates (rates to be tested by modelling). The relative gradient of the head between the land and ocean just east of Observatory Point and the resulting large flows should prevent saltwater intrusion.
- Saline groundwater is present everywhere else in the domain. Saline water originates from the Coramup Creek, groundwater regional inflow from the Esperance hinterland and the Ocean in the southeastern part of the domain where small head gradients are prevalent in the southeastern part of the domain.

Future expansion of the borefield should be targeted to locations in the southwest of the subcatchment. Furthermore, to avoid disturbance of the saltwater / freshwater interface, a shallow installation of screens is preferred and should be tailored to the local groundwater cone of depression (drawdown).

Table 13 – Groundwater Abstraction of Water Corporation Production Bores (Green: > 100 m^3/d; Yellow: 10 to 100 m^3/d; Red: < 10 m^3/d). Bores Arranged from West to East (Green Bores: East; Pink Bores: South of Pink Lake; Blue Bores: Between Pink Lake and Lake Warden; Yellow Bores: Town Area/South Lake Warden)

	Year / month	2004	2004	2006	2006	2008	2008	2010	2010	2012	2012	2014	2014	2016	2016	2018	2018	1993 - 2019	
	Bore (WC Naming)	6	12	6	12	6	12	6	12	6	12	6	12	6	12	6	12	Historical Performance Ranking	
West	Bore 01-13 (44)	0	0	0	0	0	0	0	0	0	0	0	0	0	223	416	489	34	West of Pink Lake
	Bore 29-97 (43)	207	354	268	412	334	495	874	960	289	75	348	418	58	277	280	295	6	
	Bore 32-97 (42)	338	513	303	402	222	296	336	295	0	231	476	586	337	622	408	179	4	
	Bore 28-97 (41)	320	544	274	483	255	372	450	488	91	199	404	491	268	507	154	424	3	
	Bore 27-97 (40)	42	476	0	374	170	164	73	201	158	240	1	2	139	123	23	13	14	South of Pink Lake
	Bore 03-85 (34)	0	95	0	140	0	33	143	237	98	127	65	56	1	97	21	26	29	
	Bore 02-85 (33)	6	73	44	0	0	17	1	0	5	0	0	0	0	0	0	0	36	
	Bore 01-85 (32)	60	13	49	180	0	104	123	76	34	101	14	186	135	46	0	49	28	
	Bore 10-83 (31)	7	73	0	0	0	21	55	0	90	0	0	2	1	2	0	36	30	
	Bore 08-83 (30)	51	72	24	45	46	66	67	0	68	10	6	8	55	68	24	66	25	
	Bore 01-88 (36)	9	157	39	154	0	134	157	0	137	107	15	1	124	178	1	0	24	
	Bore 02-88 (35)	9	91	58	50	0	186	62	5	112	40	0	0	177	60	99	0	20	
	Bore 09-83 (28)	62	85	33	84	44	65	25	67	34	16	71	44	14	49	56	77	26	
	Bore 11-83 (29)	4	40	27	20	56	79	80	49	72	70	7	108	1	61	27	75	23	
	Bore 03-83 (27)	0	84	0	0	0	0	0	0	0	0	0	0	1	0	0	0	32	
	Bore 02-83 (26)	206	291	178	282	174	245	270	309	251	343	243	324	0	0	0	190	9	Between
	Bore 01-83 (25)	195	285	184	358	183	243	287	337	256	49	173	94	272	366	280	344	7	
	Bore 04-91 (38)	94	50	83	150	66	105	161	204	59	221	180	13	152	198	71	130	19	South of Lake Warden
	Bore 05-91 (39)	152	247	134	265	120	179	72	256	119	309	1	0	0	174	102	192	16	
	Bore 10-00 (24)	355	622	275	480	315	455	0	548	35	639	156	48	432	504	329	269	2	
	Bore 71-80 (23)	403	620	311	587	351	497	0	0	39	610	226	576	431	579	315	337	1	
	Bore 13	0	69	4	26	95	113	0	0	46	117	30	0	0	43	0	0	27	
	Bore 01-08 (37)	0	0	0	0	0	0	148	4	100	25	156	179	1	153	79	95	33	
	Bore 10-01 (12)	6	278	3	540	206	322	0	474	14	51	60	324	0	1	1	136	15	
	Bore 09-01 (22)	8	502	0	436	180	230	81	6	91	172	270	24	3	280	108	160	13	
	Bore 31-97 (10)	211	347	0	354	68	23	0	335	45	99	253	131	203	217	98	171	11	
	Bore 01-91 (9)	128	207	117	216	43	20	169	1	130	252	180	16	148	203	77	152	18	
	Bore 11-00 (21)	308	447	200	365	230	391	0	485	30	567	35	480	330	417	166	335	5	
	Paine Rd Bore 17*	0	0	0	0	0	0	0	0	0	0	0	0	0	0	0	0	38	
	Paine Rd Bore 18*	0	0	0	0	0	0	0	0	0	0	0	0	0	0	0	0	32	
	Bore 01-00 (15)	25	367	269	412	203	338	3	7	250	0	0	0	1	6	1	34	21	
	Bore 11-01 (5)	0	272	0	0	0	0	0	0	0	0	0	0	0	0	0	0	22	
	Paine Rd Bore 19*	0	0	0	0	0	0	0	0	0	0	0	0	0	0	0	0	40	
	Bore 6A-80 (6)	27	199	127	366	260	50	0	628	193	455	59	133	0	119	0	267	8	
	Bore 09-00 (3)	40	421	340	466	275	427	1	514	245	379	3	537	0	131	0	306	10	
	Bore 4A-80 (4)	17	86	44	232	0	37	3	7	176	0	67	438	0	93	1	259	17	
	Paine Rd Bore 14*	1	9	0	0	0	0	0	0	0	0	0	0	0	0	0	0	37	
	Paine Rd Bore 1*	0	0	0	0	0	0	0	0	0	0	0	0	0	0	0	0	39	
	Bore 2A-80 (2)	23	351	246	266	4	364	3	2	85	293	85	452	1	76	6	248	12	
East	Paine Rd Bore 16*	0	0	0	0	0	0	0	0	0	0	0	0	0	0	0	0	35	

* Decommisioned

Chapter 5: Summary and Conclusions

5.1 INTRODUCTION

The Esperance drinking water aquifer is a vital source for drinking water and irrigation. DWER has issued sustainable annual abstraction rates for subareas that limit the volume that is abstracted from the aquifer. Although the abstraction rates do not exceed the limits set by DWER, saltwater intrusion from the ocean and inland sources is limiting the abstraction rates in bores located in certain areas. The sections below summarise the findings and conclusions of the research questions presented in Section 1.6.

5.2 DEVELOPMENT OF A NUMERICAL GROUNDWATER MODEL

A database with hydrological and geological information was created as part of the study that served as input for the numerical groundwater flow model MODFLOW. Timeseries of rainfall, evapotranspiration, population size and groundwater abstraction covering nearly 120 years were included. Existing bore logs in the region surrounding the Esperance subcatchment were collected and geological layer types were identified. All groundwater observations in the subcatchment from 1990 to 2019 and groundwater abstraction rates from 1993 to 2019 were collected, cleaned and filed in a monthly time step.

A literature review of the area was conducted with a focus on relevant numerical studies on saltwater intrusion in general and locally on geology, hydrology, and inland sources of salinity. The distribution of saline groundwater in the subcatchment was analysed by using bore observations and 3D data from the AEM survey in 2013. The insights of this review were used to build the hydrogeological finite-difference flow model.

QGIS in combination with Python scripting was used as a data processing tool to create a 3D geological model. The statistical processing tool PyKrige was used to elucidate the geology by applying a 3D universal (regression) Kriging algorithm. Both AEM data and bore log data were used as input.

The geological model was converted into a rectilinear MODFLOW model with approximately 270,000 active cells. The total domain was 30 layers, 275 rows and 223 columns of 9.7 x 96 x 96 m. The model was developed to be compatible with SEAWAT to allow for future inclusion of saltwater intrusion modelling by using the LPF flow package and the SMS solver from MODFLOW-USG.

Notably, lakes should not be modelled as a forcing if the dynamic behaviour of saline water has to be simulated. Decline in the lake stage due to groundwater abstraction can only be computed if the lakes are modelled as an integral part of the hydrology. Due to the incompatibility of SEAWAT with the LAK package, lake water cells were modelled with a very high hydraulic conductivity and a storage coefficient of nearly 1. A lakebed was applied to create a leaky barrier between lake water and aquifer. This setup proved to adequately simulate the hydrologic behaviour of the lakes.

The model was calibrated to match groundwater head and lake stage observations for 22 parameters with PEST++ to a reasonable accuracy. Manual adjustments of parameters were required to obtain a model in which the water balance is in equilibrium when averaged over several seasons (doesn't lose water when simulations are extended to make predictions).

Parameter statistics with GENLINPRED and IDENTPAR showed high identifiability for runoff/quickflow parameters to the lakes, the recharge and hydraulic conductivity. The runoff/quickflow parameters are highly sensitive and required to model the seasonal water level fluctuations in the lakes.

Somewhat surprisingly, the model parameters that were not identifiable are the lakebed resistances, storage coefficients and groundwater regional inflow. Explanations are summarised below.

In case of lakebed resistance, the monthly time steps of the model may be too large in comparison to the lag time between the lake stage and groundwater head.

Soil storage coefficients, in most models important to simulate seasonal head variations, are likely not identifiable here due to the dominating and antagonistic evaporation and recharge fluxes combined with the highly sensitive evaporation and recharge multipliers.

The magnitude of the regional inflow may be selected too small so that its effect is masked by other fluxes, mainly recharge.

5.3 EXTENT OF SALINE GROUNDWATER IN THE SYSTEM AND SOURCES

Salinity is widely distributed in the subcatchment due to the transportation of hyposaline to saline water by creeks to the central hydrological suite. Evaporation of surface water concentrates these salts so that salinity increases along the chain of lakes from saline in Lake Windabout to hypersaline in the terminal Pink Lake. According to literature, Lake Warden and the Pink Lake is only connected by groundwater flow whereas Wheatfield, Woody and Windabout are also connected by surface water and groundwater. Lake Windabout and Lake Warden are connected by groundwater and in wet winters by surface water during overflow events.

Borewater observations and features in the topology indicates that saline groundwater flows from the north to south and enters the subcatchment. A thin (~10 m to ~20 m thick) freshwater layer is common in the subcatchment. In the southwest of the subcatchment a thicker freshwater lens is detected by AEM.

5.4 MAJOR HYDROGEOLOGICAL AND HYDROLOGICAL CONNECTIONS AND FLOWS

Modelling suggests that rainfall and evapotranspiration control fluctuations in groundwater heads while the annual net contribution to the water balance of these fluxes is low. Over the past 26 years, the groundwater abstraction rates (~5,700 m^3/d) are 15.7 times larger than the groundwater net recharge (~360 m^3/d), where net recharge is calculated as recharge minus evapotranspiration. However, small variations in recharge (without evaporation subtracted) can have a large effect on the relative abstraction rates since the magnitude of recharge (without evaporation subtracted) is about 25 times the abstraction.

The general groundwater trends are reproduced in agreement with the conceptual models and previous numerical modelling of the aquifer. Lakes are connected by groundwater flow that is generally directed from the wetlands in the east to the terminal Pink Lake in the centre of the subcatchment. North to south groundwater flow field originating from precipitation in the subcatchment and groundwater inflow (regional inflow) in the north agree with the existing conceptual models.

Net groundwater flow enters the Pink Lake and Lake Warden while the evaporation exceeds the precipitation giving rise to hypersalinity. Runoff/quickflow is added to

direct precipitation and contributes 38% and 50% of the freshwater inflow for the Pink Lake and Lake Warden respectively.

The much less saline lake Windabout and Woody Lakes net lose water to the subsurface as the inflow from precipitation and runoff/quickflow (contributing 67% of the freshwater inflow) exceeds the evaporation. The Windabout and Woody lakes net contribute to groundwater in summer and receive a small amount of net groundwater in winter.

Coramup Creek delivers water to the Woody Lakes system and groundwater all year although slightly more in summer. The net contribution of the Coramup Creek is small (5 %) compared to the abstraction rates (~5,700 m^3/d) and the smallest of the net flows in the domain (~240 m^3/d).

On average over the last 26 years, the ocean receives a net flow of ~8,200 m^3/d which is the largest net flow (leaving) in the domain.

Regional inflow, groundwater entering in the north of the domain, is the second-largest net flow in the domain. However, this flow was unidentifiable by the PEST++ calibration for reasons that are not fully understood. It may be that the upper and lower bounds of this parameter were not selected realistically or that the regional inflow is only an insignificant part compared to the volume of recharge. This (saline) groundwater flow is currently assumed constant (at 3,770 m^3/d) and is important when the variable-density flow is included in the model.

5.5 EFFECT OF GROUNDWATER ABSTRACTION ON THE GROUNDWATER LEVELS

For different reasons the area's most susceptible of saltwater intrusion are directly south of the borefield in the Town subarea and directly south of Pink Lake. Groundwater abstraction in the Town subarea causes a local decline of groundwater (> 1 m) thereby increasing the risk of seawater intrusion. Flow vector fields indicate that the flow velocity towards the ocean decreases in the Town subarea to almost 0 m/d when abstraction takes place.

Flow vector fields and head gradient analysis show that flows are consistently high at the Observatory point with and without abstraction. The (assumed) elevated basement material prevents flow from entering the ocean in the southwest of the model and a high head gradient is maintained between Observatory Point and the ocean.

The bores directly south of the Pink Lake abstract from a relatively thin layer of freshwater and deeper saline water directly. The abstraction of groundwater would have resulted in a decline in lake stage of 0.20 m in the Pink Lake, 0.09 m in Lake Warden and 0.04 m in the Windabout and Woody Lakes.

5.6 ROLE OF THE HYPERSALINE LAKES ON SALTWATER INTRUSION

The accumulation of saline groundwater is inevitable due to the groundwater flows towards the terminal Pink Lake via the chain of lakes in the system. The concentration of salt in the lake increases due to evaporative concentration and net groundwater inflow increasing in the density of the lake water, as described in the literature. Density driven convection flows are pointed downward into the soil and this repeated process concentrates salt in the groundwater below the lake.

Lake Warden, the second last lake in the chain is hypersaline for the same reasons as the Pink Lake, however freshwater inflow per unit area is higher and the net groundwater inflow is relatively smaller.

Analysing the flow vector fields in combination with the salinity distribution demonstrate that bores directly south of the pink lake are likely abstracting a combination of fresh and saline water. Saline water distribution analysis has confirmed that the soil is saline underneath and directly south of the Pink Lake.

5.7 BOREFIELD DESIGN, OPERATION AND SUGGESTED MODIFICATIONS

It is identified that screens are currently intersecting the entire quaternary aquifer. Screens are preferably installed shallower to avoid upconing and disturbance of the fresh/saline water interface.

The production of each bore for the public water system has been analysed and ranked to their historical abstraction rates. Bores located directly south of the hypersaline Pink Lake abstract less water and are operated more infrequently than other bores in the borefield. It is assumed (conductivity of abstracted water from each bore was not available by Water Corporation) that the poor performance of bores directly south of the Pink Lake is due to the abstraction of saline water which results in shutdowns for recovery. Operational data from the borefield show that these bores are indeed performing poorly.

5.8 PREFERRED LOCATION FOR FUTURE BOREFIELD EXPANSIONS TO LIMIT SALTWATER INTRUSION

The southwest of the subcatchment is the preferred location for a future expansion of the borefield to avoid saltwater intrusion and to limit groundwater decline from its natural state.

This is partly due to the basement material layer above sea level that is being assumed to exist between Observatory Point and Eleven Mile Beach, contrary to earlier studies. Borehole data and AEM data are absent in this area. However, aerial imagery and AEM data that does exist hints at an elevated basement. The local high elevation of the land surface supports this hypothesis.

5.9 FINAL REMARKS

A finite-difference numerical model (MODFLOW) was developed capable of calculating the head and flows in the subcatchment. The accuracy of the model should be improved by more thorough calibration and the inclusion of density-dependent flow. Section 6.2 provides more details. As such, the current model should be regarded as the first step towards a complete tool that includes flows and the distribution of salts. The next revision of the model should be capable of estimating sustainable abstraction rates and calculating more accurately the areas that are at risk of saltwater intrusion.

Chapter 6: Future Work and Recommendations

6.1 INTRODUCTION

As mentioned before, the numerical flow model that was developed for this study is the first step towards a model that includes saltwater movement, i.e. density-dependent flow. Furthermore, recalibration and improved input such as geological layers, head and salinity will further enhance the model. The sections below outline the principal steps to include variable-density flow and improve the model. Suggestions are made to for applying the model to investigate the hydrology and the suitability of engineering solutions to limit saltwater intrusion as stated in Section 1.2.

6.2 INCLUSION OF VARIABLE-DENSITY FLOW AND MODEL CALIBRATION.

Point water heads must be converted to freshwater heads to adapt the model for density-dependent flow. This will have implications for the values of the heads and flow velocities. The inclusion of a saltwater wedge will increase the freshwater velocities. Furthermore, upconing may be modelled and should indicate sustainable pumping rates for each bore as well as sustainable abstraction rates for the entire area.

Improved calibration and the inclusion of density-variable flow increase the accuracy of the model. Improvements to the geological model are also suggested. The geological model can be updated as follows:

- Currently, the geological model was elucidated with a geostatistical algorithm using 2000 data points originating from the AEM data and borelogs. Another more accurate geological model was created that included the layers derived from AEM data while the model outside the AEM domain was created from bore log data with geostatistics. The MODFLOW model resulting from this procedure could not be run due to numerical issues. It is suggested to smooth out abrupt layer transitions so that the more accurate geological model can be used as input for MODFLOW and numerical issues do not arise.

- Other geostatistical software running Kriging algorithms (such as the freely available Python-based Gempy) may be a better option than PyKrige when it is known that there are locations where a geological layer is absent. PyKrige was selected for its robustness in this study.
- The assumption that the basement between Observatory Point and Eleven Mile Beach is higher than the saltwater level can have far-reaching implications for the (future) borefield design and saltwater intrusion. It is suggested to investigate if accurate bore logs or AEM data exist in this region or if a geological survey is planned in the future.

The following steps are suggested to include the sweater intrusion:

- The model is running with MODFOW-NWT which is incompatible with the SEAWAT package to simulate saltwater intrusion. This can be resolved in two ways:
    - Rewrite the model to MODFLOW 6 and use the inbuilt density and dispersion packages
    - Attempt to run the current model with the SMS solver from MODFLOW-USG which is compatible with SEAWAT
- Confirm and quantify saline water sources such as:
    - TDS concentration in rainfall
    - TDS concentration in the regional inflow. This report has described that groundwater salinity is abundant in the entire region of the subcatchment.
    - Salinity can also enter the domain by surface water flow from Coramup Creek.
- Quantify TDS concentration for each model cell as a starting position of the model:
    - The AEM dataset from the 2013 survey contains a snapshot of saline concentrations which can be reworked to the desired resolution (cells) matching the groundwater model.
    - The DWER SWIM bores contain time series with EC measurements or TDS concentrations in several locations

- TDS and/or EC data of the lakes are available
- The saline groundwater concentrations at locations outside of the AEM survey area need to be estimated

- The evaporation rate is a parameter that does not require calibration. Evaporation from the hypersaline lakes is a function of salinity and potentially has a large effect on the overall water balance of the lakes. Adjusting the evaporation rate to realistic values is recommended to improve the model's accuracy.
- Recalibrate the model after adjusting the groundwater heads to include salinity.
  - The availability of more cores for calibration is a necessity to limit the calibration run times
  - Longer time series from each observation point may be obtained directly from DWER.
  - A larger number of iterations will likely lead to parameter settings with a closer match to observations
  - Inclusion of more parameters is advised (limited by available cores)
  - Investigation of unidentifiable parameters and their thresholds
  - Use of pilot points for more accurate spatial parametrisation of the hydraulic properties of the soils

6.3 FURTHER DEVELOP THE UNDERSTANDING OF THE INTERACTION BETWEEN THE HYPERSALINE LAKES, THE SUPERFICIAL GROUNDWATER AQUIFER AND THE OCEAN.

It is recognised that the current design of the production borefield may limit abstraction rates at least at locations where a saltwater wedge is present. As shown, most wells are screened through the entire Quaternary aquifer and as such the uptake of saline water cannot be avoided in case a saline water wedge is present at the location of the bore.

As stated before, further modelling with the density-dependent flow should provide more details to further optimise and test borefield management regimes to avoid upconing, saline water abstraction and to minimise saltwater interface disturbance. Drawdowns of lakes and groundwater can be more accurately calculated and movements of saline water wedges can be calculated. This will increase the

understanding of the hydrology in the subcatchment and will aid water managers in making sustainable decisions.

6.4 ESTIMATING THE SUSTAINABLE ABSTRACTION RATES

A calibrated flow model that includes variable-density can be used to estimate the sustainable abstraction rates, i.e. a rate that can be abstracted from the aquifer for extended periods without exhausting the supply with minimal environmental impact. The sustainable extraction rate varies spatially and temporally (seasonally) which can be identified by modelling.

6.5 OPTIMISING EXISTING BOREFIELD UTILISATION AND ENGINEERING SOLUTIONS WITH SCENARIO TESTING

After the development of the variable-density model is complete, the model may be utilised as a groundwater management tool. The following may be tested and analysed:

- Investigation on how the current borefield affects saltwater intrusion in the aquifer including the role of the hypersalinity lakes.
- Abstraction of groundwater in different regions. For example, the effect on saltwater intrusion as a result of an extension of the borefield to the southwest may be modelled. It is important to note that the ocean may be separated from the aquifer due to an elevated basement (to be confirmed)
- Optimising borefield operational schemes to reduce the effects of saltwater intrusion, upconing and saline water uptake.
- Modelling the effect of population size on saltwater intrusion
- Modelling the effect of engineering solutions such as Managed Aquifer Recharge (MAR) on saltwater intrusion.
- Modelling the effect of screen depths on upconing, saltwater intrusion and saline water uptake.

Chapter 7: References

1. Kummu, M., de Moel, H., Salvucci, G., Viviroli, D., Ward, P. J., Varis, O. (2016). Over the hills and further away from coast: global geospatial patterns of human and environment over the 20th–21st centuries. *Environ. Res. Letters, 11(**3**),* 034010.
2. Short, R. (2000). *A conceptual hydrogeological model for the Lake Warden recovery catchments Esperance, Western Australia.* Department of Agriculture and Food, Western Australia, Perth. Report 200.
3. Department of Water. (2007). *Esperance Groundwater Area, Water Management Plan*. Water Resource Allocation Planning Series Report No. WRAP 16.
4. Reynolds, D. A., Marimuthu, S. (2007). Deuterium composition and flow path analysis as additional calibration targets to calibrate groundwater flow simulation in a coastal wetlands system. *Hydrogeology Journal, 15(**3**),* 515 – 535.
5. Werner, A. D., Bakker, M., Post, V. E. A., Vandenbohede, A., Lu, C., Ataie-Ashtiani, B., Simmons, C. T., Barry, D. A. (2013). Saltwater intrusion processes, investigation and management: Recent advances and future challenges. *Advances in Water Resources, 51,* 3-26.
6. Werner, A. D. (2010). A review of saltwater intrusion and its management in Australia. *Hydrogeol J 18*, 281–285
7. Oude Essink, Gualbert. (2003). Mathematical models and their application to salt water intrusion problems. 10.13140/2.1.1637.4727.
8. Costall, A.R., Harris, B.D., Teo, B. (2020). Groundwater Throughflow and Saltwater Intrusion in High Quality Coastal Aquifers. *Sci Rep 10,* 9866
9. Luyun, R.A., Momii, K., Nakagawa, K. (2011). Effects of recharge wells and flow barriers on saltwater intrusion. *Ground water, 49(***2**), 239-49
10. Kuan, W. K., Jin, G., Xin, P., Robinson, C., Gibbes, B., Li, L. (2012). Tidal influence on saltwater intrusion in unconfined coastal aquifers, *Water Resour. Res., 48,* W02502
11. Badaruddin, S., Werner A. D., Morgan, L. K. (2015). Water table salinization due to saltwater intrusion, *Water Resour. Res., 51,* 8397–8408
12. Colombani, N., Mastrocicco, M. (2017). *IOP Conf. Ser.: Earth Environ. Sci. 82* 012003
13. Sanford, W., Pope, J. (2010). Current challenges using models to forecast saltwater intrusion: Lessons from the Eastern Shore of Virginia, USA. *Hydrogeology Journal. 18*. 73-93
14. Siarkos, Ilias, Latinopoulos, Pericles. (2016). Development of constant and variable density models to study groundwater flow and saltwater intrusion in the aquifer of Nea Moudania, Greece. *European Water. 55*. 53-66.
15. Lu, Wei, Yang, Qingchun, Delgado, Jordi, Juncosa, Ricardo. (2013). Numerical modelling of saltwater intrusion in Shenzhen (China) using a 3D density-dependent model including tidal effects. *Journal of Earth System Science. 122.* 451-465

16. Mohammed S. H., Akbar A. J., Mohsen M. S. (2015). Three Dimensional Simulation of Saltwater Intrusion in a Regional Coastal Aquifer in UAE, *Procedia Engineering, 119,* 1153-1160
17. Dibaj, M., Javadi, A. A., Akrami, M. (2020). Modelling saltwater intrusion in the Pingtung coastal aquifer in Taiwan, under the influence of sea-level rise and changing abstraction regime. *Hydrogeol J 28*, 2085–2103
18. EL Hamidi, M.J., Larabi, A., Faouzi, M. (2021). Numerical Modeling of Saltwater Intrusion in the Rmel-Oulad Ogbane Coastal Aquifer (Larache, Morocco) in the Climate Change and Sea-Level Rise Context (2040). *Water 2021, 13,* 2167
19. Author Unknown. (October 10, 1911). Report of Government Geologist. *The Daily News.*
20. Simons, J. A., Alderman, A. (2004). *Groundwater trends in the Esperance sandplain and mallee subregions*. Department of Agriculture and Food, Western Australia, Perth. Report 10/2004.
21. Massenbauer, A., Esperance Catchment Support Team (WA). (2007). *Esperance Lakes catchment appraisal 2007*. Department of Agriculture and Food, Western Australia. Report 316.
22. Department of Water. (2012). *Esperance Water Reserve drinking water source protection plan - Esperance town water supply*. Report WRP 134
23. Watkins, G. (2009). *Ecological Character Description of the Lake Warden System Ramsar Site: A Report by the Department of Environment and Conservation*. Department of Environment and Conservation, Perth, Western Australia.
24. Lane J. A. K., Clarke, A.G., Winchcombe, Y.C. (2011). *South West Wetlands Monitoring Program Report 1977 – 2010.* Western Australian Department of Environment and Conservation.
25. Drew, M., Lynn, T., Ferguson, K. (2015*). Lake Warden Natural Diversity Recovery Catchment: Hydrology Program Synopsis 1997 - 2015*. Department of Parks and Wildlife (Parks and Wildlife), Wetlands Conservation Program Hydrology report WCP-HR-2015-003, Kensington, Western Australia.
26. Marimuthu, S., Reynolds, D. A., Le Gal La Salle, C. (2005). A field study of hydraulic, geochemical and stable isotope relationships in a coastal wetlands system. Journal of Hydrology. 315 (**1**–**4**), 93-116
27. Marimuthu, S. (2006). Delineation of Groundwater Flow within a Coastal Wetlands System using Hydraulic Geochemical and Stable Isotope Data. *Geological Society of Malaysia Bulletin 52*, 109-120
28. Abbott, S., (2011). *Application of Geophysical Techniques for 3D Visualization of Regolith Hydrogeological Architecture and Use of this Information for Management of Dryland Salinity in Western Australia.* [PhD – Exploration Geophysics of Curtin University, Perth]. http://hdl.handle.net/20.500.11937/1454
29. Lizamore, J. (2020). *Water quality review of Pink Lake and Associated Lakes - Technical support document for the Esperance Pink Lake Feasibility Study*. Shire of Esperance
30. McCafferty, P. B., Devenish, M., Burton H. M., Jackson, M., North, M., Winchester, W. (2013). Assessment and Remediation of Lead

Contamination in Esperance, Western Australia. *E3S Web of Conferences, 1, 10002*. doi 10.1051/e3sconf/20130110002
31. Heyworth, J. S., Mullan, N., (2009). Environmental Lead and Nickel Contamination of Tank Rainwater in Esperance, Western Australia: An Evaluation of the Cleaning Program. *J. Water Resource and Protection 1,* 1-57
32. Department of Water. (2019). *Frequently Asked Questions - PFAS and Esperance Water Supplies.* https://www.der.wa.gov.au/images/documents/our-work/community-updates/FAQs%20%20Esperance%20PFAS.pdf
33. Hodgkin, E.P., Hesp, P., (1998). Estuaries to salt lakes: Holocene transformation of the estuarine ecosystems of south-western Australia. *Mar. Freshwater Res.49,* 183–201
34. George, R., Clarke, J., English P., (2008). Modern and palaeogeographic trends in the salinisation of the Western Australian wheatbelt: a review. *Australian Journal of Soil Research, 46,* 751–767
35. Short, R., Salama, R., Pollock, D., Kin, P., Hatton, T.J., Bond, W.J., Paydar, Z., Cresswell, H.P., Gilfedder, M., Moore, A., Simpson, R., Salmon, I., Stafanski, A., Probert, M., Huth, N., Gaydon, D., Keating, B. (2000). *Assessment of salinity management options for Lake Warden catchments, Esperance WA. Groundwater and crop water balance modelling.* Agriculture WA, Esperance. Report No.:20/00. http://hdl.handle.net/102.100.100/205836?index=1
36. Myers, J. S., (1995). *Geology of the Esperance 1:l 000 000 sheet: Western Australia Geological Survey*, 1:l 000 000. Geological Series Explanatory Notes, 1 Op.
37. Overheu, T. D., Muller, P. G., Gee, S. T., Moore, G. A. (1993*). Esperance land resource survey.* Department of Agriculture and Food, Western Australia, Perth. Report 8.
38. Timms, B. V. (2009). Study of the saline lakes of the Esperance Hinterland, Western Australia, with special reference to the roles of acidity and episodicity. *Natural Resources and Environmental Issues: Vol. 15(*44)
39. Raper, G.P., Speed, R.J., Simons, J.A., Killen, A.L., Blake, A.I., Ryder, A.T., Smith, R.H., Stainer, G.S. Bourke, L. (2014). *Groundwater trend analysis for south-west Western Australia 2007–12.* Department of Agriculture and Food, Western Australia, Perth. technical report 388
40. Mernagh, T.P. (2013). *A review of Australian salt lakes and assessment of their potential for strategic resources*. Geoscience Australia: Canberra. Record 2013/39
41. Galloway, D., Bestow, T. Loh, I. (1986). *The report on investigations into the hydrology and use of Pink Lake at Esperance*. Department of Conservation and Environment Perth, Western Australia. Bulletin, 262, 9p.
42. Massenbauer, T. (2020). *Esperance Pink Lake Feasibility Study*, Shire of Esperance (2020), Report ESPER-855161
43. Street, G. J., Abbott, S. (2007). Study of groundwater flow in sediments and regolith defined by airborne geophysical surveys. https://doi.org/10.1071/ASEG2007ab141

44. Department of Water and Environmental Regulation (2020). *Esperance groundwater evaluation 2012-2020, an evaluation of the 2007 Esperance groundwater area water management plan.* Perth, Western Australia.
45. Gee, S. T., Simons, J. A. (1997). *Catchments of the Esperance region of Western Australia*. Department of Agriculture and Food, Western Australia, Perth. Report 165.
46. Johnson, S. L., Baddock, L. J. (1998). *Hydrogeology of the Esperance Mondrain Island 1:250000 Sheet: Western Australia*. Water and Rivers Commission, Hydrogeological Map Explanatory Series, Report HM 2, 24p
47. Rockwater. (2018). *Planned Landfill Site Esperance - Results of Pumping Tests. Shire of Esperance* https://www.esperance.wa.gov.au/sites/default/files/publication/files/18-01a_pumping_test_results.pdf
48. Talis (2017). *Phase 1 Hydrogeological Investigation - Lot 12 Kirwan Road*. Shire of Esperance. https://www.esperance.wa.gov.au/sites/default/files/publication/files/te16039-esperance_phase_1_site_investigation_site_19.1c_-_resized.pdf
49. Allen, R., Pereira, L., Raes, D., Smith, M. (1998). *FAO Irrigation and drainage paper No. 56.* Food and Agriculture Organization of the United Nations. 56. 26-40
50. Lymburner, L., Tan, P., McIntyre, A., Thankappan, M., Sixsmith, J. (2019*). Dynamic Land Cover Dataset Version 2.1*. Geoscience Australia. http://data.gov.au/dataset/0cb242e2-daed-4507-a42e-73892c0941a1
51. Brodie, R.C. (2014). *South West Coastal Plain & South Coast TEMPEST AEM Survey, Western Australia.* Geoscience Australia, Canberra. http://dx.doi.org/10.4225/25/542E1D13558F5
52. Geoscience Australia (2019). *What is airborne electromagnetics?* ABARES. https://www.agriculture.gov.au/ag-farm-food/natural-resources/salinity/salinity-mapping/what_is_airborne_electromagnetics
53. Gallant, J. C., Dowling, T. I., Read, A. M., Wilson, N., Tickle, P., Inskeep, C. (2011). *1 second SRTM Derived Digital Elevation Models User Guide.* Geoscience Australia. www.ga.gov.au/topographic-mapping/digital-elevation-data.html
54. The Esperance Bay Historical Society. (n.d.). *Esperance History*. Retrieved 2019, from https://www.esperancehistory.com.au/esperance-history-timeline/
55. The Esperance Bay Historical Society. (n.d.). *Brief Outline of Esperance's history since World War One*. Retrieved 2019, from http://htawa.net.au/WA-100-years/files/community/Esperance-snapshot-100-years-e.pdf
56. City population: Population statistics for countries, administrative divisions, cities, urban areas and agglomerations – interactive maps and charts. *Esperance Urban Centre.* Retrieved 2019, from https://www.citypopulation.de/en/australia/westernaustralia/_/513002__esperance/
57. Australian Bureau of Statistics. Regional Population Growth, Australia, 2005-06. Retrieved 2019, from https://www.abs.gov.au/ausstats/abs@.nsf/Previousproducts/3218.0Main%20Features42005-

06?opendocument&tabname=Summary&prodno=3218.0&issue=2005-06&num=&view=
58. https://www.waterwest.com.au/wp-content/uploads/2018/07/Water-Opportunities-Final-Report.pdf
59. USGS, (2016). *SEAWAT Version 4: A computer program for simulation of multi-species solute and heat transport*. Retrieved 2019 from https://water.usgs.gov/ogw/seawat/summaryv4.html
60. Nield, D. A., Simmons, C. T., Kuznetsov, A. V., Ward, J. D. (2008). On the evolution of salt lakes: Episodic convection beneath an evaporating salt lake. *Water Resour. Res., 44.* W02439
61. Harbaugh, A.W. (2005). MODFLOW-2005, The U.S. Geological Survey modular ground-water Model - the Ground-Water Flow Process: U.S. Geological Survey Techniques and Methods 6-A16
62. Harte, P.T., (1994). Comparison of Vertical Discretisation Techniques in the Finite-Difference Models of Ground-water Flow: Example from a Hypothetical New England Setting. U.S. Geological Survey, Open-File Report 94-343
63. Hengl, T. A. (2009). *A Practical Guide to Geostatistical Mapping*.
64. Goovaerts, P. (1997). *Geostatistics for Natural Resource Evaluation*.
65. Murphy, B. (2021). *PyKrige Documentation - Release 1.6.0.* https://geostat-framework.readthedocs.io/_/downloads/pykrige/en/stable/pdf/
66. Niswonger, R. G., Panday, S., Ibaraki, M. (2011). MODFLOW-NWT, A Newton Formulation for MODFLOW-2005. U.S. Geological Survey Techniques and Methods 6-A37
67. Freeze, R. A., Cherry, J. A., (1979). *Groundwater*. First Edition. Prentice Hall, Englewood Cliffs, USA (ISBN: 0-13-365312-9)
68. Schenk, H. J., Jackson, R. B., (2002). Rooting depths, lateral root spreads and below-ground/above-ground allometries of plants in water-limited ecosystems. *Journal of Ecology 90*, 480–494
69. Bakker, M., Post, V., Langevin, C. D., Hughes, J. D., White, J. T., Starn, J. J., Fienen, M. N. (2016). Scripting MODFLOW Model Development Using Python and FloPy. *Groundwater, 54*(**5**), 733–739
70. Doherty, J. (2020a). *PEST - Model-Independent Parameter Estimation—User Manual Part I: PEST, SENSAN and Global Optimisers*. (7th edition). Watermark Numerical Computing, Brisbane, Australia.
71. Doherty, J. (2020b). PEST - *Model-Independent Parameter Estimation—User Manual Part II: PEST Utility Support Software.* (7th edition). Watermark Numerical Computing, Brisbane, Australia.
72. White, J. T., Hunt, R. J., Fienen, M. N., Doherty, J. E. (2020). *Approaches to highly parameterized inversion: PEST++ Version 5, a software suite for parameter estimation, uncertainty analysis, management optimization and sensitivity analysis.* (Report No. 7-C26; Techniques and Methods, p. 64). USGS Publications Warehouse.
73. Doherty, J., Hunt J. R., (2008). Two statistics for evaluating parameter identifiability and error reduction. *Journal of Hydrology, 366*, 119–127
74. Doherty, J., Moore, C. (2020). Decision Support Modeling: Data Assimilation, Uncertainty Quantification, and Strategic Abstraction. *Groundwater, 58*(**3**), 327–337

75. Doherty, J. (2003), Ground Water Model Calibration Using Pilot Points and Regularization. *Groundwater, 41*. 170-177
76. Doherty, J.E., Fienen, M.N., Hunt, R.J., (2010). *Approaches to highly parameterized inversion: Pilot-point theory, guidelines, and research directions.* U.S. Geological Survey Scientific Investigations Report. 2010–5168, 36 p.
77. Marimuthu, S. (2020). *Water Balance for Pink Lake and Lake Warden Esperance - Technical support document for the Esperance Pink Lake Feasibility Study*. Shire of Esperance
78. Bear, J., Verruijt, A. (1987). *Modeling groundwater flow and pollution: With computer programs for sample cases*. Dordrecht: D. Reidel Pub. Co.